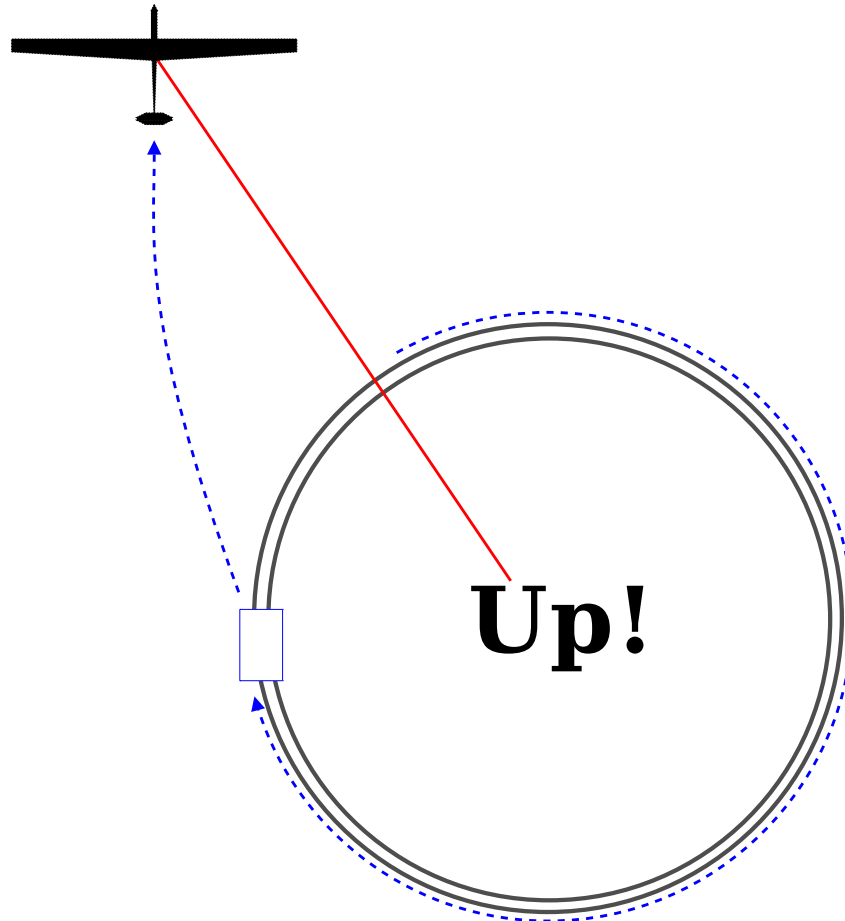


Delft University of Technology
Faculty of Aerospace Engineering

Master of Science Thesis



How to Launch and Retrieve a Tethered Aircraft



Author:
Eelke Bontekoe
Student Number:
1335561

Supervisor:
Dr.Ir. Mark Voskuijl

August 16, 2010



Delft University of Technology
Faculty of Aerospace Engineering

Master of Science Thesis

Up!

How to Launch and Retrieve a Tethered Aircraft

Author:

Eelke Bontekoe

Student Number:

1335561

Supervisor:

Dr.Ir. Mark Voskuijl

Reviewers:

Prof.dr. G.J.W. van Bussel

Dr.ir. M. Voskuijl

Dr. M.D. Pavel

Ir. Soren Sieberling

August 16, 2010

Preface

This thesis is the result of my research done as final part of the master of science program Sustainable Energy Technology at the TU Delft. Even though this master is rooted at the Faculty of Applied Science, I conducted my research in cooperation with the faculty of Aerospace Engineering because of my specialization in the field of wind energy. Furthermore the assignment I took is probably even more aircraft related than other wind energy projects, since I decided to do my research in the field of Airborne wind energy at the small start-up company Ampyx Power.

Many thanks go out to my supervisor Mark Voskuijl. First of all, for being open to supervise me on this project. In the end that is what made it possible to choose this topic. Moreover I thank him for the advice on which steps to take during the research and his useful comments on everything I wrote.

Then of course I would like to thank my colleagues at Ampyx Power. Starting with Richard for inspiring me into the field of airborne wind energy, with the interesting kite course he gave at the TU Delft. Bas for sharing his knowledge and experience on the Powerplane concept and the rotational platform. And for making sure that good coffee was always at hand.

Sören was a great help throughout my research, especially for running Matlab simulations. He also took the time to answer any aerospace engineering related question I had. Mathieu for persuading me to use Ubuntu which consequently forced me to write this report in L^AT_EX; A decision I will never regret. Illias for being the only person in the company who finally overtook my example of not eating meat.

Further on, I would like to thank my parents for providing me their unlimited support. My friends and family for giving me a wonderful life next to the research, and last but definitely not least my girlfriend Cora for being the love of my life.

Eelke Bontekoe,
Delft, August 16, 2010

Summary

The basic model of the principle of crosswind power as described by Miles M. Loyd in 1980 [Loyd, 1980], promises a high energy revenue from airborne wind energy. With a growing awareness of the need of sustainable energy resources and the current technological possibilities, different initiatives are undertaken to harvest the energy of wind at higher altitudes. One of these initiatives is the Powerplane, which makes use of a glider type aircraft with a wing span of 36 meters for producing 1 MW of electric power. The aircraft flies patterns in the sky such that it produces a high tension in the connecting tether. The system generates power as the tether is unwound from a drum located at the ground under this high tension. When the tether is fully unwound, the aircraft performs a dive while the tether is quickly retrieved with a minimum tension. The difference in tension during retrieval and unwinding allows net energy to be generated.

Before the 1 MW Powerplane can be put on the market as a working system, several technological hurdles must be taken. A conventional wind turbine is always firmly situated at its operational altitude as soon as it is installed. On the contrary, the Powerplane needs a method to get there. Therefore one of the main design challenges is the step between an idle state on the ground, and generating energy at operational altitude. This challenge is the main objective of the research done in this thesis: to find out how the aircraft can be launched and retrieved such that the Powerplane will be a competitive system for wind energy generation.

There are many different ways for doing this, but which way is most feasible? To answer this question, first of all the main requirements a launch and retrieval system has to comply with are outlined. A functional analysis lead to different design options, of which the most interesting options were analysed more extensively by various methods. Combining promising design options gave three concepts. One concept based on buoyancy, a concept making use of propeller thrust and one which uses a rotational platform to launch the aircraft. Analysing these concepts in a trade-off resulted in abandoning the buoyancy concept, but the other two required more research. This resulted in an improvement of the propeller thrust concept by combining it with a circular runway. The operating principle of the rotating platform concept is analysed by means of computer simulations. Even though the results of the simulations were promising, they were not convincing.

Before a definite decision on the concepts can be made, more research is required. The effect of the added weight of the propeller thrust concept should be determined by studying the Powerplane concept in general. The concept of the rotational platform needs to be investigated more to make sure that the operational altitude can be reached without additional equipment. Nevertheless, the research outlined in this thesis and the recommendations made, provide a firm basis to find the optimum solution for launching and retrieving the aircraft. I hope the content of this research will help to make the concept of Airborne Wind Energy a step closer to becoming a world wide success.

Contents

1	Introduction	11
1.1	Problem description	11
1.2	Aims and objective	12
1.3	Structure	12
2	The Powerplane concept	13
2.1	Basic model of crosswind power	13
2.2	Operating principle of Powerplane	15
2.3	Comparison wind turbine	16
2.3.1	Wind shear	16
2.3.2	Capacity factor	17
2.3.3	Material use	18
2.4	Competitors	18
2.4.1	Joby energy and Makani Power	18
2.4.2	Pumping laddermil	19
2.5	Parameters aircraft	20
2.5.1	Development of 10 kW and 100 kW aircraft	20
2.5.2	Lift and Drag	21
2.5.3	Load factor	21
2.6	Conclusion	22
3	Design requirements	23
3.1	Aircraft related requirements	23
3.1.1	Main dimensions aircraft	23
3.1.2	Minimum velocity	24
3.1.3	Maximum velocity	24
3.1.4	Maximum acceleration	24
3.1.5	Additional thrust	24
3.1.6	Landing controllability	24
3.1.7	Additional weight on aircraft	25
3.2	Operational requirements	25
3.2.1	Minimum altitude and cable length the aircraft should be able to reach	25
3.2.2	Operating conditions	25
3.2.3	Time span for launching	26
3.2.4	Time span for landing	26
3.2.5	Forces on aircraft	27
3.2.6	Forces on landing / launching mechanism	27
3.2.7	Forces during extreme conditions	27
3.3	Peripheral requirements	27
3.3.1	Prepared for park set-up	27
3.3.2	Autonomous operation	27
3.3.3	Safety	27
3.3.4	Lifetime	27
3.3.5	Cost-efficient	28

3.3.6	Reliability	28
3.3.7	Cable wear	28
3.4	Summary	28
4	Design option analysis	31
4.1	Basic design option tree	31
4.2	Functional analysis diagrams	31
4.3	High velocity lift-off	32
4.3.1	Launch velocity	33
4.3.2	Launch distance	34
4.3.3	Power	34
4.3.4	Conclusion	35
4.4	Using buoyancy	35
4.4.1	Maintain operating area	36
4.4.2	Drag of a Zeppelin	37
4.4.3	Retain shape	37
4.4.4	Cope with gas leakage	38
4.4.5	Docking in the sky	39
4.5	Climb with a propeller	39
4.5.1	Optimum angle of attack	40
4.5.2	Aircraft with cable	41
4.5.3	Cable tension	43
4.5.4	Required shaft power	43
4.5.5	Mass of electric motor	45
4.5.6	Required energy	45
4.5.7	Battery mass	46
4.5.8	Total mass	46
4.5.9	Cost	47
4.5.10	Propeller	47
4.5.11	Conclusion	48
4.6	Climb with air pressure	48
4.6.1	Adiabatic expansion	48
4.6.2	Possible amount of impulse	49
4.6.3	Required impulse for climbing	49
4.6.4	Pressure vessel	49
4.6.5	Conclusion	50
4.7	Accelerate with propeller	50
4.7.1	Distance of ground run	50
4.7.2	Power	51
4.7.3	Energy	51
4.8	Accelerate with an external system	52
4.9	Launch with a rotational platform	52
4.9.1	Minimum radius of turn for a conventional flight	53
4.9.2	Tether for centripetal force	55
4.9.3	Minimum radius of turn for tethered flight	55
4.9.4	Test set-up proof of concept with rotating platform	59
4.10	Conclusion	61
5	Concepts	63
5.1	Concept: Buoyancy	63
5.2	Concept: Propeller thrust	64
5.3	Concept: Rotating platform	64
5.4	Operational procedure rotating platform	65
5.5	Comparison	67
5.6	Discussion of trade-off results	69
5.6.1	Aircraft related requirements	69

5.6.2	Operational boundaries	70
5.6.3	Peripheral requirements	70
5.7	Conclusion	70
6	Climbing with aircraft thrust	71
6.1	Winch limitations	71
6.2	Different approach to minimum height	71
6.2.1	Flight path	72
6.2.2	Launch with headwind	72
6.2.3	Launch with tailwind	73
6.3	Climbing to operational altitude with aircraft thrust only	73
6.4	Launch with a circular track	73
6.5	Improved Propeller thrust concept	74
6.5.1	Launch and climb	74
6.5.2	Landing on a circular track	74
6.5.3	Discussion of concept	75
6.6	Conclusion	75
7	Simulation of a rotating launch	77
7.1	Simulation model	78
7.1.1	Model structure	78
7.1.2	Mass and inertia block	79
7.1.3	Forces and Moments block	79
7.1.4	Equations of Motion	81
7.1.5	State computations block	82
7.1.6	Sensor dynamics	82
7.1.7	Actuator dynamics	83
7.1.8	Cable	83
7.1.9	Rotating launch	83
7.1.10	Start of simulation	83
7.2	Simulation approach	83
7.3	Simulation results	84
7.3.1	Reference simulation	84
7.3.2	Coordinates	84
7.3.3	Lag angle ζ	85
7.3.4	Launch angle ξ	85
7.3.5	Cable	85
7.3.6	Velocities	87
7.3.7	Attitude and actuator demands	87
7.3.8	Optimizing controller	89
7.4	Optimizing airspeed	89
7.5	Sensitivity analysis	90
7.5.1	Effect of wind	91
7.5.2	Changing desired bank angle	91
7.5.3	Varying desired velocity	94
7.5.4	Varying desired reel out speed	94
7.5.5	Varying arm length	94
7.6	Required power	95
7.7	Physical appearance	95
7.8	Circular track	97
7.9	Conclusion and recommendations	97

8 Conclusion and recommendations	99
8.1 Research on reversed pumping	99
8.2 Improve and utilize simulation model	99
8.2.1 Specifications 1 MW aircraft	100
8.2.2 Rotating launch	100
8.2.3 Reversed pumping and winching	100
8.2.4 Winch parameters	100
8.2.5 Propeller thrust	100
8.3 Modular prototype	100
A List of symbols	105
B Increase altitude with help of the winch	107
B.1 Airborne winching	107
B.2 Reversed pumping	107
C Specifications Dyneema Cable	109
D Design options	111
E Functional Analysis Diagrams	115
F Airfoil characteristics Easyglider	119
G Data of Terex Crane	123

Chapter 1

Introduction

Ampyx Power is a pioneering technology start-up company that is at the forefront of Airborne Wind Energy. Ampyx is developing the Powerplane, a machine that aims to extract energy from the wind much more economically than wind turbines. The principle of operation is shown in figure 1.1. The aircraft flies patterns in the sky such that it produces a high tension in the connecting tether. The system generates power as the tether is unwound from a drum located at the ground under this high tension. When the tether is fully unwound, the aircraft performs a dive and the tether is quickly retrieved with a minimum tension, in order to minimize power losses. The difference in tension during retrieval and reel out allows net energy to be generated.

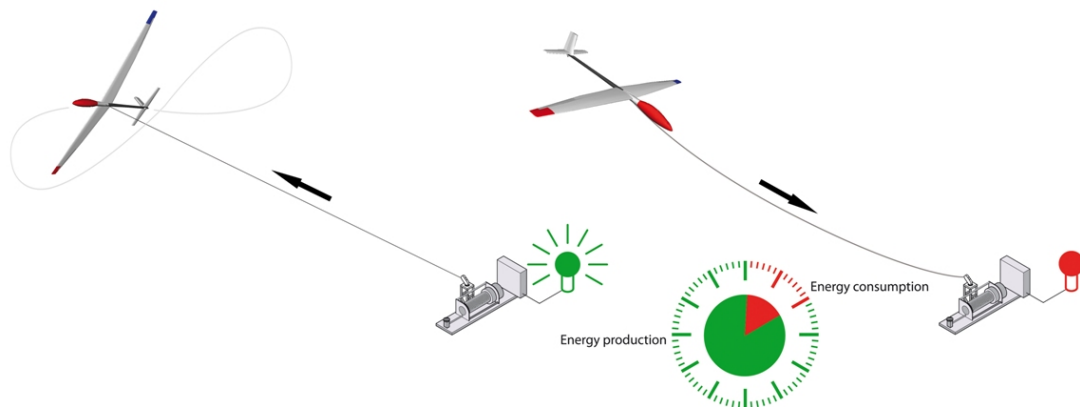


Figure 1.1: Graphic representation of the Powerplane concept

1.1 Problem description

One main requirement for the Powerplane to be an economically attractive wind energy system, is to work fully autonomously, just like conventional wind turbines. Circumstances will take place where the aircraft cannot remain airborne. In these cases the aircraft must be landed or retrieved automatically. Before the system can generate energy again, the aircraft must also automatically reach its operational altitude and an appropriate cable length. An 'off the shelf' solution for these operations is not available, nor has the company developed such a system yet. Therefore the research question becomes:

How to launch and retrieve the tethered aircraft of the Powerplane system

In this statement, launching means getting the aircraft from the ground station to an appropriate altitude, velocity and cable length. Retrieving means returning the aircraft from a certain height and velocity back to the ground station. The main function the system has to accomplish is represented in figure 1.2.

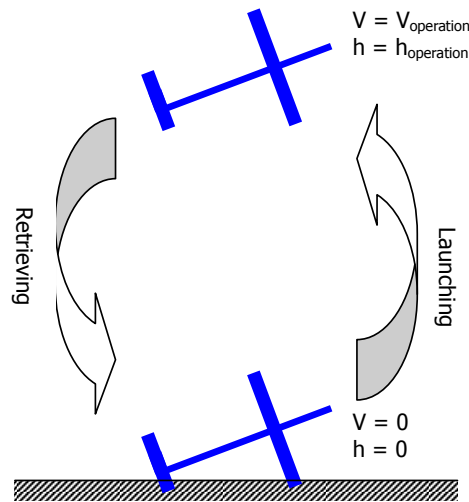


Figure 1.2: Graphic representation of main function

1.2 Aims and objective

The main objective of the research is to find out how the aircraft can be launched and retrieved such that the Powerplane will be a competitive system for wind energy generation. The results of these findings will be used to give recommendations for a more extensive and detailed design of the launch and retrieval system.

1.3 Structure

First of all the Powerplane system is described more elaborately. Crosswind power, the main principle it operates on, are explained and a general look into Ampyx Power and its the main competitors are given. There are a lot of requirements attached to launching and retrieving the aircraft. Before finding solutions for the main function, it must be clear what these requirements are and what the importance of these requirements is. Then different design options regarding the main function are analysed more deeply and divided into different functions in functional analysis diagrams. As a result of these diagrams specific questions arise, which will be answered if necessary. Different concepts will be suggested by means of the functional analysis diagrams and the associated research. The concept that most satisfactory meets the requirements will be defined by means of comparison chart. The most attractive concept will then be defined and analysed more extensively to come up with the final design recommendations.

Chapter 2

The Powerplane concept

The most efficient principle to gain energy with the help of an aircraft is using crosswind power. Which means that the aircraft is not facing into the wind, but its moving approximately transverse to the wind. This is comparable to how a wind turbine operates. The motion of a turbine blade is also perpendicular to the wind, having an average velocity above the wind speed. The lift force on the blade is the major contributor to power generation. Figure 2.1 shows these similarities, a remark to this picture is the fact that the Powerplane operates at a higher altitude than the turbine.

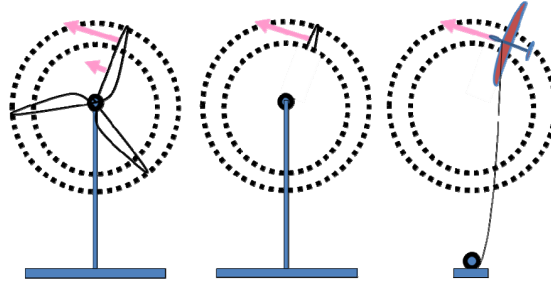


Figure 2.1: Comparison between wind turbine and Powerplane

In case of the Powerplane, the aircraft flies a closed path downwind from the ground station having a crosswind airspeed increased above the wind speed. The aerodynamic lift force resulting from this motion is not only sufficient to support the weight of the cable and the aircraft but also to generate power. This power is generated by pulling a load downwind with a certain velocity. Physically this means reeling out a cable from a drum with a velocity V_L and a tension T . To understand how this works, a simplified two dimensional analysis is made as described in [Loyd, 1980] in paragraph 2.1. This analysis brings out how generated power increases quadratic with the 'glide number'; $\frac{C_L}{C_D}$ of the aircraft and linear with the 'minimum power required condition'; $\frac{C_L^3}{C_D}$.

2.1 Basic model of crosswind power

Figure 2.2 shows the forces and velocities on a massless tethered aircraft, flying a crosswind path. As described in the previous chapter, power P is generated by pulling a load T downwind, with a velocity V_L .

$$P = TV_L \quad (2.1)$$

As tether drag is ignored, the total drag \bar{D} is the aircraft drag. Perpendicular to this drag is the lift \bar{L} . The tether tension at the aircraft \bar{T} is in line with the wind speed \bar{V}_W , and perpendicular to the crosswind velocity \bar{V}_C . In case of the Powerplane, V_L is the cable reel out velocity. Since this velocity is in the same direction as the wind speed, it reduces the effective wind speed at the aircraft to $\bar{V}_W - \bar{V}_L$.

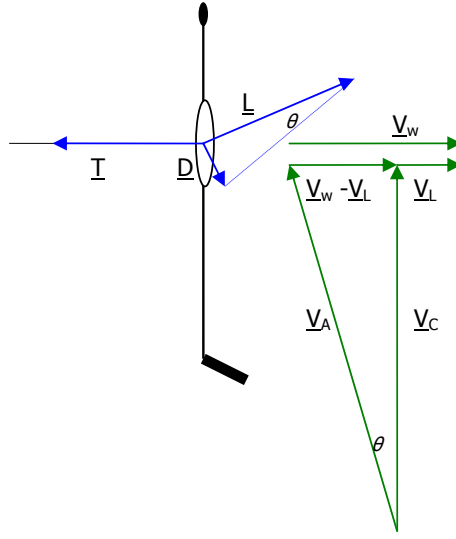


Figure 2.2: Velocities and forces on a weightless tethered aircraft, flying a crosswind path

The relative velocity of the aircraft through the air \bar{V}_A is parallel to the drag. Now the velocities and forces form similar right triangles, so

$$\tan \theta = \frac{D}{L} = \frac{V_W - V_L}{V_C} \Rightarrow V_C = (V_W - V_L)L/D \quad (2.2)$$

For normal operating conditions the angle θ is very small, making \bar{V}_A and \bar{V}_C approximately equal in magnitude. Thus

$$V_A = (V_W - V_L)L/D \quad (2.3)$$

The lift is

$$L = \frac{1}{2} \rho C_L S V_A^2 \quad (2.4)$$

Substituting into 2.3 gives

$$L = \frac{1}{2} \rho C_L S (V_W - V_L)^2 \left(\frac{L}{D}\right)^2 \quad (2.5)$$

A large L/D also makes \bar{L} and \bar{T} approximately equal in magnitude, so 2.1 can be rewritten to

$$P = L V_L \quad (2.6)$$

When the weight of the aircraft and the tether drag are neglected and the aircraft is assumed to have constant velocity, the power at a certain operating condition can be expressed in terms of wing surface area (S), lift coefficient (C_L), wind power density (P_W) and a function F , which will be specified later. This will result in

$$P = P_W S C_L F \quad (2.7)$$

P_W is a function of the air density (ρ) and the wind velocity (V_W)

$$P_W = \frac{1}{2} \rho V_W^3 \quad (2.8)$$

The function F from 2.7 can now be derived by combining 2.8, 2.5 and 2.6 and simplifying to

$$F = (L/D)^2 (V_L/V_W) (1 - V_L/V_W)^2 \quad (2.9)$$

L/D is a function of the angle of attack α which is assumed to be constant at constant velocity. Therefore the maximum value of this function occurs at

$$V_L/V_W = 1/3 \quad (2.10)$$

Up! *How to Launch and Retrieve a Tethered Aircraft*

Resulting in a maximum value F_{max} of

$$F_{max} = 4/27(L/D)^2 \quad (2.11)$$

Combining this equation with equation 2.1 and 2.8 results in the quadratic relation between power production and the glide number

$$P_{max} = \frac{2}{27}\rho V_W^3 S C_L (L/D)^2 \quad (2.12)$$

In terms of C_L and C_D this is

$$P_{max} = \frac{2}{27}\rho V_W^3 S \frac{C_L^3}{C_D^2} \quad (2.13)$$

Which proves the linear relation between the maximum achievable power production and the 'minimum power required'-condition for aircraft ($\frac{C_L^3}{C_D^2}$). The parameters Ampyx Power approximately aims for in case of the 1MW system, is a wing surface area (S) of 130 m^2 . When it operates at maximum lift coefficient (C_L) of 1.3 it has an L/D of 18.6. Leading to a maximum power output as a function of the wind velocity as shown in graph 2.3. The air density ρ at an altitude of 500m. is 1.18 kg/m^3 . [ISO 2533:1975,]. Since the aircraft flies at relatively low altitudes and with low altitude variations, the variation of air density with height are neglected. The maximum potential power production of the 1MW system is calculated for different wind speeds and plotted in figure 2.3. A wind velocity of 5 m/s at ground level, which is a reasonable average for coastal areas, results in 10 m/s at an operational altitude of 500m. The graph indicates that at under these conditions the maximum potential power generation rises to above 5 MW. Even though this number is at ideal conditions, with no cable drag or other losses and with a purely crosswind motion, it is very promising.

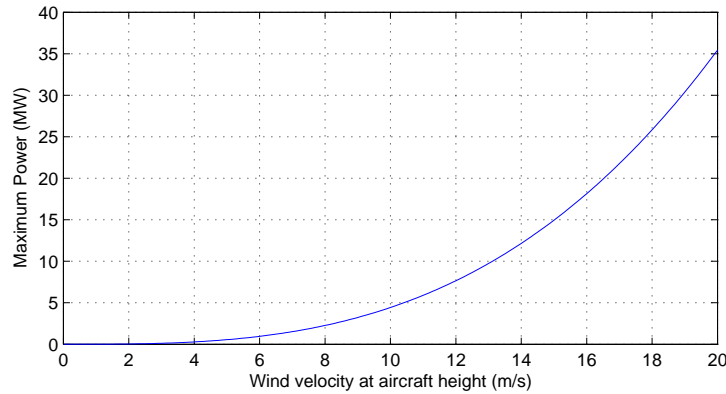


Figure 2.3: Maximum potential power output for a crosswind tethered aircraft with a wing area of 130 m^2

2.2 Operating principle of Powerplane

Ampyx Power plans to use a glider type rigid aircraft to generate energy by making use of the crosswind power as described above. This aircraft will be controlled with ailerons, rudder, elevators and (possibly) flaps, similar to other aircraft. By using these controls to adjust both angle of attack and crosswind motion, the tension in the tether can be varied by orders of magnitude. The winch, located on the ground, will have a drum with a diameter of 0.5 m to reel the cable in and out.

In the power production phase, the aircraft flies perpendicular to the wind, increasing the airspeed and the tension in the cable (Figure 2.4, left). This high tension will be used to pull the cable off the drum, thus rotating this drum under a high tension. The flight path is still to be optimized, but its expected to have a power production phase of about 1 minute, pulling out the cable with a torque of 75kNm, at a rate of 130 rpm. The reel out velocity V_L as stated in paragraph 2.1 in this case is about 3.4 m/s. The rotation of the drum can be transformed into electric power by an alternator and delivered to

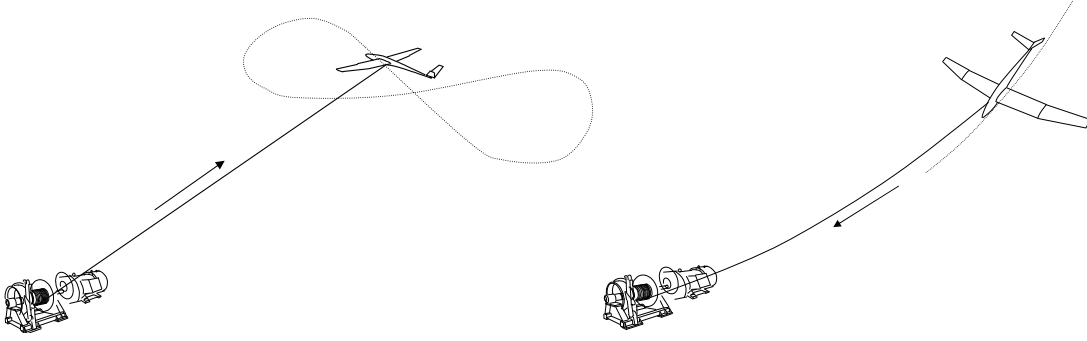


Figure 2.4: Schematic representation of the power production phase (l) and the retrieval phase (r) of the Powerplane

the grid. After the production phase, the tether is fully deployed meaning that there is almost no tether remaining on the drum. Now the aircraft will be controlled in such a way that the cable tension is very low by diving towards the drum as in figure 2.4 on the right. During this dive, the alternator will be used the other way around. Electric energy will be used to rotate the drum for about 9 seconds under a high rate of 900 rpm with a torque of only 3kNm. [Lansdorp, 2009] Maximizing the tether tension during the power production phase and minimizing tension during retrieval will finally result in a net power production. The momentary shaft power (P_{shaft}) can be found as a function of torque (T) and angular velocity (ω) with

$$P_{shaft} = T\omega \quad (2.14)$$

So the average generated shaft power can be calculated with

$$P_{av} = \frac{\omega_{gen}T_{gen}t_{gen} - \omega_{ret}T_{ret}t_{ret}}{t_{gen} + t_{ret}} \quad (2.15)$$

With the given numbers for T and ω in this example the average amount of shaft power is 0.85 MW. The 1 MW output power stands for the maximum power rating of the generator. Standard wind turbines are generally also rated to their maximum power production at rated wind speed [DWIA, 2003]. Because this limiting factor, at higher wind speeds, the power production remains constant. In case of stall controlled turbines it will even decrease [Burton, 2001]. Up scaling the Powerplane system for generating more energy at higher wind speeds can be simply done by changing the generator only. In this case only the reel out velocity will be increased, while the torque remains constant. This way the forces acting on the aircraft and cable also remain constant, but power increases linear with the reel out speed.

2.3 Comparison wind turbine

The advantage of the Powerplane compared to a wind turbine is very clear when it comes to material use. First of all a big steel tower is replaced by a cable and an autopilot. But the benefits of flying at higher altitude are also related a better utilization of the installed capacity. The following paragraphs describe how this makes the energy generation of a 1 MW Powerplane system comparable to a wind turbine of 2 MW.

2.3.1 Wind shear

Wind velocity increases with height, due to the wind shear effect which is related with the ground roughness z_0 , a number ranging from 0.0002 on water to 1.6 for a very large city with skyscrapers. The turbulence caused by this roughness results in a loss of wind speed close the ground. The wind speed V_w at operational height h_{op} can be calculated with the help of the speed V_{ref} at the reference height h_{ref} [DWIA, 2003].

$$V_w = V_{ref} \frac{\ln(\frac{h_{op}}{z_0})}{\ln(\frac{h_{ref}}{z_0})} \quad (2.16)$$

Figure 2.5a shows that when z_0 is 0.2 (agricultural land with some obstacles) the wind speed at 500 m is always twice as much as at reference height. A reference wind speed of 7 m/s at 10 m. then doubles to 14 m/s at 500 m. This effect results in a higher average potential wind speed for the Powerplane operating at 500 meter compared to a wind turbine with a hub height of up to 140 meter [Burton, 2001]. This is shown in figure 2.5b, where the wind speed at operating height of a wind turbine with a tower of 100 m. (which is rather high) and the Powerplane are compared. With a wind speed of 7 m/s the speed at operating height for the wind turbine is 11.1 m/s while the Powerplane operates with a wind speed of 14 m/s. Moreover, equation 2.8 shows there is a cubic relation between the potential wind power production and the wind speed [Burton, 2001], hence a 25 % increase of wind speed means a 95 % increase of potential power.

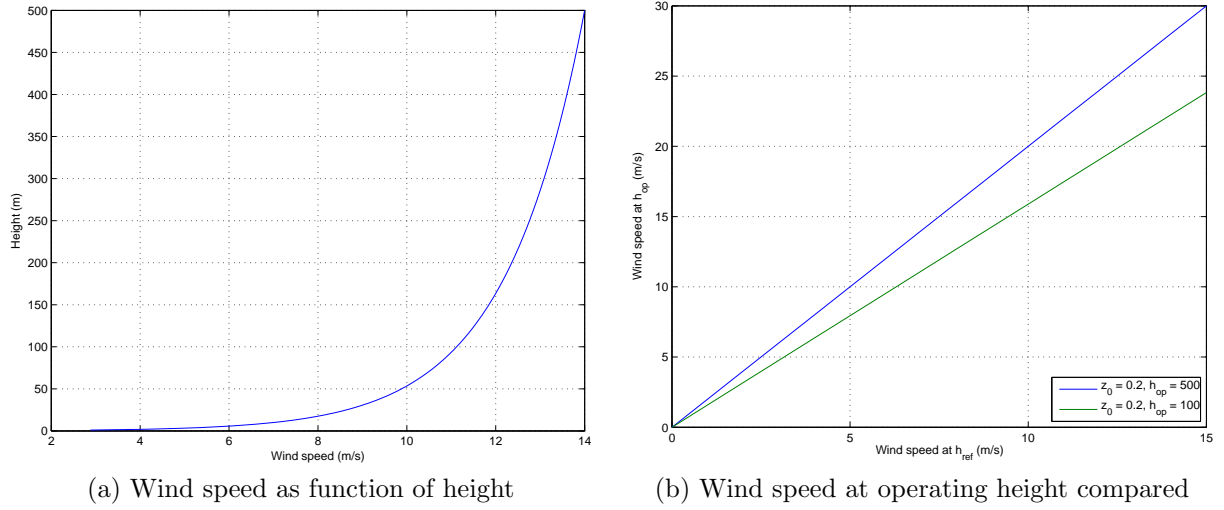


Figure 2.5: Advantage of wind shear effect to Powerplane

2.3.2 Capacity factor

Similar to conventional wind turbines, the maximum power production is limited to the installed capacity of the generator. But the annual energy output is also defined by the amount of time the system operates at this maximum. This is defined by the capacity factor (CF) which is a function of the actual amount of energy produced over time (E_{act}) and the amount of energy that would have been produced if the system operated at maximum output 100% of the time (E_{max}).

$$CF = \frac{E_{act}}{E_{max}} \quad (2.17)$$

Imagine a Powerplane generating 1 MW at a wind speed at operational height of 14 m/s compared to a wind turbine operating at 100 meters. The yearly amount of time that the wind speed is above 14 m/s value is much less than at an altitude of 500 m. For this reason the capacity factor of the Powerplane is estimated to be about 65 % compared to an average of 25 to 30% for conventional wind turbine [DWIA, 2003]. This makes a 1 MW Powerplane comparable to a 2 MW wind turbine. An important remark to make is the fact that the installed generator capacity is to be optimized. At higher wind speeds, more energy generation could take place without increasing the forces on the Powerplane and the ground station itself, but only by increasing the reel out speed (V_L). The most cost efficient generator capacity in this case is still to be optimized.

2.3.3 Material use

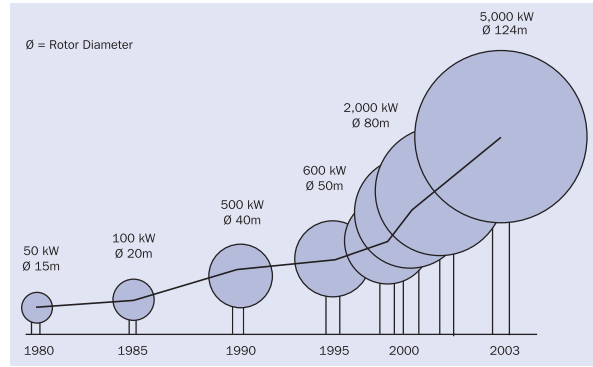
The DeWind D8.2 (figure 2.6a), a typical 2 MW wind turbine has a radius (R) of 40 m. and an average blade chord length (c_{av}) of approximately 2.5 m.[DeWind, 2010]. This resembles the radius at this rated power as shown in figure 2.6b. The total blade area (A_{blade}) can be defined as

$$A_{blade} = Bc_{av}R \quad (2.18)$$

Resulting in A_{blade} for this 3 bladed (B) turbine of about $300 m^2$. The turbine has its nominal power of 2 MW at a wind speed of 13.5 m/s at a hub height of 80 to 100 m. The maximum theoretical power for a Powerplane as shown in figure 2.3 at this wind speed is above 10 MW. The total laminate weight of every blade is 6.1 tonnes, resulting in a total blade weight of more than 18 tonnes. Compared to the 3.5 tonnes of weight for a complete Powerplane, a great material reduction can be achieved on the blades only, not to mention the reduction on the steel tower. A 60 meter tower, suitable for a 2 MW wind turbine already weighs 80 metric tonnes [DWIA, 2003]. With increasing size of wind turbines (2.6b) even larger Powerplanes will effect in a significant material reduction.



(a) DeWind D8.2



(b) Growth in Size of Commercial Wind Turbine Designs [EWEA, 2009]

Figure 2.6: Conventional wind turbines and the Powerplane compared

The advantages on material use also reflect in the installation costs. The bigger a wind turbine becomes, the higher transportation and installation costs become.

2.4 Competitors

As the advantages of crosswind power compared to conventional wind energy generation are clear, more companies and research institutes have put their effort into developing systems which make use of this principle. Three of them are described in the following paragraphs.

2.4.1 Joby energy and Makani Power

Both Joby energy and Makani Power have focused their attention on power generation using a rigid wing with propellers (figure 2.7). While the rigid wing flies crosswind patterns, increasing its velocity above the wind speed, energy is generated by the propellers which rotate as a result of this high velocity. Electricity is generated at high altitudes by generators connected to these propellers. Long electricity lines are used to transport this electric energy to the ground [JobyEnergy, 2010, MakaniPower, 2010]. An advantage of this system is that the problem of launching and landing is solved by using the propellers the other way around. The wing flies itself to operational altitude or down to the ground base by using its propellers. Energy to power these propellers comes from the electricity grid and is transported through the electricity lines. In case of the Powerplane system, electricity generation takes place on land, eliminating the need of long electricity lines and keeping heavy and expensive equipment at ground level. This enables cheaper and faster technology development.

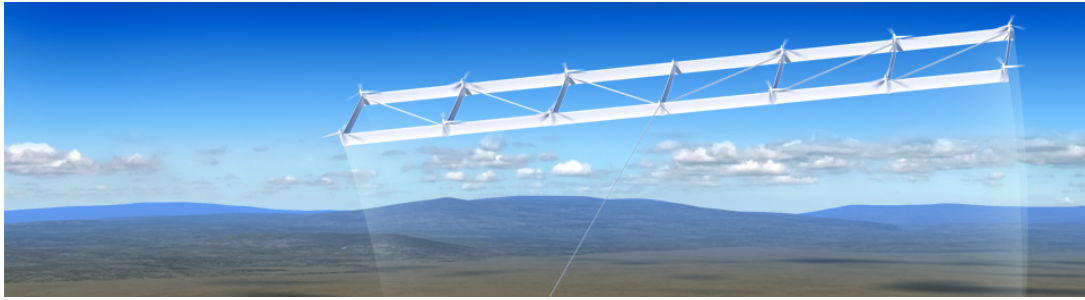


Figure 2.7: Artist impression of airborne energy generation by Joby Energy [JobyEnergy, 2010]

2.4.2 Pumping laddermil

Delft University of technology is developing the Pumping Laddermill (figure 2.8). This system consists of a long array of kites, attached to a main tether. For a 100 MW Pumping Laddermill, for example, some 50 kites are distributed evenly in the top 5 km of the tether [Lansdorp and Ockels, 2005]. The kites will fly patterns to make use of the crosswind power to pull out the main tether under a high tension. When the tether is fully unwound the kites are controlled such that the tension is low and tether is retrieved again.



Figure 2.8: Artist impression of the pumping laddermill

The advantage of flying at an altitude of 5 km. compared to the 500 m. the Powerplane operates on, is the fact that wind is more consistent and wind velocity is higher at higher altitudes. Even though the density of air decreases with altitude, the cubic relation between power and velocity results in a higher potential energy gain. But operating at this altitude also demands a much longer tether, which increases tether drag and weight, thus decreasing the energy gain. Not to mention that making use of airspace at these altitudes require changes in regulations as it can conflict with air traffic and military conventions. For Ampyx Power the optimum between cable drag and weight and energy gain is calculated to be at an altitude of 500 m., this also facilitates the installation of wind parks from a regulatory point of view, as much less airspace is involved. Besides that, the use of rigid aircraft instead of kites enables the use of proven technology, not only for building the system, but also for controlling it. This way the Powerplane

can be developed cheaper and faster.

2.5 Parameters aircraft

The aircraft for the Powerplane system will be a lightweight, unmanned glider type aircraft. Ampyx Power currently tests with its second 10 kW test prototype. The optimum aircraft parameters for the 1 MW version are modeled and presented in [Ruiterkamp, 2009], these will be used as a baseline and are described in the following paragraphs.

2.5.1 Development of 10 kW and 100 kW aircraft

The main wing of the first aircraft (figure 2.9 left) consists of rigid polyurethane foam, reinforced with a carbon fiber spar. To decrease the labour intensity and weight and improve the flight performance, the current aircraft (figure 2.9, right) is made out of glass- and carbon fibre reinforced epoxy, which is moulded by means of hand layup. This method facilitates the production of more similar aircraft, so the loss of an aircraft because of a crash during a test does not result in big delays in the research. Development

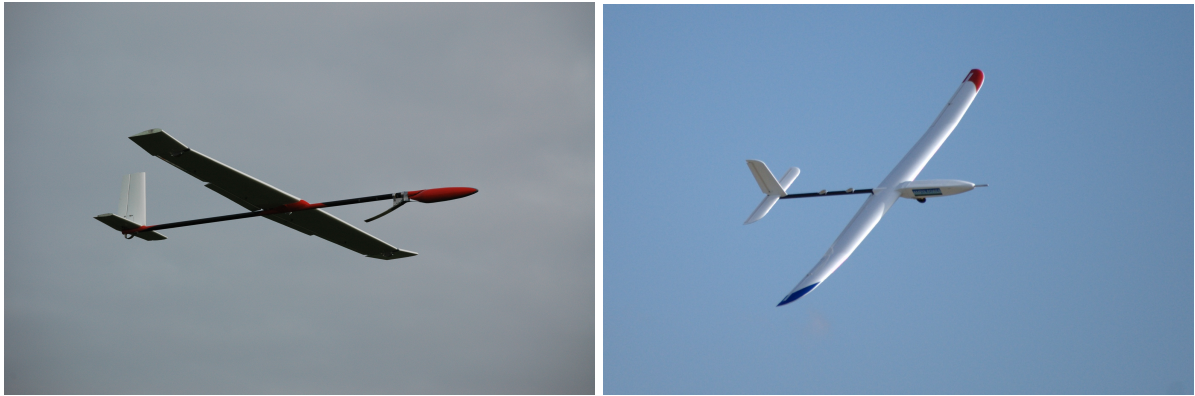


Figure 2.9: First (l) and current (r) 10 kW test aircraft during a test flight

of the 1 MW system takes place with an intermediate step of a 100 kW system. A conceptual sketch of this aircraft is shown in figure 2.10. The 1 MW system will most probably have a similar shape.

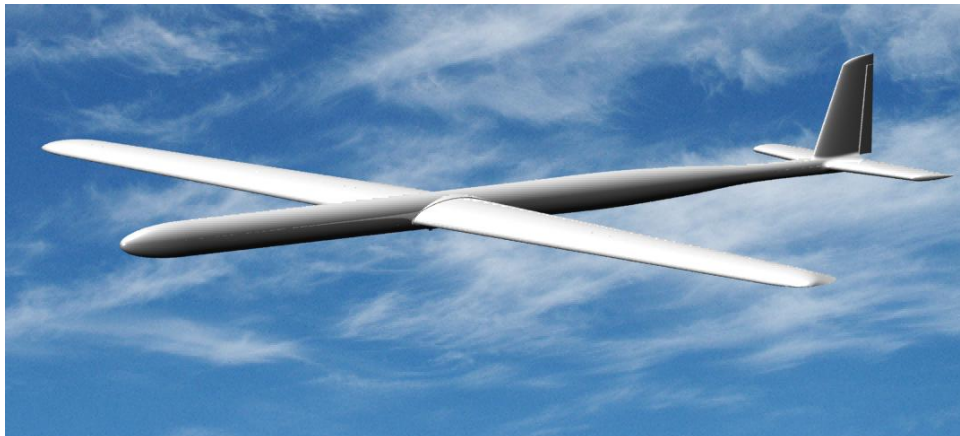


Figure 2.10: Conceptual sketch of 100 kW aircraft [Klok, 2010]

The main dimensions of these aircraft are shown in table 2.1. These dimensions are the current optimum aircraft dimensions to generate the specified amount of power, during computer simulations. The weight is expected to increase linear with power rating, nevertheless the 1 MW aircraft is projected

to have a weight of 3500 kg to have a safety factor, in case the weight finally becomes higher than expected. In addition to these numbers, the 1 MW aircraft is estimated to have a main wing with a tip

Table 2.1: Main dimensions of Powerplanes

	10 kW	100 kW	1000 kW
Length (m)	4	8	30
Wingspan (m)	5.5	13.8	36
Wing surface (m^2)	3	19	130
Weight (kg)	25	250	3500

chord (C_t) of 2.9 m. and a root chord (C_r) of 4.3 m.

2.5.2 Lift and Drag

The linear part of the lift curve (C_L) and the drag curve (C_D) of the aircraft are based on the following equations

$$C_L = C_{L_0} + C_{L_\alpha} \alpha = C_{L_\alpha} (\alpha - \alpha_0) \quad (2.19)$$

$$C_D = C_{D_0} + K C_L^2 \quad (2.20)$$

With $C_{L_0} = 0.4$, $C_{L_\alpha} = 0.105$, $C_{D_0} = 0.01$, $K = 0.0354$ from [Ruiterkamp, 2009] this results in the C_L and C_D curve as shown in figure 2.11. α_0 is found where no lift is generated (C_L is 0) which is at -3.8° . The maximum C_L is the point where stall occurs and the linear relation with α disappears. This happens at a $C_{L_{max}}$ of 1.3.

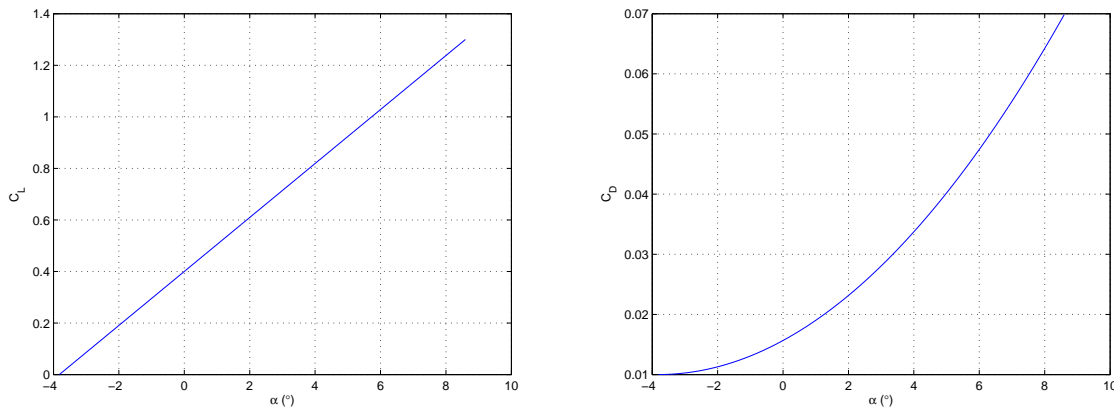


Figure 2.11: C_L (only linear part) and C_D versus angle of attack of 10MW aircraft

The graph on the right in figure 2.12 shows how the lift to drag ratio varies with the angle of attack (α). At $C_{L_{max}}$ this ratio is 18.6. The aircraft produces the largest amount of lift with the least drag (maximum C_L/C_D) at an angle calculated by

$$\alpha = \frac{\sqrt{C_{D_0} K} - C_{L_0} K}{C_{L_\alpha} K} \quad (2.21)$$

Resulting in a maximum C_L/C_D of 26.6 at an α of 1.3° . In figure 2.12 this point is presented as the top of the L/D graph.

2.5.3 Load factor

In case of conventional aircraft, a structural design is based on the load factor (n), which is a function of lift (L) and weight (W).

$$n = \frac{L}{W} \quad (2.22)$$

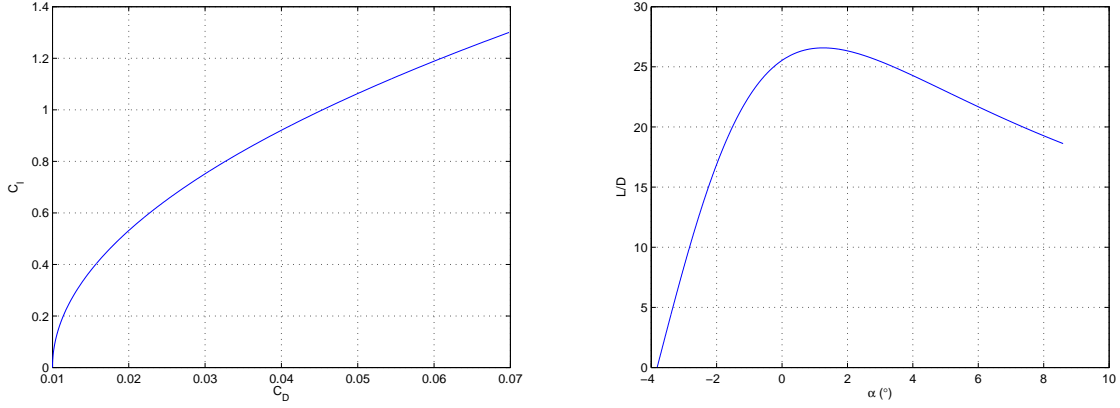


Figure 2.12: The lift drag polar (l) and the glide ratio versus α (r) of the 10MW aircraft

Normally L considers the total lift of not only the main wing, but also the aircraft fuselage and the tail wing. The fuselage and the tail wing of the 1 MW aircraft are not expected to influence the total lift of the aircraft significantly. Therefore the lift is calculated by

$$L = \frac{1}{2} \rho C_{L_{max}} S V_{max}^2 \quad (2.23)$$

And the weight is

$$W = \frac{m}{g} \quad (2.24)$$

The 1 MW aircraft will be designed to operate at a maximum velocity (V_{max}) of 60 m/s. With a maximum lift coefficient ($C_{L_{max}}$) of 1.3, a surface area (S) of 130 m² and a ρ of 1.18 this results in a maximum L of 360 kN and a load factor of 10.5. Compared to manned air planes, this number seems rather high, though a remark to be made is that this aircraft will be unmanned. Hence no human being has to experience the forces acting under these circumstances. Besides that, the lift generated while flying at this velocity is not generated for flying itself, but merely for creating tension in the tether.

2.6 Conclusion

After outlining the main principle of crosswind power, the Powerplane system is described in this chapter. The advantages compared to conventional wind energy systems and other airborne wind energy initiatives are explained. Together with the main aircraft parameters of the Powerplane system this provides a framework on which the design requirements in the following chapter are based.

Chapter 3

Design requirements

The basis of the design project lies in determining which necessary requirements the design must satisfy. The following paragraphs describe these requirements and how they are defined. A large part of the main project still remains in a conceptual phase. This makes the definition of certain parameters rather difficult. Therefore the requirements are determined in different ways such as:

- Determined by specifications given by Ampyx Power, there is already broad tacit knowledge built up in the company because of years of experience.
- Determined by computer modeling. During the project, another researcher builds a model with Matlab-simulink, which simulates the use of a rotational platform to launch an aircraft. Especially in case the final concept will be a rotational platform, certain parameters will be based on this model.

The requirements are divided into three different sections, first of all the requirements related to the aircraft are described, followed by the operational requirements and the system requirements. In a subsequent phase of the research various concepts will be compared in a trade of chart with different weight factors. These factors are related to the importance of each requirement in terms of the full system and will also be defined in the following sections. The chapter will conclude with a short overview.

3.1 Aircraft related requirements

The main function is mainly related with an aircraft remaining in conceptional phase during the whole project, therefore some characteristics may be changed to facilitate the launching and landing procedure. As long as these changes do not influence the capabilities of the system to produce power. Besides that, developments and findings in the research and tests of the 10 and 100 kW systems, the computer models and other researchers can result in changes of the aircraft. The optimum aircraft parameters as it currently has been modeled and presented in [Ruiterkamp, 2009] and described in 2.5 will be used as a baseline. No fundamental changes to these specifications are expected to take place. The aircraft for the 1 MW system will be a lightweight, unmanned glider type aircraft. Ampyx Power is currently testing with its second 1 kW system.

3.1.1 Main dimensions aircraft

The land and launch system must be capable of operating with an aircraft with main dimensions as described in paragraph 2.5. The wing span of the aircraft will be 36 meters, with a chord of 4.34 m at the root and 2.90 m at the tip of the main wing, the surface will be approximately 130 m^2 . The length of the aircraft from nose to tail will be 30 m. The total weight is estimated to be 3500 kg. Even though some minor changes on the aircraft can take place, the overall size of the aircraft is of such an importance for its performance that a weight factor of 5 is given for this requirement

3.1.2 Minimum velocity

The stall velocity (V_{stall}) is the minimum velocity the aircraft can have in straight and level flight. At this velocity the generated lift is just enough to support the weight of the aircraft while the angle of attack is such that the lift coefficient is maximum ($C_{L_{max}}$) [Torenbeek, 1982].

The generated lift under these circumstances can be calculated by

$$L = \frac{1}{2} \rho V^2 S C_{L_{max}} \quad (3.1)$$

Where weight is a function of the aircraft mass and the gravity and must be equal to L

$$W = mg = L \quad (3.2)$$

Combining these equations and rearranging to V gives

$$V_{stall} = \sqrt{\frac{2mg}{\rho S C_{L_{max}}}} \quad (3.3)$$

With the parameters from the former paragraph, a V_{stall} of 18.4 m/s is obtained at an air density of 1.2 kg/m³.

Flying at maximum angle of attack is not the most desirable flight condition as the aircraft is in a state where stall is just about to occur. To have some freedom to manoeuvre and in order to avoid stalling due to wind gusts, a safety margin of 20 % will be taken into account [Ruijgrok, 2007].

$$V_{min} = 1.2 V_{stall} \quad (3.4)$$

Resulting in a minimum velocity V_{min} of 22 m/s. Since flying below this velocity is not really considered as an option, it receives a weight factor of 5.

3.1.3 Maximum velocity

The maximum velocity the aircraft will be designed for is based on the maximum velocity which will be reached during operation plus the effect of wind gusts. This is estimated to be 60 m/s. Operating above this velocity results in larger forces on the aircraft. Especially the effect of an increased lift, combined with increasing cable drag, which both occur on higher velocities, result in larger overall forces on the aircraft structure. Gusts increase the peak loads in this case. These considerations result in a weight factor of 5.

3.1.4 Maximum acceleration

The sensitive measurement equipment inside the aircraft can cope with a maximum acceleration of 10g. But since the tether will most probably be attached to the hull of the aircraft, accelerating from this location will result in a momentum on the wing attachments. For these reasons the maximum acceleration of the aircraft is set to be 5g or $\pm 50 \text{ m/s}^2$ with a weight factor of 5.

3.1.5 Additional thrust

The aircraft will be equipped with a propeller and a generator to produce electricity for the on-board equipment during operation. Some of this energy will also be stored in batteries as a buffer. Therefore the propeller could also be used to give additional thrust of about 0.5 to 1.5 kW.

3.1.6 Landing controllability

Figure 3.1 illustrates the range of touchdown of the aircraft, when it lands on an airfield on the given weather conditions, compared to a reference point. It shows that the aircraft is controllable in such a way that the point of touchdown will be within a range of 20 meter lengthwise and 5 meters in width. The landing system should be able to adapt itself to this range to facilitate a safe landing. This requirement is of such an importance that it has a weight factor of 5. But this requirement only counts for cases in which this type of landing is used. As the cable will be attached to the aircraft, a smaller range can be achieved by using the cable for aircraft orientation.

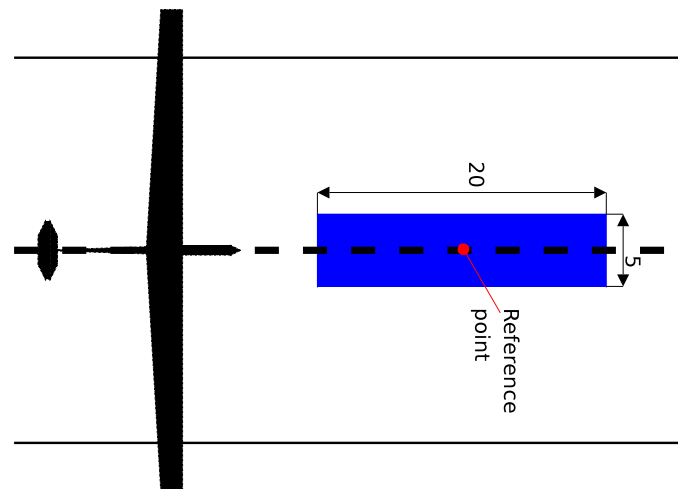


Figure 3.1: Range of touchdown of the 1 MW Powerplane

3.1.7 Additional weight on aircraft

Modifications on the aircraft to make the landing / launching system work, such as attachment points or even additional thrust should be as light as possible, but preferable should stay below 200 kg. The low weight is especially important for the ability of the aircraft to fly at a low velocity, which could facilitate the launching and landing process. During operation, the aircraft generates such an amount of lift that the weight becomes less important. This results in a weight factor of 3.

3.2 Operational requirements

3.2.1 Minimum altitude and cable length the aircraft should be able to reach

This requirement can be based the following three statements:

- The wind velocity at this altitude is large enough to let the aircraft increase its own altitude by its generated lift.
- The aircraft is at proper altitude to fly its energy generating patterns. This altitude is estimated to be 500m.
- The unwound cable length is large enough to be able to winch up the aircraft, this is described in appendix B The cable length for this operation is set to 400 m. at a favourable angle of 30° which leads to an altitude of 200 m, although an altitude of 125 m could be possible.

Launching must be possible at different weather conditions (paragraph 3.2.2). Since the wind is an uncontrollable parameter, the first option is not always feasible. In any case, winching is possible with the installed equipment for energy generation. Therefore either option two or three can be considered as a main requirement for the system. A weight factor of 5 is given, since this is the main requirement for the system.

3.2.2 Operating conditions

Since the system will be used outside in the open field, it should withstand weather conditions like rain, hail and lightning. The wind velocity at ground level, is an important factor influencing the possibility to land and launch. The mechanism has to be designed to land the aircraft with a wind velocity between 0 and 28 m/s. Launching should be possible at wind velocities of 0 to 14 m/s. Wind velocities above 10 m/s at ground level especially inland are not occurring very frequently and therefore the ability to launch above this velocity would in most cases not influence the capacity factor thus the yearly gain of the Powerplane too much [Canada, 2010]. Also very high wind speeds can be forecast quite precise, so

reaching the upper wind velocity for landing could most likely be prevented. For these reasons a weight factor of 3 is given to this requirement. The wind direction determines the orientation of the aircraft related to the ground station. The cable must be able to be oriented 360° in the horizontal plane around the ground station and in between 27° and 60° in the vertical plane. (figure 3.2)

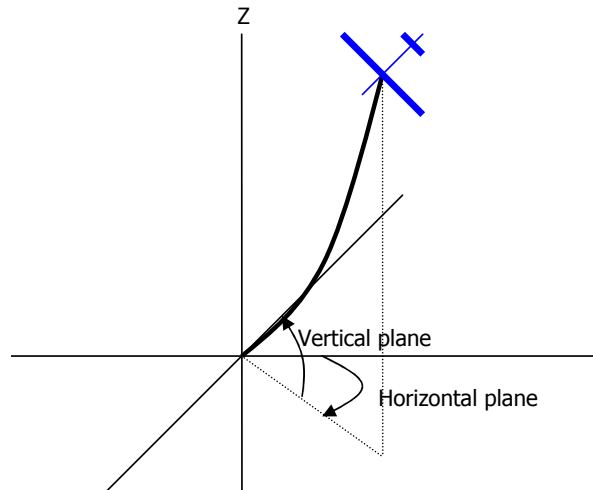


Figure 3.2: Cable angles during operation

3.2.3 Time span for launching

Whenever weather conditions are suitable to launch the aircraft, energy generation is possible. This means the time launching takes is a loss of potential energy yield. Therefore this time can be seen as a trade-off between the loss of energy yield and the cost of increasing launching velocity. In a later stadium of designing the final launching mechanism more effort can be put in this trade-off. For now the main requirement is to keep launching time as low as possible. The uncertainty of this requirement results in a low weight factor of 2.

3.2.4 Time span for landing

There are three main circumstances for landing:

1. No wind: There is not enough wind to generate energy.
2. Emergency landing: There's a failure in the system, another aircraft accidentally enters the reserved airspace or a trauma helicopter has to pass through.
3. Extreme weather conditions: Weather not suitable for the aircraft to stay airborne is forecast.
4. Maintenance: In case of regular maintenance on the aircraft or ground station the aircraft generally must be landed.

For testing purposes circumstance 1 and 3 are most significant, since system failures are common at this stage of the process. In case of the final system especially circumstance 2 is important. Rapid adaptation to weather conditions could result in a larger range of operation and therefore larger energy yield. Trade-off between costs to decrease landing time and energy yield is something that could be done for the final system, although as described before, the maximum weather conditions mostly do not occur that frequently. Since airborne wind energy and unmanned aircraft still have to prove their reliability to the general public, safety issues are important for accepting this technology. Therefore the possibility for an emergency landing is important. For now the maximum time it may take to get from energy generation to rest will be set to 2 minutes with a weight factor of 4.

3.2.5 Forces on aircraft

At the locations where the aircraft will be attached to the launching mechanism the resultant forces during operation at these attachments should not damage the aircraft. These forces strongly depend on the way the aircraft will be launched and the shape of the connection unit. Therefore this requirement will be specified later according to the chosen launching mechanism. For now preferably the forces are such that the aircraft needs least modifications. This requirement has a weight factor of 3.

3.2.6 Forces on landing / launching mechanism

The mechanism should be strong enough to withstand the forces it will be subject to during operation. Forces during landing and launching strongly depend on the chosen mechanism and will be specified later. As soon as the aircraft flies its energy generating patterns, it will pull the cable with a force of 400 kN. This value is based on the optimum ratio between cable tension (T) and cable velocity (V_L) to generate approximately 1 MW [Ruiterkamp, 2009]. This force will be in any horizontal direction with an angle with the horizontal plane between 27° and 60°.

3.2.7 Forces during extreme conditions

Extreme conditions like sudden large wind gusts, an error in the autopilot or an emergency stop could result in very large forces on the mechanism. Especially in the test phase, these conditions are likely to happen. How large these forces could become is dependent on the chosen concept, so this will be specified later. The maximum force the cable can withstand is 1314 kN, so this can be seen as an upper limit without a safety factor. The ability to withstand this force is very important and therefore has a weight factor of 5.

3.3 Peripheral requirements

3.3.1 Prepared for park set-up

The goal of Ampyx is to design 1 MW generators for use in wind parks of about 50 MW. For safety reasons the distance between separate generators must be approximately 600m. Separate systems should not hinder each others performance. Costs for ground use at expected location (deserted Canadian areas) are only €150 per hectare per year, but a smaller area use, results in a higher the energy density. This influences how the Powerplane competes with other systems. Therefore the weight factor for this requirement is set to 4.

3.3.2 Autonomous operation

The set-up has to work fully autonomously, while manual override must be possible for maintenance. Autonomous operation is indispensable, since this is the only option to make this technique a cost efficient means of energy generation, consequently a weight factor of 5 is given to this requirement.

3.3.3 Safety

Large forces and high velocities could lead to dangerous situations. According to the chosen concept features such as an emergency break, overload protection or covering certain moving parts should be applied to avoid damage or injuries. But, if possible, preventing the need of such systems could be a more workable option. The amount and type of different systems within the chosen concept can also increase the possibility of failure and unsafe situations. As described before, safety is also an important issue due to general acceptance of the technology, hence a weight factor of 5 is given.

3.3.4 Lifetime

The goal of Ampyx Power is to provide a total system with a lifetime of 20 years. Although certain parts like the cable probably will need replacement during this period, it is desirable to have a system

which operates with least modifications as possible. A reason for this system lifetime is to have a strong position amongst established competitors in the green energy field, such as wind turbines and solar PV. These systems have a comparable lifetime [DWIA, 2003].

3.3.5 Cost-efficient

A wind turbine of 2 MW costs about 2.5 Million Euro [EWEA, 2009], the goal of Ampyx Power is to have a cost effective solution which will be an adequate competitor in the energy market. Therefore costs have to be less than 1/3 of a comparable turbine. For each 1 MW generator, the initial costs for the landing/launching mechanism may be €85.000 for commercial series production. Operational costs should be as low as possible. A weight factor of 5 is given to this requirement since a strong competition with even fossil fuels must be obtained.

3.3.6 Reliability

Even though reliability is a tricky issue, since this term can be explained in different ways. The downtime of the system has been defined to be at the highest 15% for the first years, going down to 10% in the following years. To stay below this value its desirable to keep the amount of moving and controlled parts as low as possible and to make use of proven technologies as much as possible.

3.3.7 Cable wear

The cable must be handled in such a way that cable wear will be minimized. This means that the path of the cable from the drum to the aircraft requires minimal obstacles or deflections. Contact between the cable and any surface should be minimized. Whenever cable guides are used, these should be suitable for the utilized cable. The Dyneema cable will have a diameter of 40 mm, further specifications can be found in appendix C. Preferably the cable must stay attached to the aircraft during any operation. Cable wear is one of the main operational costs, which should be as low as possible. Replacing the cable also results in downtime thus a lower overall energy yield of the system. Consequently it is a factor 5 requirement.

3.4 Summary

Table 3.1 shows a summary of the requirements listed in this chapter. The list provides the basis of research towards the baseline design of the system. In the following chapter the main function is divided into different functions and possible solutions are given. Every design option can be analysed by comparing it with the requirements described in this list.

Table 3.1: Short-list of requirements

		Factor
Aircraft related requirements		
Main parameters aircraft	Surface (S): 130 m ² Wing span: 36 m Maximum lift coefficient ($C_{L_{max}}$): 1.3 Maximum L/D: 26.6 Mass (m): 3500 kg Propeller power: 0.5 – 1.5 kW Height of operation (h_{op}): 500 m	5
Minimum velocity	V_{stall} : 18.4 m/s V_{min} : 22 m/s	5
Maximum velocity	V_{max} : 60 m/s	5
Maximum acceleration	a_{max} : 50m/s ²	5
Touchdown range	< 5 m in width, < 20 m lengthwise	5
Additional weight of system on aircraft	< 200 kg	3
Operational boundaries		
Minimum altitude/ cable length	h_{min} : 125 – 200 m, l_{min} : 400m	5
Operating conditions	Wind velocity during launching: 0 – 14 m/s Wind velocity during landing: 0 – 28 m/s Cable orientation horizontal plane: 360° Cable orientation vertical plane: 27° – 60°	3
Time span for launching	Least as possible	2
Time span for landing	< 2 minutes	4
Forces on aircraft	Cable tension during normal operation (T_{op}): 400 kN	3
Extreme forces	Maximum cable tension (T_{max}): 1314kN	5
Peripheral requirements		
Prepared for park set-up	Operating area: 600 x 600 m Costs for field rent: €150 per 10000 m ² /year	4
Autonomous operation		5
Safe operation		5
Lifetime	20 years	4
Initial cost	<€ 85.000	5
Operational cost	Least as possible	5
Reliability	85 – 90 % uptime	5
Cable wear	Least as possible	5

Chapter 4

Design option analysis

Now the aims and objective of the research are defined and the most important design requirements are known, it is time to find solutions. A nice and motivating way to kick-off such a phase is by a brainstorm session. This chapter starts with the results of such a session. To find more design options and unravel all options into different problems to be solved, functional analysis diagrams are made. Main questions rising from these diagrams are explained by calculations, literature research and field tests. The results of this chapter will be used for defining and comparing the concepts in chapter 5.

4.1 Basic design option tree

To gather many different ideas regarding the main function *Launch and retrieve a tethered aircraft*, a brainstorm session was held. The session was divided into two parts: Launch and retrieve. Figure 4.1 shows a design option tree which can be considered as a summary of the brainstorm session. To clarify the keywords in the tree, artist impressions of every option are shown in appendix D.

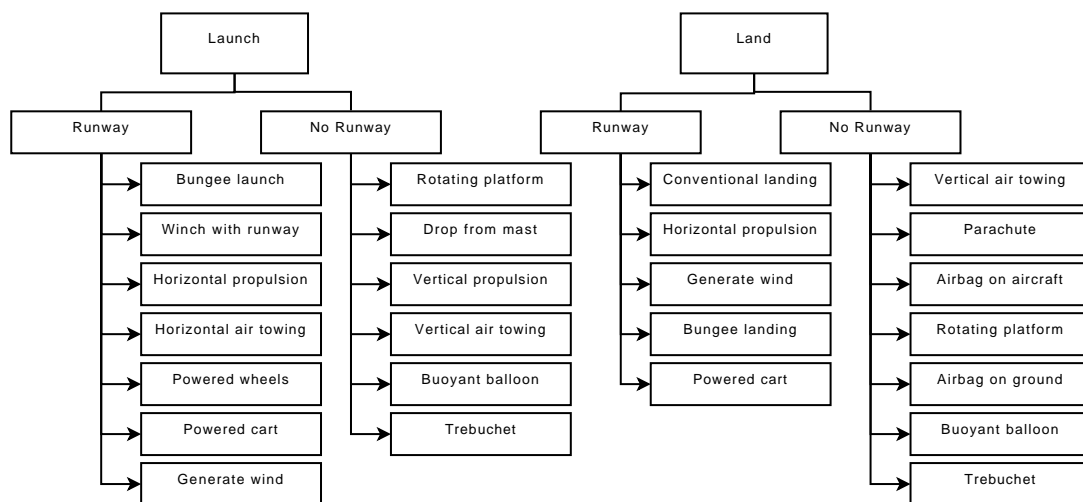


Figure 4.1: Basic design option tree for launching and landing

Even though the tree covers many solutions, a deeper analysis is made in the following paragraphs by making use of functional analysis diagrams.

4.2 Functional analysis diagrams

The brain storm session reveals that many options are available. On the other hand it approaches the design problem in such a way that the scope is narrowed because only complete solutions to, for

example, launching are given. Using a functional analysis diagram cuts the main function into parts of other functions which all have their own solutions attached. This approach increases the amount of possible options and provides an organized overview of design problems and their solutions. In the diagram, blocks of functions are presented as figure 4.2a and the different options to carry out these functions (figure 4.2b) are attached with arrows. In case a solution comes with a new function, a new function block is created with its solutions and so on.

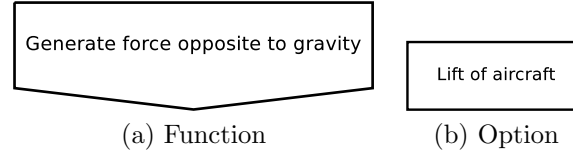


Figure 4.2: Building blocks of Functional Analysis diagram

For intelligibility, the main function is divided into three phases:

- Take off: This phase can be described by the part from where the aircraft stands still on the ground station until it leaves the ground.
- Climb: The aircraft flies from just above ground level to its required height and/ or distance.
- Land: Returning from operational height and distance to standstill on the ground station.

For every phase a different diagram is built, which can be found in appendix E. The fact that the diagrams are pushed all the way to the back in the appendix, does not mean that they are not important, it is just because all diagrams are too large to show in between the text of this chapter. The diagrams form the backbone of the solutions investigated in this chapter and the definition of the concepts. During creation of the functional analysis diagrams, some solutions came out being impossible to adopt within the requirements. These options are not further researched. Options that need more research or calculations to find out how they would meet the requirements are highlighted yellow in the diagrams. The rest of this chapter describes the research on these options. A remark to make is the fact that most effort is put in 'take off' and 'climbing'. For most solutions, landing appears to be less of an issue. In many cases it is just the reverse of launching, where almost no energy has to be put in the system, since it is available as potential or kinetic energy in the aircraft.

4.3 High velocity lift-off

A way to accelerate the aircraft to a high velocity is by using a linear induction motor (LIM). A system based on this technique is currently being developed to serve as a new launching mechanism to replace the steam catapult system in aircraft carriers. Figure 4.3 is a schematic image of this system, known as EMALS (Electro Magnetic Aircraft Launch System) [GeneralAtomics, 2010, Doyle et al., 1995].

The system consists of a linear induction motor with a moveable armature to connect to the aircraft. A power conversion module which generates the proper pulse to power and accelerate the induction motor and an energy storage system, based on a flywheel, to provide a large amount of energy over a very short time-scale. The developed system is expected to meet the requirements, specified in the table below.

Table 4.1: EMALS requirements

End velocity	28-103 m/s
Max Peak-to-Mean Tow Force Ratio	1.05
Launch Energy	122 MJ
Cycle Time	45 seconds
Weight	< 225,000 kg
Volume	< 425 m ³
End velocity Variation	-0 to +1.5 m/s

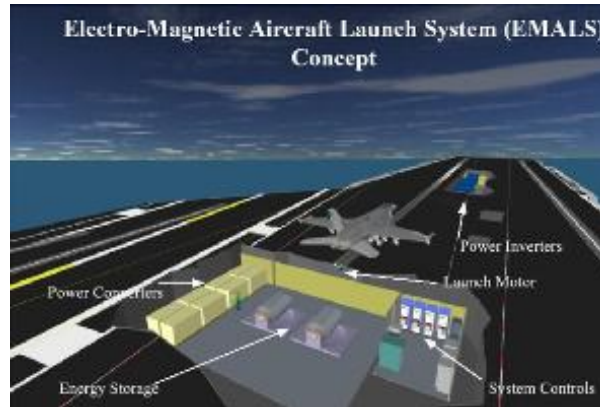


Figure 4.3: Schematic image of EMALS

Although a system designed to launch fighter jets from carriers is much larger than a system launching a 3500 kg glider type aircraft. EMALS is an example of what a launching mechanism for a high velocity launch can consist of.

4.3.1 Launch velocity

When no additional power is available for the climb phase, all energy to reach the end height must be 'in' the aircraft as kinetic energy. During climb this energy is converted into potential energy until the aircraft reaches operation height at a velocity just above the stall velocity, the specific energy at this situation is denoted as the energy height (H_e). Figure 4.4 gives a graphic representation of the two energy states.

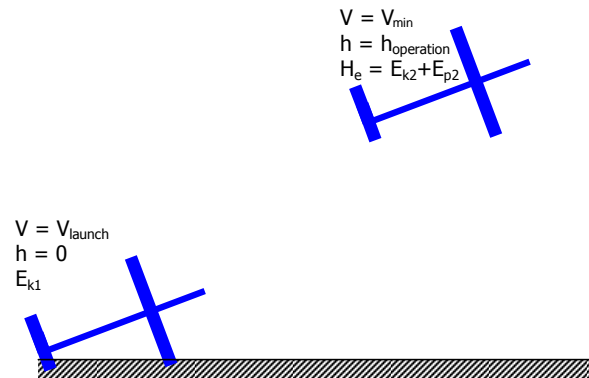


Figure 4.4: Two energy states of high velocity lift-off

The direction of the initial velocity is neglected in the calculations. The necessary final velocity is assumed to be equal to the minimum velocity (V_{min}) of the aircraft. The cable drag and aircraft drag can be significant, especially at a higher velocities. But for a first calculation these forces are neglected. When this approach gives a very promising result, more effort can be put in a more realistic model, where direction and drag are taken into account. Alternatively, when results are poor, no time has to be put further analysis.

The kinetic energy as function of the velocity is:

$$E_k = \frac{1}{2}mV^2 \quad (4.1)$$

The potential energy is:

$$E_p = mgh \quad (4.2)$$

The energy height (H_e) in case the aircraft flies in horizontal direction at a constant height can be calculated by

$$H_e = mgh_{op} + \frac{1}{2}mV_{min}^2 \quad (4.3)$$

Balancing the kinetic energy at the start with the energy height gives

$$\frac{1}{2}mV_{launch}^2 = mgh_{op} + \frac{1}{2}mV_{min}^2 \quad (4.4)$$

m cancels out, leaving

$$\frac{1}{2}V_{launch}^2 = gh_{op} + \frac{1}{2}V_{min}^2 \quad (4.5)$$

Rearranging to the launching velocity (V_{launch}) gives

$$V_{launch} = \sqrt{2gh_{op} + V_{min}^2} \quad (4.6)$$

This function is plotted in figure 4.5 for an operation height of 0 to 500 meter.

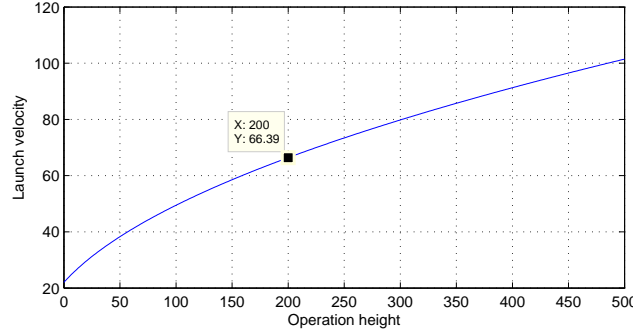


Figure 4.5: Required start velocity as function of reachable operation height, drag is neglected

The figure shows that for an operation height (h_{op}) of 200 m. a constant gravity g of 9.81 m/s^2 and a V_{min} of 22 m/s, the initial velocity turns out to be 66 m/s. This is already well above the maximum velocity of 60 m/s, while aircraft and cable drag have not been taken into account yet.

4.3.2 Launch distance

The distance it takes to reach this velocity if the aircraft is accelerated with the maximum allowable acceleration (a_{max}) of 50 m/s^2 can be calculated by

$$s = \frac{v_{launch}^2}{2a_{max}} \quad (4.7)$$

In this case, to reach a velocity of 66 m/s, an airstrip of at least 44 m. must be available.

4.3.3 Power

Even though mass cancels out in the equations of motion, it is an important factor in the necessary work the launching mechanism has to provide to the aircraft. The mass of the aircraft is 3500kg. Using equation 4.3 for a h_{op} of 200 m gives a required work of 6.9 MJ. The unit for Power is W or J/s, so to derive the necessary power, first the time span of launching has to be derived.

$$\Delta t = \frac{v_{launch}}{a_{max}} \quad (4.8)$$

This results in a time span of 1.3 seconds which means that the necessary power of the launching device is in this case is just above 5 MW. Special measures should be taken to be able to store and

instantaneously deliver this amount of energy, since the electricity connection at the site will most probably be similar to the rated power of the Powerplane, which is 1 MW. Besides the cost of these special measures, the cost of a machine, for example a Linear Induction Motor (LIM), delivering this amount of power will most probably cross the maximum initial cost of 85 k€. For example, the cost of a 6 MW train locomotive, using this technique is estimated to be 3 million \$ [Turman et al., 1995]

4.3.4 Conclusion

A high velocity lift-off system as analysed in this section is not feasible when looking at the aircraft requirements and the cost of such a system.

4.4 Using buoyancy

A balloon filled with a gas lighter than air can be used to pull the aircraft up to a height where the aircraft can be dropped to fly itself down to the operational height. For this purpose a kind of weather balloon could be used as shown in figure 4.6. The dimensions of this balloon can be estimated by the following calculations.



Figure 4.6: Weather balloon

$$F_b = V_{\text{balloon}} g (\rho_{\text{air}} - \rho_{\text{gas}}) \quad (4.9)$$

Where the buoyancy force (F_b) has to compensate the gravity force on the balloon itself, the cables of the aircraft and the balloon, and the aircraft.

$$F_g = \Sigma m g = F_b \quad (4.10)$$

The total weight (Σm) of all the parts described above is estimated to be 4500 kg. The volume of the balloon then becomes

$$V_{\text{balloon}} = \frac{\Sigma m}{\rho_{\text{air}} - \rho_{\text{gas}}} \quad (4.11)$$

Table 4.2 shows that a balloon with a radius of almost 10 m. would be large enough to contain enough lifting gas to balance the total weight. The weight difference of helium and hydrogen compared to the weight of air give a negligible size difference between both gases. In cost however, the differences are much higher, since the cost of hydrogen and helium are estimated to be approximately 10 €/kg and 80 €/kg.

Leakage will take place for both gases, because of the permeability through the skin of the balloon. This could make helium more expensive in use. Hydrogen is much cheaper to buy and it could be made

Table 4.2: Cost and volume of buoyant gas

Gas	$\rho(kg/m^3)$	$V(m^3)$	Radius (m)	Amount of gas (kg)	Estimated cost (€)
Hydrogen	0.00899	3943.87	9.80	35.45	354.47
Helium	0.01785	3974.74	9.83	70.95	5675.93

on the spot by electrolysis, since the electricity needed for this conversion will be generated on the same location. When there is a surplus in generated electricity, this can be used for hydrogen generation. This could bring the hydrogen costs down to zero, dependent on plant cost and the electricity market. The largest disadvantage is the high flammability of hydrogen. Even though the use of hydrogen is never proven to be the cause, the Hindenburg disaster still remains in the minds of the lighter than air vehicle designs [Brown, 1998]. Therefore the general trend nowadays remains in using Helium as lifting gas. For this purpose Helium will be very expensive, almost €5700 at the start, plus the losses due to permeability.

4.4.1 Maintain operating area

During operation the balloon will drift away from its operating area because of the drag force which will be induced by the wind velocity at the balloon and at the cable. It is reasonable to neglect the cable drag in this case, since the drag on the balloon is assumed to be several magnitudes larger. The total drag force F_D then becomes

$$F_D = \frac{1}{2} \rho V_w^2 C_D A \quad (4.12)$$

The shear effect makes the wind velocity (V_w) increase with height. At the balloon height (h_b), the wind velocity can be calculated by [DWIA, 2003]

$$V_w = \frac{V_{ref} \ln(h_b/z_0)}{\ln(h_{ref}/z_0)} \quad (4.13)$$

Since the operating area is limited to 600x600 meter, the drift distance should not exceed this value. An additional cable could be used to keep the balloon within its area, but this increases the risk of the aircraft hitting a cable during operation. Another option is to use a larger balloon with more lifting gas, increasing the buoyant force. The ground cable balancing this additional lift (L_D) is acting at a given angle when the balloon is at minimum operational height and at the edge of the operating area. This results in a horizontal component of the cable tension T_{hor} which balances the drag.

$$T_{hor} = F_D \quad (4.14)$$

Figure 4.7 gives a simplified impression of the forces on the balloon and how the drift distance (d) and the balloon height (h_b) are related to the drag force and the additional lift (L_D), giving

$$L_D = F_D \frac{h_b}{d} \quad (4.15)$$

This means that a larger balloon uses a part of its buoyancy (F_B) to overcome weight (L_W) and a part for the drag (L_D). Neglecting the increase in weight due to increasing balloon size this means that

$$L_D = F_B - W \quad (4.16)$$

Increasing the balloon radius not only results in a larger lift force, but also in a larger drag force. Assuming that the weight of the lifting gas can be neglected as these values are small compared to the weight of air, the radius where drag, cable tension and lift forces balance can be found by rewriting equation 4.15 and 4.16 as functions of the radius to

$$L_D = \frac{1}{2} \rho v_b^2 C_D \pi r^2 \frac{h_b}{d} = \frac{4}{3} \pi r^3 \rho_{air} g - \Sigma m g \quad (4.17)$$

When the balloon height lies 50 m above h_{min} , at 250 m, using a C_D of 0.6 for the balloon [White, 2008] and a mass of both the balloon, cables and lifting equipment Σm of 4500 kg, these functions are equal at a radius of 13 m, resulting in a volume of 9400 m³. The drag force on the balloon

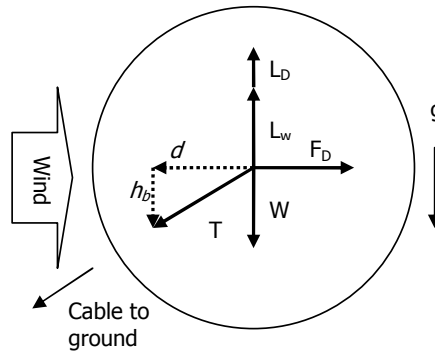


Figure 4.7: Forces on balloon

is then approximately 150 kN. This will result in a gas cost and a balloon size of more than twice as big as expected when buoyancy is only used to balance weight. Also the operational costs will increase significantly, since the gas losses increase with the size of the balloon skin.

4.4.2 Drag of a Zeppelin

Using a more aerodynamic shape, for example the cigar-like shape a Zeppelin has, would decrease the drag coefficient to C_D of only 0.1 [White, 2008]. Now the amount of lifting gas used to stay within the operating area also decreases. In this case the volume is not related to the radius such as with a spherical balloon. For a simplified analysis the shape is regarded to be a cylinder with a length of 10 radii and a diameter of 2 r. (figure 4.8, [Aerospace, 2009]). The length is taken a bit shorter than the real length, to compensate the conical shape of the nose and the tail. The weight is assumed to be 500 kg more, since the surface of this shape is much larger.



Figure 4.8: Zeppelin Aerwin

In this case the additional buoyancy force to stay within the operating area can be obtained from

$$L_D = 10\pi r^3 \rho_{air} g - \Sigma mg \quad (4.18)$$

Solving this for r provides us with a radius of 5.2 m. and a length of 52 m. This results in a drag force of only 4 kN, which is much smaller than a sphere, since both the drag coefficient and the surface are much smaller. The necessary volume is 4500 m^3 , which is only about 14% more. A Zeppelin shape therefore proves to be a much more suitable solution.

4.4.3 Retain shape

The main difference between a Zeppelin and a blimp is the way the airship keeps its shape. A Zeppelin has a rigid structure, while a blimp is completely flexible. Pressurization in this case provides the structure.

Even though the use of Zeppelins got a bad reputation due to the Hindenburg disaster, more promising developments in this category of air traffic took place the past decades [Liao and Pasternak, 2009]. Blimps on the other hand are more used as aerostat, which can be defined as an unmanned tethered balloon, designed to keep a payload at a certain altitude. One of the leading companies, designing and delivering these systems is TCOM. Their aerostats are mainly designed and used for:

- Radar Surveillance.
- Passive Electronics & Communications Surveillance
- Electro-optical/Infra-red Camera Surveillance
- Communications Relay / Networking

The largest aerostat (TCOM 71M) of 16.000 m³ can only lift a payload of 1600 kg. This does not agree with the calculations made in paragraph 4.4, where a body of 4500 m³ should be able to lift a payload of 3500 kg. The payload per volume ratio now differs almost a factor of 8. The main reason for this difference has to do with the height that has to be reached. The TCOM 71M is designed to reaching an altitude of 4600 m. with its payload. The air density at this altitude is only half as much as at lower altitudes, leading to a much smaller density difference between the lifting gas and the surrounding air. Therefore the buoyant force is much smaller, so a larger amount of lifting gas is necessary [Ruijgrok, 2007, pg.41], resulting in a larger required volume of lifting gas (equation 4.9). To cope with the volume difference between ground level and operational height special measures must be taken. Besides that a lower density also results in a lower pressure. As the shape of a aerostat is mainly defined by a slight overpressure this also should be taken care of. The aerostat solves these issues by means of an additional air envelope, which can take up and release air, as shown in figure 4.9 [TCOM, 2009]. When the Aerostat increases height, it releases air. This way the volume of the buoyant gas has the ability to increase, maintaining the relative overpressure.

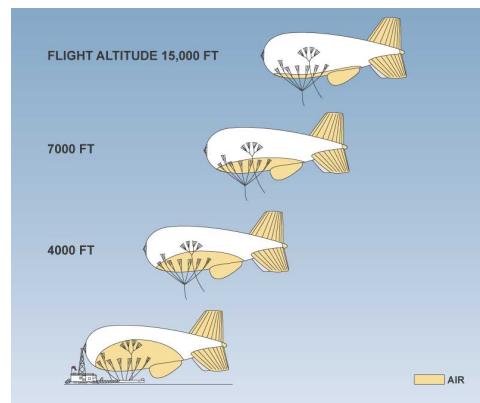


Figure 4.9: Aerostat releasing air to keep its shape at any height

The final reason for the smaller payload is the weight of the system itself. Reaching an altitude of 4600 m. compared to an altitude of 250 m. means a tether of more than 15 times longer. The tether for these aerostats not only keeps the system at its place, but also works as lightning protection, control wiring and power connection for the electric system. Therefore the cable mass will significantly reduce the payload capabilities.

The variety in air density and relative pressure at ground level and at 250 meter height is so small [Anderson, 2008] that in case of using a blimp for this purpose this effect can be neglected.

4.4.4 Cope with gas leakage

Hydrogen molecules are the smallest molecule available. So they can penetrate any skin material, leading to loss of hydrogen and buoyancy. Even though this phenomena is mentioned in many documents

regarding lighter than air vehicles, real numbers for hydrogen leakage are not very well known or documented [Fulton, 2008]. In old publications a number of 10 litres per square meter per day are mentioned for rubber like skins [ACA, 1911]. Polyurethane skin has a 3% helium loss per day. But Magenn Power inc., a company which has developed a "Floating Wind Generator" (figure 4.10) claims to have a helium leakage of only 6% per year [Magenn, 2010]. Therefore more research must be done on the decision of how to cope with gas leakage and the cost of alternatives. For example the use skin material with very low porosity could eliminate a refilling system, but the cost of a refilling system could be much lower than the cost of this material. Finding this optimum lies beyond the scope of this thesis.

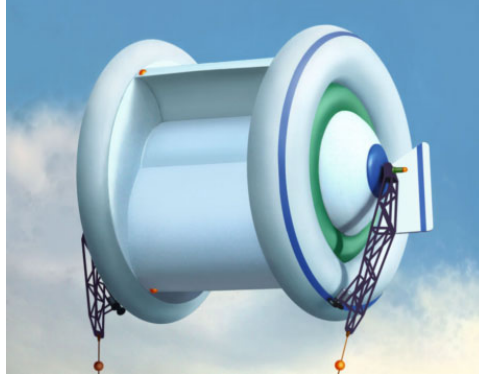


Figure 4.10: MARS 100kW floating wind generator of Magenn Power Inc.

4.4.5 Docking in the sky

When the aircraft flies in a controllable way, it has a velocity of at least 22 m/s, with a mass of 3500 kg. This means that colliding with an attachment unit in the sky would result in a big shock. Two options to decrease this shock could be:

- Fly an upward path in line with the cables until it connects to the attachment unit. Because of the flight path, the main direction of the aircraft inertia will be in line with the cables and opposite to the gravity. So kinetic energy will be slowly converted into increasing height until the aircraft stands still and can be taken down.
- The aircraft will just fly into the attachment unit. The kinetic energy will be converted into elastic deformation of the cables, a downward motion of the balloon or a combination of the two.

It is hard to say which one of the options is preferable without doing more research and having more knowledge on the rest of the system.

4.5 Climb with a propeller

After the aircraft has an initial velocity equal to its minimum velocity, it is possible to climb with the aid of a propeller. This section investigates some main characteristics about this option.

When an aircraft performs a steady, un-accelerated climbing flight as represented in figure 4.11, the thrust force (T) is not only acting to overcome drag, but also supports a component of weight.

$$T = D + W \sin \gamma \quad (4.19)$$

Multiplying this equation with the velocity along the flight path gives

$$TV_{\infty} = DV_{\infty} + WV_{\infty} \sin \gamma \quad (4.20)$$

In equation 4.20 the left hand side represents the power available TV_{∞} . The required power for level flight P_R is given by DV_{∞} . The vertical velocity $V_{\infty} \sin \gamma$ is also referred to as the rate of climb RC

$$RC = V_{\infty} \sin \gamma \quad (4.21)$$

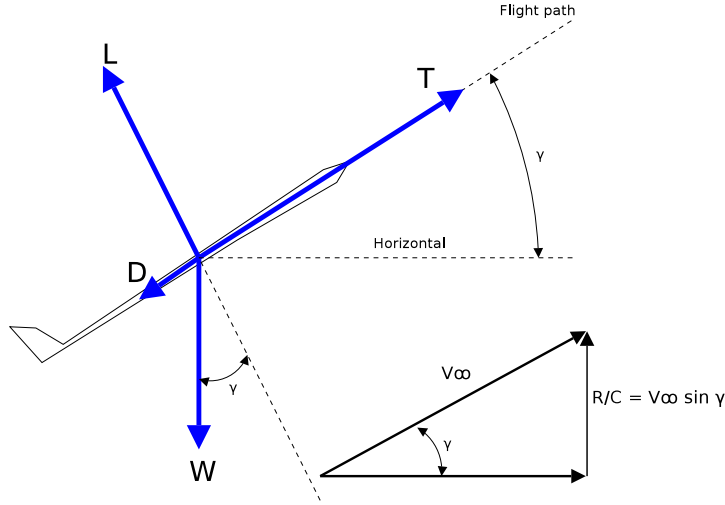


Figure 4.11: Aircraft in climbing flight

If we divide power into two parts, DV_∞ can be referred to as the power required for flight. For climbing flight, however, a part of the weight should also be overcome by the thrust. Since the lift vector is not exactly counteracting against the weight vector (figure 4.11). For small angles of climb though, (below 20°) it is reasonable to ignore this [Anderson, 2008]. So the required power for climbing P_C can be written as

$$P_C = DV_\infty + WRC \quad (4.22)$$

4.5.1 Optimum angle of attack

Assuming that the aircraft will not have an electric connection with the ground, the energy to climb must come from within the aircraft so an energy carrier such as a battery must be used. Since this would add up to the weight of the aircraft, it is desirable to keep the energy need as low as possible. This can be done by flying with the most efficient angle of attack. As described in 4.19 the required thrust equals the total drag summed with the weight multiplied by $\sin\gamma$. The drag can be minimized by flying at an optimum velocity. Assuming level flight, this optimum lies at the point where the lift force balances the weight of the aircraft and the lift to drag ratio is maximum.

The lift force can be calculated with the help of the lift coefficient (C_{L_a}), the wing surface (S), the air density (ρ) and V_∞ . This results in a lift of

$$L = \frac{1}{2}\rho C_L S V_\infty^2 \quad (4.23)$$

The minimum flight velocity where $L = W_a$ (V_{stall}) can be obtained from

$$V_{stall} = \sqrt{\frac{2W_a}{\rho C_{Lmax} S}} \quad (4.24)$$

To have some freedom to manoeuvre and in order to avoid stalling due to wind gusts, a safety margin of 20 % will be taken into account [Ruijgrok, 2007], similarly as described in paragraph 3

$$V_\infty = 1.2V_{stall} = \sqrt{\frac{2W_a}{\rho C_L S}} \quad (4.25)$$

Where W_a comes from

$$W_a = m_a g \quad (4.26)$$

The aircraft drag D_a can be calculated in a similar way as the lift

$$D_a = \frac{1}{2} \rho C_D S V_\infty^2 \quad (4.27)$$

Every C_L gives a different V_∞ to balance the aircraft weight. And every given C_L has a corresponding C_D (figure 2.12). Combining these equations results in the drag curve of figure 4.12. The point denoted as $C_{L_{max}}$ in this graph is the point where stall occurs, at V_{stall} . The curve shows that with a minimum drag D_{min} of 1860 N, the velocity is about 34 m/s, C_L at this state is about 0.52. This point can also be referred to as the point with the maximum L/D. A propeller would normally be designed to operate most efficiently at this state. The next paragraph describes why in case of the Powerplane a different point of design must be chosen.

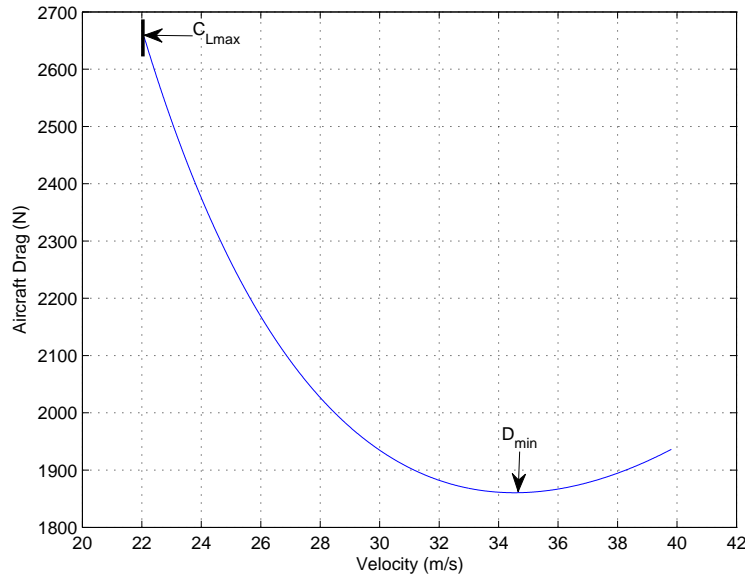


Figure 4.12: Aircraft drag as function of minimum airspeed when lift balances weight

4.5.2 Aircraft with cable

The main difference with a regular aircraft is the fact that there is a cable attached which also induces drag and has a weight. The significance of the cable drag is investigated in this paragraph.

The cable drag can be approximated by assuming that the cable velocity (V_c) at any point in the cable is a linear function of the aircraft velocity (V_∞)

$$V_c(s) \approx \frac{s}{l} V_\infty \quad (4.28)$$

Where l is the cable length and $s \in [0, l]$ is a spatial coordinate along the cable. Figure 4.13 shows the drag force (dD_c) on a cable element (ds) and how the drag increases as $s \rightarrow l$. This drag is balanced by the moment (M_c) represented at $s = 0$. M_c can be found by summing the drag force of each element dD_c multiplied with its distance s from $s = 0$ until $s = l$. This results in a total moment due to the drag given by

$$M_c = \int_0^l \frac{1}{2} C_{D_c} \rho d \frac{s^3}{l^2} V_\infty^2 ds = \frac{1}{8} C_{D_c} \rho d_c l^2 V_\infty^2 \quad (4.29)$$

In this equation d_c is the cable diameter and C_{D_c} is the cable drag coefficient. The cable is not a rigid element, so in reality M_c should be 0. Therefore an equivalent drag force from the cable on the

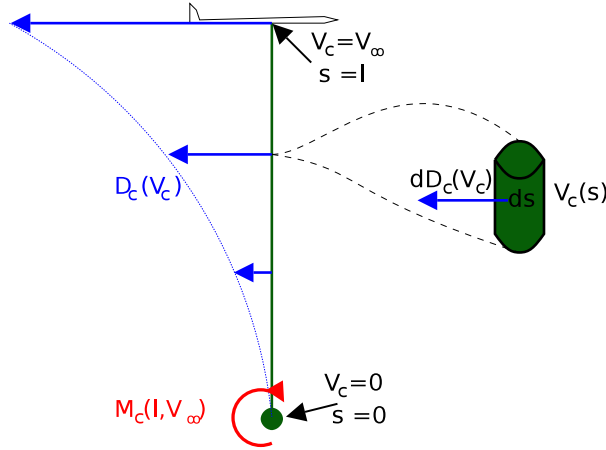


Figure 4.13: Representation of drag on the cable

aircraft can be assumed to balance the total drag on the cable. This force D_c is calculated by dividing M_c by the cable length.

$$D_c = \frac{M_c}{l} = \frac{1}{8} C_{D_c} \rho d_c l V_\infty^2 \quad (4.30)$$

The total drag force D_t consists of the aircraft drag D_a and the cable drag D_c .

$$D_t = D_a + D_c = \frac{1}{2} \rho C_{D_a} S V_\infty^2 + \frac{1}{8} C_{D_c} \rho d_c l V_\infty^2 \quad (4.31)$$

The weight in equation 4.22 is now not only the weight of the aircraft, but also the weight of the cable, which is a function of the cable length l_c

$$W_c = m_c g l_c \quad (4.32)$$

So the total weight becomes

$$W_t = W_a + W_c = m_a g + m_c g l_c \quad (4.33)$$

Following the same procedure as in the former paragraph, but now for different cable lengths, provides a similar graph as figure 4.12. Only now it is clearly visible that the longer the cable, the more significant the cable drag is. Increasing cable drag decreases the share of the aircraft drag on the total drag. Consequently the optimum speed decreases to a point where the aircraft flies at maximum C_L , thus maximum C_{D_a} . But since the aircraft is able to fly at a lower velocity with maximum C_L the cable drag is minimal. This means that for every cable length, a minimum drag force can be obtained by changing the pitch angle such that the aircraft flies at an optimum velocity.

The C_L for this optimum can be calculated by finding the maximum value of L/D as function of the cable length, using 4.23 and 4.31

$$L/D = \frac{\frac{1}{2} \rho C_L S V_\infty^2}{\frac{1}{2} \rho C_{D_a} S V_\infty^2 + \frac{1}{8} C_{D_c} \rho d_c l V_\infty^2} \quad (4.34)$$

rearranging and substituting C_{D_a} as function of C_L from equation 2.20

$$L/D = \frac{C_L S}{(C_{D_0} + K C_L^2) S + \frac{1}{4} C_{D_c} d_c l} \quad (4.35)$$

Which has a maximum value for every l at $C_{L_{opt}}$ of

$$C_{L_{opt}} = \sqrt{\frac{C_{D_0} + \frac{1}{4S} C_{D_c} d_c l}{K}} \quad (4.36)$$

This means that minimizing the energy it takes to climb involves a varying pitch angle such that C_L varies from 0.53 to $C_{L_{max}}$ for a cable length of 0 to 540 meters.

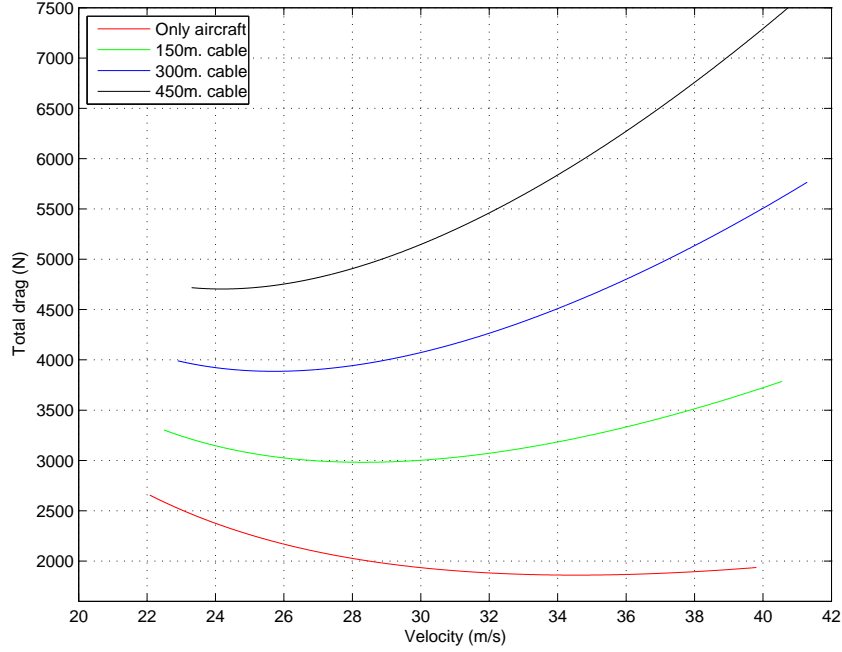


Figure 4.14: Total drag as function of minimum airspeed when lift balances weight

4.5.3 Cable tension

A minimum amount of cable tension should always be present to make sure that the cable does not get tangled while reeling out. This tension (T_0) is estimated to be 100 N. As the tension will be opposite to the direction of the aircraft and constant, it can be added to the drag force of equation 4.31. D becomes

$$D = D_t + T_0 = \frac{1}{2}\rho C_{D_a} S V_\infty^2 + \frac{1}{8}C_{D_c} \rho d_c l V_\infty + T_0 \quad (4.37)$$

Incorporating this tension in figure 4.14 means shifting every graph 100 N. upwards.

4.5.4 Required shaft power

To calculate the power required from an electric motor (shaft power, P_s), the efficiency should be taken into account. A reasonable average value of the propeller efficiency can be stated as 86% [Loftin, 1985]. This number is rather conservative, since the propeller can be optimized for one main purpose: climbing flight at given velocity range. The required shaft power can be calculated by

$$P_s = \frac{DV_\infty + WRC}{\eta_{prop}} \quad (4.38)$$

The weight in equation 4.38 is not only the weight of the aircraft, but also the weight of the cable, which is a function of the cable length. The path the aircraft will fly during fly-out is not known yet, but for the required power, we only need the maximum length, because at this point the drag force will be the largest when the climb angle varies (as shown in figure 4.14). If we assume that the aircraft remains within its maximum operating area, the cable is a straight line from the ground station to the aircraft and the ground station is situated in the exact center of the area. Then the length will be at maximum

$$l_{max} = \sqrt{2\left(\frac{1}{2}d_{max}\right)^2 + h_e^2} \quad (4.39)$$

h_e represents the final height of the climb-out phase and d_{max} is the maximum width of the operating area. Now when m_c is the weight of the cable in kg/m the total cable weight becomes

$$W_c = m_c g l_{max} = m_c g \sqrt{2\left(\frac{1}{2}d_{max}\right)^2 + h_e^2} \quad (4.40)$$

The power the aircraft should be supplied with, depends on the maximum power. The necessary power as function of the climb angle can be found by combining equations 4.21, 4.38, 4.37 and 4.40.

$$P_s = \frac{\{T_0 + D_a + D_c + (W_a + W_c)\sin\gamma\}V_\infty}{\eta_p} = \frac{\{T_0 + \frac{1}{2}\rho C_{D_a} S V_\infty^2 + \frac{1}{8}C_{D_c}\rho d_c l_{max} V_\infty^2 + (m_a + m_c l_{max})g\sin\gamma\}V_\infty}{\eta_p} \quad (4.41)$$

The time of climb (t_{climb}) can be obtained from equation (4.21) and the height (h_e).

$$t_{climb} = \frac{h_e}{V_\infty \sin\gamma} \quad (4.42)$$

The most efficient $C_{L_{opt}}$ of equation 4.36 for a cable length of l_{max} gives a C_L of 1.25. V_∞ for this value is obtained from equation 4.25, where W is W_t of equation 4.33 with $l_c = l_{max}$. C_{D_a} is also related with C_L and calculated by equation 2.20. This results in the parameters given in the table 4.3

V_∞	η_p	m_a	m_c	g	h_e	d_{max}	S_a	ρ	C_{D_a}	C_{D_c}	d_c
23.8m/s	0.86	3500kg	0.885kg/m	9.81m/s ²	200m	600m	130m ²	1.2kg/m ³	0.064	1.2	0.04m

Table 4.3: Parameters used for propeller power calculations

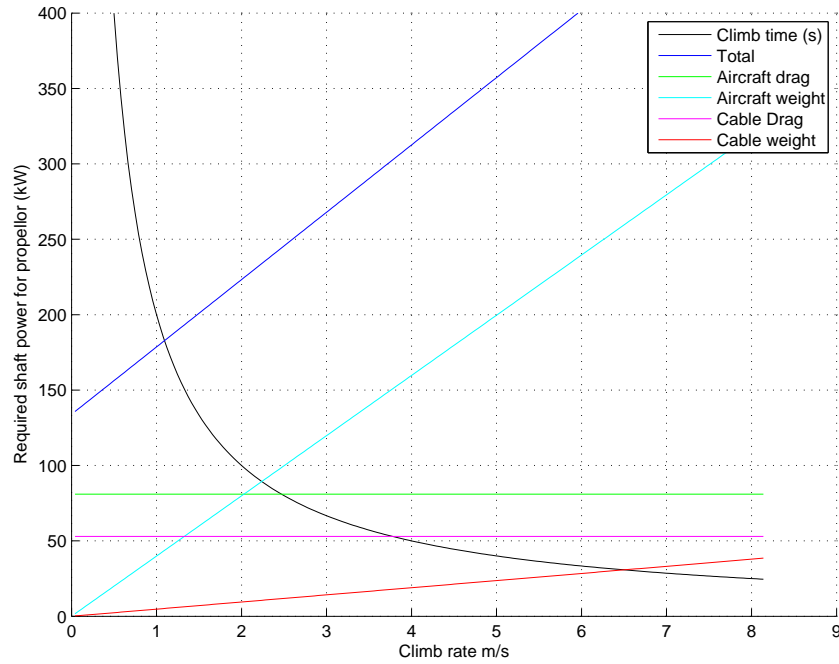


Figure 4.15: Required shaft power and climb time as function of rate of climb.

With the parameters from table 4.3 this function is plotted against the climb rate in figure 4.15¹. It shows that the the required shaft power increases linearly from about 135 to 400 kW for a climb rate between 0 and 6 m/s. Since the drag is not a function of the climb angle, the required power to balance the aircraft drag and the cable drag are constants of respectively 81 and 53 kW.

¹In the graph climb time is in seconds, though it uses the kW axes

4.5.5 Mass of electric motor

Using a battery powered electric motor instead of a combustion engine is preferred as such a motor requires less maintenance and has a higher reliability [Nemry et al., 2009]. Besides that an electric motor fits much better into the Powerplane system as it has the ability to make use of its own generated energy and does not rely on fossil fuels. The additional mass on the aircraft is an important requirement (paragraph 3). Now the required shaft power is calculated, an estimation can be made for the mass of the electric motor. This mass (m_b) for any P_s can be obtained from

$$m_b = \frac{P_s}{p_{w_m}} \quad (4.43)$$

Where p_{w_m} represents the power to weight ratio of the motor. To estimate this ratio research on electric motors suitable for this purpose is done. UQM technologies sells electric motors for Electric Vehicles ranging from 50 to 150kW with a p_{w_m} of 1.22 to 1.65 kW/kg [UQM, 2010]. Alternatively, lighter electric motors which are engineered specially for aircrafts are also available. Yuneec Ltd. has designed an electric aircraft with a 40 kW motor weighing only 17 kg. [Yuneec, 2008]. An image of this aircraft is shown in figure 4.16



Figure 4.16: left: Yuneec e430 electric aircraft, right: PML Hi-Pa drive installed in mini

Finally PML flightlink markets integrated drive and controller units (Hi-Pa Drive) which are already demonstrated in electric cars (figure 4.16, right) with a maximum power of 40 - 120 kW weighing only 18 - 25 kg ($p_{w_m} = 2.22 - 4.8$ kW/kg) [PML, 2006]. This concludes that a power to weight ratio of 2.5 kW/kg can be assumed to be commercially available. This value will be used as an average for weight calculations later in this chapter.

4.5.6 Required energy

To provide the electric motor with electric energy, it is possible to use batteries. The amount of energy which should be available for climbing, can be calculated by multiplying the required power of equation 4.41 with the climb time (equation 4.42). Though, during climbing the required power varies, since the cable length increases from 0 to maximum, and the optimum pitch angle varies with cable length. In case of the cable weight, this can be tackled by using the average weight which is exactly half of the end weight. Since the flight path is not known yet, the drag part of the cable and the aircraft are a bit harder to estimate. A typical way the aircraft could fly up is by flying to the end of the field and then flying circles with a radius of half the field width. In reality this means that the cable length becomes 300 m. in about 10 to 15 seconds, when the aircraft flies a straight path. Followed by a relatively slow increase to l_{max} . Therefore the average cable drag is assumed to be 85 % of its maximum value. The optimum C_L for most of the climbing procedure is defined for a cable length above 300 m. and varies from 1.07 to 1.25. But as the maximum is defined to be 1.1, C_L , C_D and V_∞ for the required energy are similar as in paragraph 4.5.4. Besides this a motor η_m and a battery efficiency η_b of both 95% are taken into account. Finally adding a factor for kWh gives

$$E_b = \frac{T_0 + D_a + 0.85D_c + (W_a + 0.5W_c)\sin(\gamma)}{\eta_p\eta_m\eta_b} \frac{h_e}{\sin\gamma} \frac{10^{-6}}{3.6} \quad (4.44)$$

4.5.7 Battery mass

Similar to the motor mass, the battery mass is also an important issue. The batteries with the best energy to weight ratio which are widely available on the market, are lithium ion and lithium polymer batteries. When also the casing material is taken into account, the energy to weight ratio (e_{w_b}) of these batteries ranges from 0.100 to 0.150 kWh per kg. [Scrosati and Garche, 2010]. The total mass of the batteries can be calculated by

$$m_b = \frac{E_b}{e_{w_b}} \quad (4.45)$$

The value m_b will be used in the following chapter for estimating the total mass. A remark on the use of these batteries could be the danger of explosion which lithium ion batteries tend to have. The use of these batteries in electric vehicles and many consumer products such as laptops, power tools, electric bicycles and cellphones underlines that this would not really be a threat. Besides that the aircraft will not be flying around in densely populated areas. Hence the risk of people getting hurt because of exploding batteries is very low.

4.5.8 Total mass

The total mass can be calculated by adding the battery mass to the motor mass

$$m_{total} = \frac{P_s}{p_{w_m}} + \frac{E_b}{e_{w_b}} \quad (4.46)$$

Figure 4.17 shows how the battery mass and the motor mass varies with the climb rate, where e_{w_b} is 0.125 kWh/kg and p_{w_m} is 2.5 kW/kg. It reveals that the required shaft power and, together with, that the motor weight, increases with the climb angle. Contrary to the motor mass, the battery mass decreases with the angle due to the fact that a higher instantaneous power results in much less climb time. So the climb angle can be optimized for mass by choosing the minimum value. The graph of the total mass shows in this case, that an optimum of 141 kg is situated around a climb rate of 1.8 m/s, where P_s is 215 kW. The climb time in this case is just more than 2 minutes. The dotted lines represent the worst case ($e_{w_b} = 0.100, p_{w_m} = 1.22$) and the best case ($e_{w_b} = 0.150, p_{w_m} = 4.5$) with an optimum at respectively 242 kg and 89 kg.

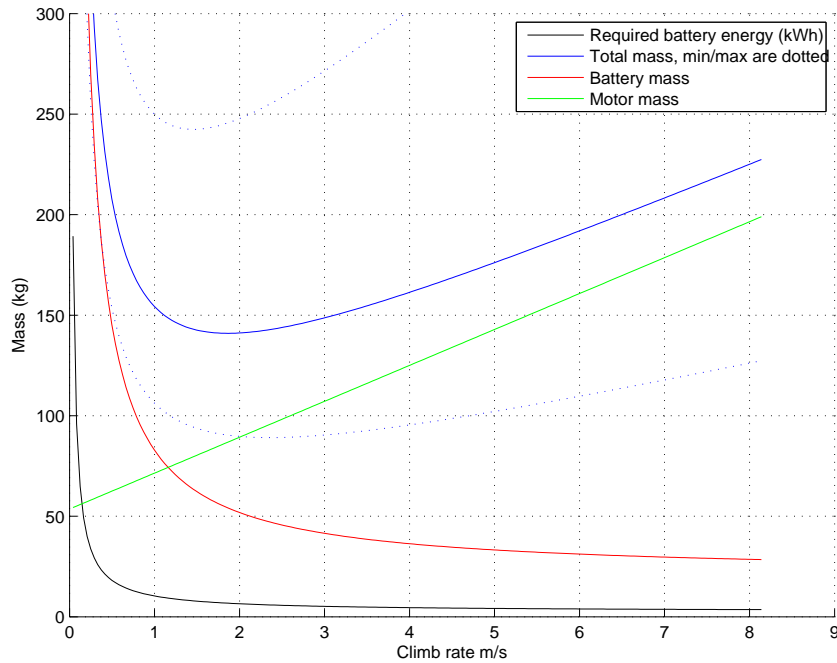


Figure 4.17: Mass of electric propulsion as function of the climb rate

4.5.9 Cost

Just as in the former paragraph, an optimum can also be found for the cost of the system. This can be done by replacing e_{w_b} with the energy to cost ratio e_{c_b} and p_{w_m} with the power to cost ratio p_{c_m}

$$C_{b+m} = \frac{P_s}{p_{c_m}} + \frac{E_b}{e_{c_b}} \quad (4.47)$$

Research on the cost for electric vehicles states that the MPM80 of UQM technologies costs €310 when produced in very large series $> 200k/yr$ [Lipman and Delucchi, 2006]. This motor has a power of 80kW and weighs 50kg. p_{w_m} will then be 0.26 kW/€. The motor is a bit heavier than estimated earlier and the quantity will be a bit smaller first, so a more conservative statement for p_{w_m} is decided to be 0.09 kW/€. The price of a complete lithium battery pack is expected to be €700 per kWh, but dropping down to €140 in 2030. [Nemry et al., 2009] Therefore e_{c_b} for 2015 is assumed to be about 1/500 kWh/€. With these parameters the cost can be plotted as in figure 4.18.

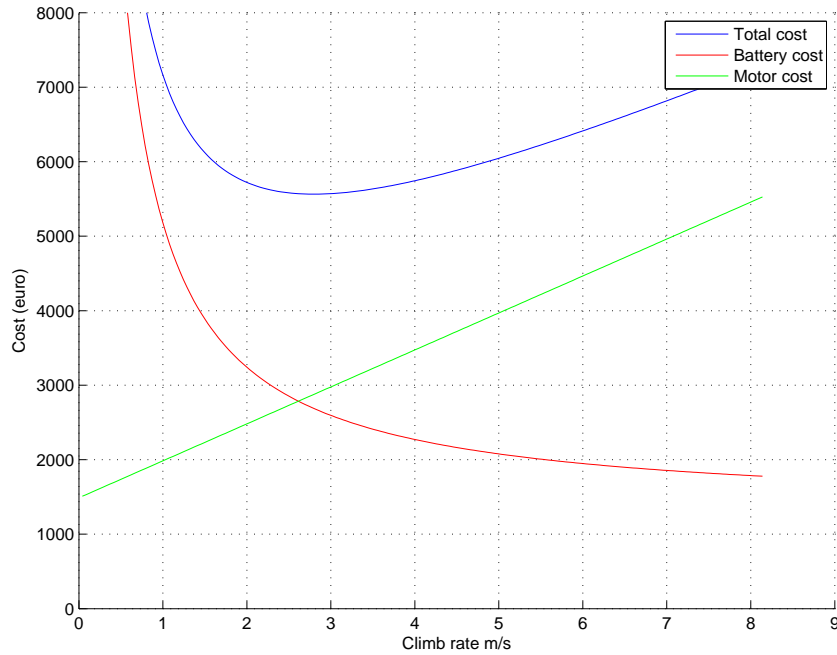


Figure 4.18: Battery cost plus motor cost versus climb rate

This graph shows that with the chosen parameters the cost graph has a similar shape as the graph of the weight. In this case the cost optimum lies at a rate of 2.8 m/s with a cost of 5.5 k€. Though the slope of the graph is quite small, the total cost ranges in between 5.5 and 8 k€ for the plotted climb rates.

4.5.10 Propeller

The propeller should be lightweight and have a high efficiency in its working range. But another important feature is that the propeller should not induce too much drag while the aircraft flies its energy generating patterns. To decrease the drag several options are possible such as:

- Variable pitch propeller: During energy generation the blades are pitched into feathering position [MT-Propeller, 2010]
- Retractable propeller (figure 4.19a): The propeller retracts itself into a position where it does not influence the aircraft drag. For example folding into the nose cone or hiding behind doors similar to landing gear doors [Lange-Aviation, 2010].

- Foldable propeller (figure 4.19b): The blades fold at their attachment points aligning lengthwise with the aircraft flight direction.



Figure 4.19: a: Foldable propeller in folded position b: Retractable propeller, in operation on PIK-20 aircraft

For a weight and size estimation, the MTV-23 of MT-Propeller can be taken as an example. This 3-blade electric variable pitch propeller for light aircraft has an infinitely variable pitch range from take-off to feathering position, is designed for a constant speed and has electronic pitch control [MT-Propeller, 2010]. Further parameters are shown in table 4.4

Table 4.4: Technical data of MTV-23 Propeller

Material blades	Natural-Composite with fiber reinforced epoxy cover.
Material hub	Forged / milled aluminium alloy
Max. Power	261 kW @ 2700 rpm
Max. Diameter	213 cm
Weight with 193 cm	25 kg
Weight of spinner	1.5 kg
Weight of control unit	0.5 kg

These parameters show that a propeller suitable for having a climb rate of 3.5 m/s weighs 25 kg.

4.5.11 Conclusion

When a climb rate of 3.5 m/s is taken into account, the total weight of propeller, batteries and motor (with controller) add up to approximately 165 kg. This is nicely below the projected 200 kg, leaving room for peripheral elements such as wiring, cooling etcetera. The costs of motor and batteries in this case are below €6000. Including the propeller and other elements, such a system for climbing is expected to remain below €10.000 when produced in large series.

4.6 Climb with air pressure

Using air pressure as means of propulsion has the advantage that the equipment to generate this pressure can stay on the ground. The aircraft is only equipped with a pressure vessel, a nozzle to release the pressure efficiently and some control equipment. This could decrease weight and increase simplicity, thus increasing the reliability of the system.

4.6.1 Adiabatic expansion

The difference in specific internal energy of the initial and final state of 1 kg of air determines the amount of energy available through adiabatic expansion of air stored at 200 bar.

$$\Delta u = C_v(T_1 - T_2) \quad (4.48)$$

Where the temperature T_2 can be calculated by

$$T_2 = T_1 \left(\frac{P_1}{P_2} \right)^{\frac{k-1}{k}} \quad (4.49)$$

A k of 1.4, P_1 of 200 bar, P_2 of 1 bar, $C_v = 0.71$ kJ/kg K and a T_1 of 288 K results in a T_2 of 65 K. The available energy is 160 kJ per kg of air. This seems promising, but an efficient way to make use of this energy must be found.

4.6.2 Possible amount of impulse

Using compressed air blowing out of a nozzle as means of propulsion for a glider plane is investigated by a research group [Jackson and Pearson, 1974]. A computer model verified by a scaled prototype resulted that a system holding 45 kg of air at 207 bar gave an impulse of 22.2 kNs. So the average impulse of such a system is about 0.5 kNs/kg. This amount of impulse can only be reached in case the aircraft already has its minimum velocity.

4.6.3 Required impulse for climbing

When the aircraft already has its minimum velocity, the amount of impulse required to climb to the required altitude with the aircraft can be calculated by the thrust (T) and the time

$$I = T \Delta t \quad (4.50)$$

T is again a function of the total drag D , weight W and the minimum tension T_0 .

$$T = D + W \sin \gamma + T_0 \quad (4.51)$$

so

$$I_{total} = (D + W \sin \gamma + T_0) t_{climb} \quad (4.52)$$

With the variables given in paragraph 4.5 this results in an impulse as function of the climb rate as in figure 4.20. To define the amount of pressurized air required for climbing, these numbers can be simply multiplied by two (as 1 kg represents 0.5 kNs). For example a climb rate of 5 m/s requires 1000 kg of air. Compared to the aircraft weight, this is of such a significance that it actually should have been added to the calculation as well. But first of all, the weight of a system carrying this air is investigated.

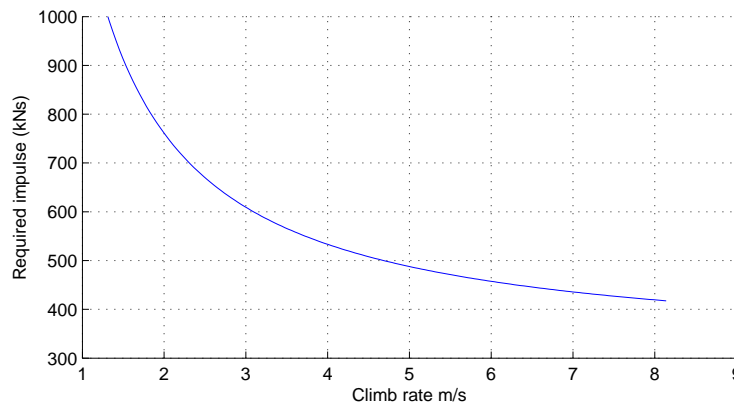


Figure 4.20: Required impulse as function of climb rate

4.6.4 Pressure vessel

Carbon composite cylinders used for the aviation industry capable of holding 200 Bar typically weigh about 0.42 kg per liter of storage volume [Worthington, 2010]. This holds for sizes of up to 26 liters. Fuel cylinders of the same manufacturer meeting the same pressure and having a size of 300 liters weigh

0.37 kg per liter of storage volume. At a pressure of 200 bar, the specific weight of air is 237 kg/m^3 . This means that the factor between the weight of air and the weight of the vessel it holds, is in these cases respectively 1.77 and 1.56. For an increased size this factor probably can be decreased down to 1.2. This also meets the calculations made in [Jackson and Pearson, 1974] where the vessel is estimated to weigh 1.2 times the weight of the air it holds.

4.6.5 Conclusion

When air pressure is used as propulsion for climbing, as described in this section, the total weight of the pressure vessel would be at least 500 kg, when a climb rate of 8 m/s is achieved. Climbing at a smaller rate demands even a larger weight. This number increases when the weight of the pressure vessel and the containing air is taken into account. Besides that, the size of a vessel storing for example 800 kg of air at 200 bar is about 3400 liter. Both weight and size of the system will influence the performance of the Powerplane significantly. Therefore climbing by means of air pressure with a nozzle is not regarded to be a suitable option. Instead of using a nozzle, pressurized air could also be used for powering an air motor in combination with a propeller. But compared to using a battery powered electric motor, this only adds complexity to the system. Hence this option is not investigated.

4.7 Accelerate with propeller

The propeller-motor combination from the paragraph 4.5 could be used for accelerating to lift off velocity. To estimate how this option relates itself to the system requirements the following calculations are made.

4.7.1 Distance of ground run

The distance a body of mass m requires to accelerate to velocity V under a constant force F is given by

$$s = \frac{V^2 m}{2F} \quad (4.53)$$

Figure 4.21 shows the forces acting on an aircraft during take off. The force F from equation 4.53 not only consists of the thrust T and the aircraft drag D , but additionally a roll resistance R must be taken into account. This force is given by

$$R = \mu_r(W - L) \quad (4.54)$$

Where μ_r is the coefficient of rolling friction which varies from 0.02 for a relatively smooth, paved surface to 0.1 for a grass field. $W - L$ is the net normal force exerted between the wheels and the ground.

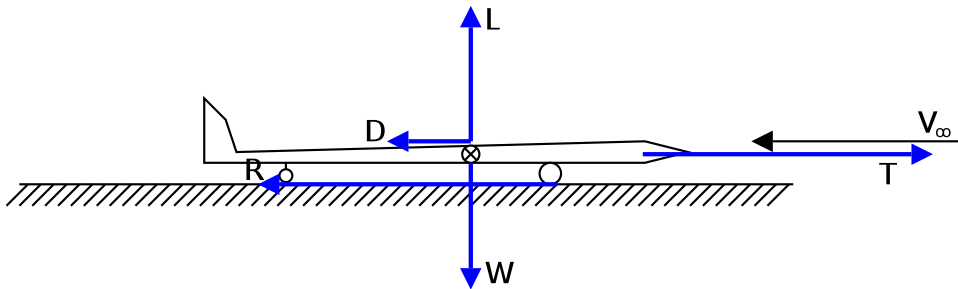


Figure 4.21: Forces on an aircraft during take-off

F becomes

$$F = T - D - R = T - D - \mu_r(W - L) \quad (4.55)$$

Here we assume that T is reasonably constant, D (eq. 4.27) and L (eq. 4.23) are functions of V , which is not constant during acceleration. [Anderson, 2008] states that the average force can be taken to be

equal to its instantaneous value at $0.7V_{LO}$. Where the lift-off velocity (V_{LO}) is typically 20% higher than the stall velocity to ensure a margin of safety during take-off.

$$V_{LO} = 1.2V_{stall} = 1.2\sqrt{\frac{2W}{\rho_{\infty}SC_{L_{max}}}} \quad (4.56)$$

The weight of the cable is neglected since at the start the cable is very short, so W is the aircraft weight W_a from equation 4.26. Combining this with eq. 4.53 and 4.55 results in an equation for the ground run distance s_{LO}

$$s_{LO} = \frac{1.44W^2}{g\rho_{\infty}SC_{L_{max}}\{T - [D + \mu_r(W - L)]_{0.7V_{LO}}\}} \quad (4.57)$$

Further on the thrust is calculated from the shaft power by

$$T = \frac{P_s\eta_p}{0.7V_{LO}} \quad (4.58)$$

Where the propeller efficiency (η_p) is taken as .65 assuming that the propeller has its optimum efficiency at V_{∞} .

4.7.2 Power

When the shaft power (P_s) is assumed as the main adjustable parameter for this launching method, it can easily be used to represent weight and cost from paragraph 4.5. Therefore the ground run distance is plotted as a function of this parameter with a μ_r of 0.02 and 0.1 and also in a situation in which drag and resistance are ignored. Figure 4.22 shows that with a motor at the optimum weight situation (P_s is 215 kW, paragraph 4.5.8), the ground run distance would be in between 94 and 117 m. With a motor of 500 kW, the ground run distance is below 60 m., though this means a motor weight of at least 100 kg and a different propeller must be used. Especially at lower shaft power, the effect of the ground roughness is significant.

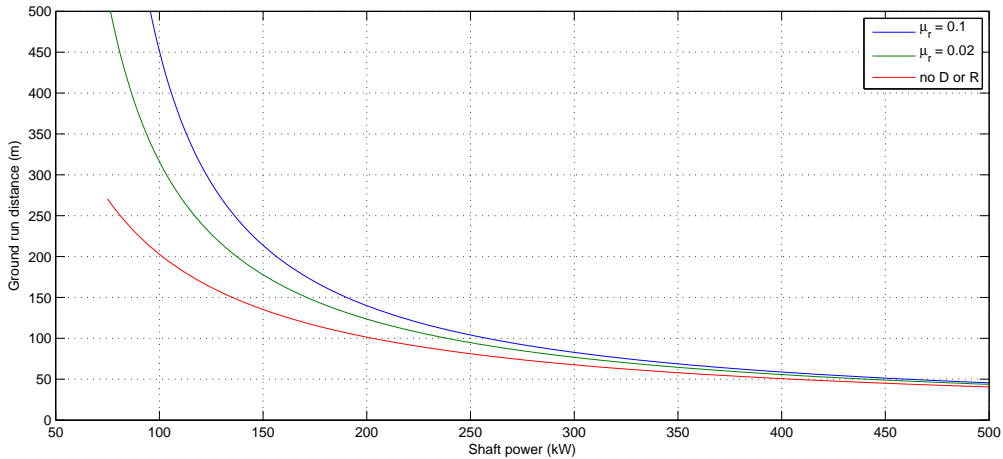


Figure 4.22: Ground run distance as function of shaft power

4.7.3 Energy

The energy the motor uses, will add to the battery weight. To estimate the energy use, the electric power can be multiplied with the launch time. The launch time comes from

$$t_{launch} = \frac{s_{LO}}{V_{av}} \quad (4.59)$$

So the launch energy can be calculated by

$$E_{launch} = \frac{P_s t_{launch}}{\eta_b \eta_m} \frac{10^{-6}}{3.6} \quad (4.60)$$

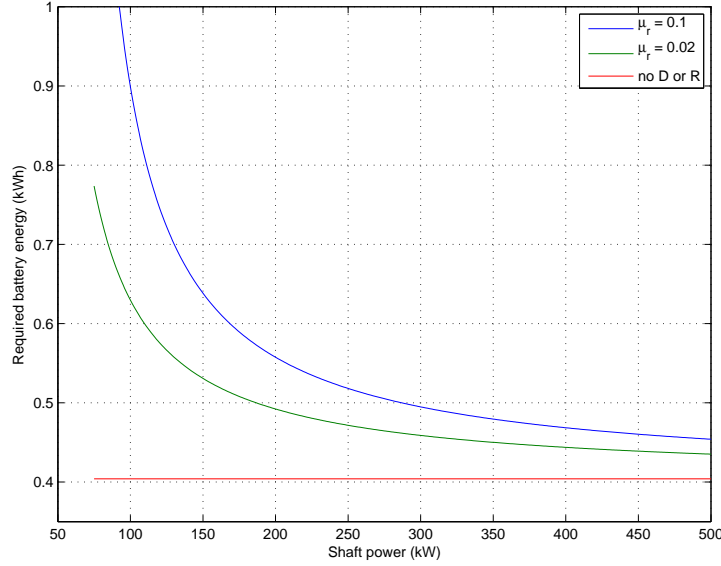


Figure 4.23: Ground run energy as function of shaft power

Figure 4.23 shows that the required energy decreases with the shaft power. This is due to the declined ground run distance which decreases the run time, thus the losses to drag and roll resistance. The required energy ranges from 0.9 kWh on a grass field with 100 kW shaft power to .44 kWh on a paved surface with 500 kW. This means an additional weight of 4 to 8 Kg and additional cost of €250 to €500 (with the average values of paragraph 4.5).

4.8 Accelerate with an external system

Since acceleration with a propeller requires either high power or a long ground run, an external system on the ground can be used as an alternative. This means that the power and also the energy-carrier for lift-off does not have to be incorporated in the aircraft. Weight becomes less important and even a grid connection could be possible. Without going into detail about the system itself, it can be assumed that converting power of the actuator into velocity of the aircraft happens much more efficient compared to using a propeller.

For the ground run distance again equations 4.57 and 4.58 are used. In this case η_{prop} is replaced with a conversion efficiency (η_c) of .95 and μ_r ranges from negligible (e.g. linear motor) to 0.1 (e.g. wheels on grass field). This results in a similar plot (figure 4.24 as figure 4.22). Though the higher efficiency results in a shorter ground run and the range of the external power is much larger. The graph also shows that when the thrust is very large, the influence of drag and roll resistance becomes negligible. With 2 MW of power, the ground run becomes than 10 meters, 20 meters can be reached with 1 MW. The energy it takes to launch becomes less important, but it can be stated that with a negligible drag and resistance, it will be around .5 kWh for any amount of power.

4.9 Launch with a rotational platform

A method currently used as a performance test for power kites, is using a rotational platform for launching and testing. The kite is pulled via a tether by a rotating arm. The apparent wind caused by this motion makes the kite generate enough lift for launching and performing tests. The method is simple, only

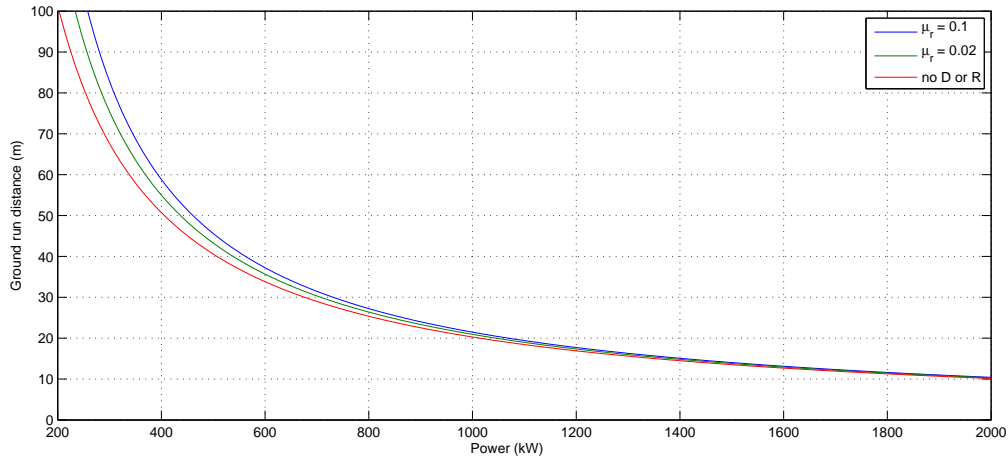


Figure 4.24: Ground run distance as function of external power

needs a relatively small ground surface area, and can also be executed with no wind or low wind speeds [Stevenson et al., 2005]. Ampyx Power aims for a system based on a rotating platform as well, but the company is still unsure if this is a suitable solution. First of all it is unknown if this method will be suitable for large rigid aircrafts. Some basic boundary conditions of this method are analysed in this section and a test is performed with a small prototype.

4.9.1 Minimum radius of turn for a conventional flight

For calculating the minimum radius of turn of an aircraft, the assumption is made that the aircraft takes a steady, non side slipping banked turn. The effect of the tether will be ignored now. That means that the tether has no weight and also does not counteract on the centrifugal force. At these conditions the horizontal component of the lift causes the inward centripetal force which pulls the aircraft towards the center of turn. Both resultant aerodynamic force ($\mathbf{R} + \mathbf{T}$) and the sum of the weight and the outward centrifugal force ($\mathbf{W} + \mathbf{C}$) are in the plane of symmetry of the aircraft. The instantaneous conditions on the spiral flight path are described by:

$$T - D - W \sin(\gamma) = 0 \quad (4.61)$$

$$W \cos(\gamma) \sin(\mu) - C \cos(\mu) = 0 \quad (4.62)$$

$$-L + W \cos(\gamma) \cos(\mu) + C \sin(\mu) = 0 \quad (4.63)$$

When the origin of the system is put at the center of gravity and level flight ($\gamma = 0$) is assumed, the angle of roll equals the bank angle ($\mu = \Phi$). The forces working on the aircraft in a turn to the right under these conditions are shown in 4.25. From this figure the following equations can be found.

$$T - D = 0 \quad (4.64)$$

$$L \sin(\Phi) - C = 0 \quad (4.65)$$

$$-L \cos(\Phi) + W = 0 \quad (4.66)$$

From the figure and the equations we see that the centripetal force is completely balanced by the centrifugal force, which is given by

$$C = \frac{W}{g} \frac{V^2}{R} \quad (4.67)$$

Further on we know that the lift force follows from

$$L = C_L \frac{1}{2} \rho V^2 S \quad (4.68)$$

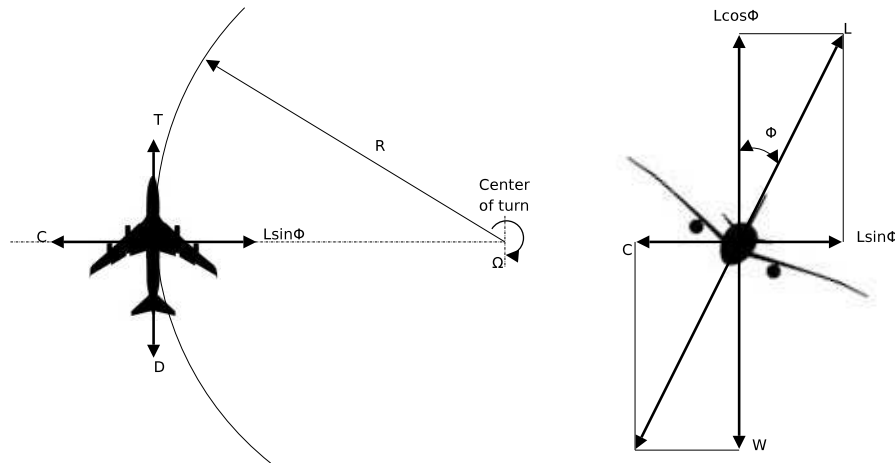


Figure 4.25: Forces on the aircraft during a steady level true banked turn

Substituting C and L in equation 4.65 and rearranging to R gives

$$R = \frac{W}{S} \frac{2}{\rho} \frac{1}{g} \frac{1}{C_L \sin \Phi} \quad (4.69)$$

The velocity necessary to balance the weight with the vertical part of the lift force can be found by substituting L into equation 4.66 and rearranging to V. A safety factor of 1.2 is added similar to paragraph 3.1.2.

$$V_{min} = 1.2 \sqrt{\frac{W}{S} \frac{2}{\rho} \frac{1}{C_L \cos \Phi}} \quad (4.70)$$

Equation 4.69 and 4.70 are plotted against the bank angle in one graph (figure 4.26). The graph shows that when the bank angle reaches 90°, the velocity runs to infinite. This is obvious, since an increasing bank angle results in a decreasing component of lift to balance the weight. Therefore the total lift force must be increased by increasing the velocity. The radius of turn works the other way around, as the fraction of lift going to the centripetal force increases with the bank angle. Therefore the radius increases to infinite with a bank angle reaching zero.

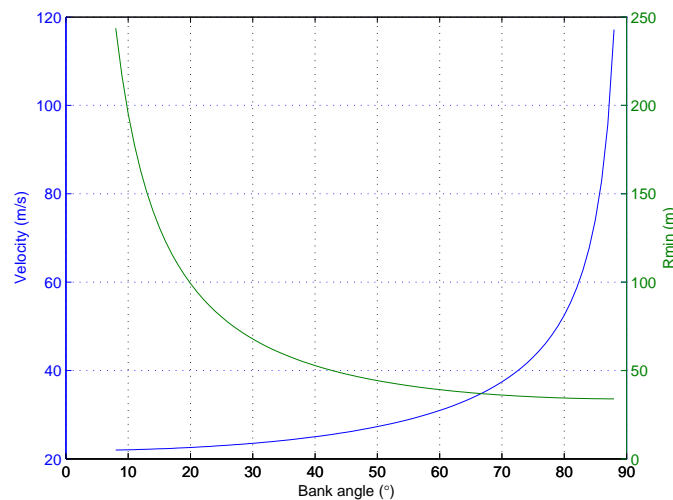


Figure 4.26: Minimum Velocity and Radius of turn as function of the bank angle of the 10MW aircraft

The graph reveals that using this approach would lead to a radius of at least 35 meters if the velocity remains below the required 60 m/s. At this state the bank angle is 83° , which means that almost all of the lift force goes into balancing the centrifugal force. A small deviation of the bank angle could easily lead to crashing the aircraft into the ground with 60 m/s. Besides that most of the energy will be lost into the drag, because of the high velocity. These drawbacks demand a different approach for a launching procedure with a rotating platform.

4.9.2 Tether for centripetal force

The aircraft is tethered and the tension in this cable acts in the direction of the center of turn. Using the cable to act as centripetal force is an easy option, as long as this force remains below the maximum allowed cable tension. Hence in this case it is best to abandon the conventional approach of banking to balance the centrifugal force. Remain within the limits of the cable is not really an issue, flying at 40 m/s with an arm of 30 m. results in a C of 187 kN, which is relatively small compared to the maximum cable tension of 1314kN. Another advantage is that the cable keeps on being tensed, lowering the risk of it getting tangled. Above all, the radius to rotate around becomes smaller. But when rotating at a smaller radius, other phenomena will take place which can not be ignored.

4.9.3 Minimum radius of turn for tethered flight

Investigating what is important when rotating around a small radius, is done by the calculations and a field test, described in the following paragraphs.

Easyglider

The following calculations are done for the “Easyglider”, a model aircraft which was planned to be used for a scaled test (figure 4.27). Characteristics of the aircraft are defined as in appendix F, and shown in table 4.5. Even though dimensions differ from the large 1 MW aircraft, terms as lift coefficient are expected to be similar. The approach used here, can be repeated for the 1 MW aircraft as soon as more data on this is available.



Figure 4.27: The Multiplex Easyglider

Wingspan b	Overall length l	Chord c	Surface S	Max Lift Coeff. $C_{L_{max}}$	Weight W	Wing loading W/S
1.8 m	1.13 m	0.20 m	0.416 m ²	1.3	8.63 N	20.7 N/m ²

Table 4.5: Characteristics of Easyglider Electric

Velocity difference

Assuming that all the lift force will be used to counterbalance the gravity, the most efficient way to go up is with a zero bank angle. But having zero bank angle and a small radius, means that the difference in air velocity from the tip of the inner wing and the outer wing tip is large, as shown in figure 4.28.

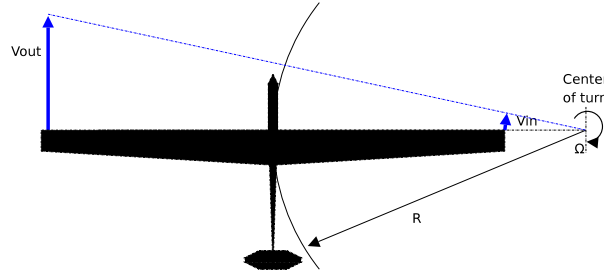


Figure 4.28: Difference in velocity along aircraft with small radius

Lift distribution

Since the liftforce is determined by the square of the velocity, the force generated by the outer wing of the plane will be much larger than the force of the inner wing. This results in a roll moment, making the aircraft bank towards the center of turn. A way to prevent this is by using the ailerons. These can be used to reduce the C_L of the outer wing and increase the C_L of the inner wing. To calculate what this liftforce would be, the wing surface can be divided into areas with a 'fixed' C_L (without ailerons) and with a variable C_L . The liftforce per section can then be calculated by integrating along the wing surface.

So there is lift L

$$L = C_L \frac{1}{2} \rho V^2 S \quad (4.71)$$

In this case the velocity V is a function of the rotational velocity Ω and the radius R

$$V = 2\pi\Omega R \quad (4.72)$$

And the surface can be written as a function of the radius and the chord c .

$$S = cdr \quad (4.73)$$

This means that the liftforce for every infinitely small radius can be calculated by

$$dL = C_L \frac{1}{2} \rho (2\pi\Omega r)^2 cdr \quad (4.74)$$

Every surface has a begin radius, an end radius and a given C_L so the lift of the surface can be integrated as

$$L = C_L \rho c 4\pi^2 \Omega^2 \int_{r_{begin}}^{r_{end}} 1 + r^2 dr \quad (4.75)$$

Balancing with ailerons

Using the ailerons to balance the lift means that the outer aileron will be set to having a low C_l and the inner side will have a high C_l as shown in figure 4.29. Assuming that the low C_l will be above zero, the lift distribution along the wing will look somewhat like the graph in this figure. Balancing the lift on the inner and on the outer wing means that

$$C_{L_{high}} \rho c 4\pi^2 \Omega^2 \int_{r_1}^{r_2} 1 + r^2 dr + C_L \rho c 4\pi^2 \Omega^2 \int_{r_2}^{r_3} 1 + r^2 dr = C_L \rho c 4\pi^2 \Omega^2 \int_{r_4}^{r_5} 1 + r^2 dr + C_{L_{low}} \rho c 4\pi^2 \Omega^2 \int_{r_5}^{r_6} 1 + r^2 dr \quad (4.76)$$

Which can be simplified to

$$C_{L_{high}} \int_{r_1}^{r_2} 1 + r^2 dr + C_L \int_{r_2}^{r_3} 1 + r^2 dr = C_L \int_{r_4}^{r_5} 1 + r^2 dr + C_{L_{low}} \int_{r_5}^{r_6} 1 + r^2 dr \quad (4.77)$$

Equation 4.77 is only a function of the radii and the C_L . Javafoil can be used to calculate the minimum and the maximum C_L for different aileron settings, by changing the shape of the airfoil. The

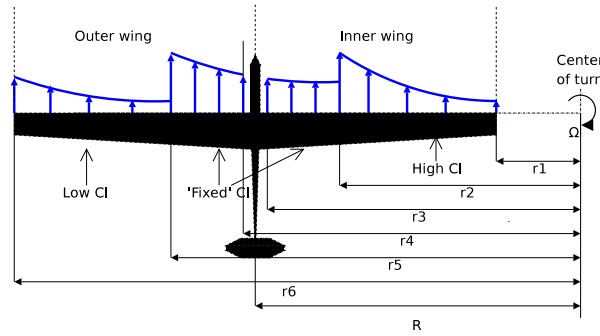


Figure 4.29: Schematic graph of glider with lift distribution when flying a circular pattern with a small radius and having the ailerons set to provide a balanced lift

manual of the Easyglider [Kühn, 2009] provides that the maximum upward position of the aileron is 20 mm and it can go down to -8mm which is a rotation of 22° and -9° respectively. Modeling the airfoil for different aileron settings, gives the plot, shown in figure 4.30. Since control of the aircraft is such that the setting of both ailerons are linked (moving one aileron up means moving the other down), the values are plotted as a function of the rotation of the outer aileron δ_a .

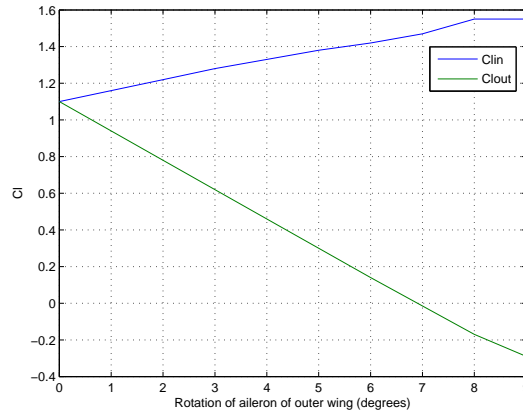


Figure 4.30: Lift coefficient of inner and outer aileron as a function of the rotation of the outer aileron (δ_a)

At maximum settings, this results in a C_{Lmin} of -0.29 and a C_{Lmax} of 1.55 at a pitch angle of 5° . Graph 4.30 also shows that up to a rotation of 8° the function is almost linear. This means that the lift coefficients can be approximated as

$$0 < \delta_a < 8 \quad (4.78)$$

$$Cl_{out} = -0.16\delta_a + Cl \quad (4.79)$$

$$Cl_{in} = 0.055\delta_a + Cl \quad (4.80)$$

Substituting equation 4.79 and 4.80 into 4.77 results in a function with δ_a as a variable. The values for r_1 to r_6 can be written as a function of R and the distances of the section from the center of the aircraft, as shown in figure 4.31 and table 4.6

Since these distances are given aircraft parameters, equation 4.77 can be solved for δ_a at any given R , as long as R is larger than the length of one wing (d_{end}). This is shown in figure 4.32. It also shows that even at a very small radius the rotation is below 8° , which means that the linear functions can be used and that the setting stays within the aircraft its possibilities.

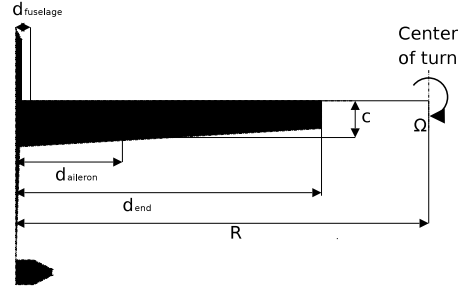


Figure 4.31: measurements of aircraft

r1	r2	r3	r4	r5	r6
$R - d_{end}$	$R - d_{aileron}$	$R - d_{fuselage}$	$R + d_{fuselage}$	$R + d_{aileron}$	$R + d_{end}$
R-0.76	R-0.35	R-0.05	R+0.05	R+0.35	R+0.76

Table 4.6: r as function of R and distances at aircraft

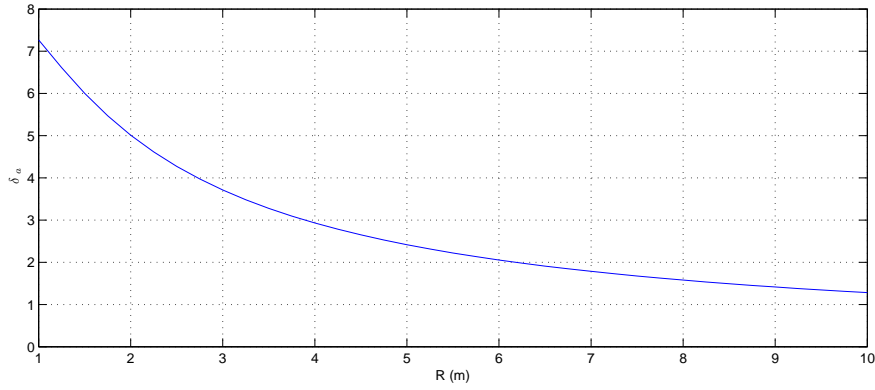


Figure 4.32: Aileron setting for balanced lift as function of the radius

Aileron balancing in practice

Now we have learned that there is an optimum setting for every radius, it is possible to calculate what the total generated lift would be at different radii and different rotational velocities. The total lift can be calculated by adding the generated lift for every section as in equation 4.81.

$$L_{total} = \rho c 4\pi^2 \Omega^2 \left(C_{L_{high}} \int_{r_1}^{r_2} 1 + r^2 dr + C_L \int_{r_2}^{r_3} 1 + r^2 dr + C_L \int_{r_4}^{r_5} 1 + r^2 dr + C_{L_{low}} \int_{r_5}^{r_6} 1 + r^2 dr \right) \quad (4.81)$$

Using the variables given in table 4.6, a chord (c) of 0.20 m. and a ρ of 1.2 Kg/m³ and calculating the total lift for a radius of 0 to 5 m. at a rotational velocity (Ω) of 0.5 to 3 rev/s results in figure 4.33. The red line in the graph represents the minimum necessary lift L_{min} which is calculated by

$$L_{min} = 1.2W \quad (4.82)$$

As long as the total generated lift is larger than L_{min} the aircraft should be able to lift off. The graph shows that for example with a radius of 4.5 m. the minimum velocity for a possible lift-off is 0.5 rev/s. while at a radius of 1 m, the velocity has to be as high as 3 rev/s. It also shows that the benefit of increasing the velocity, while increasing the radius returns an increasing value of the total lift. This is due to the fact that at a low radius the total lift coefficient is smaller compared to working at a high radius, because of the aileron settings.

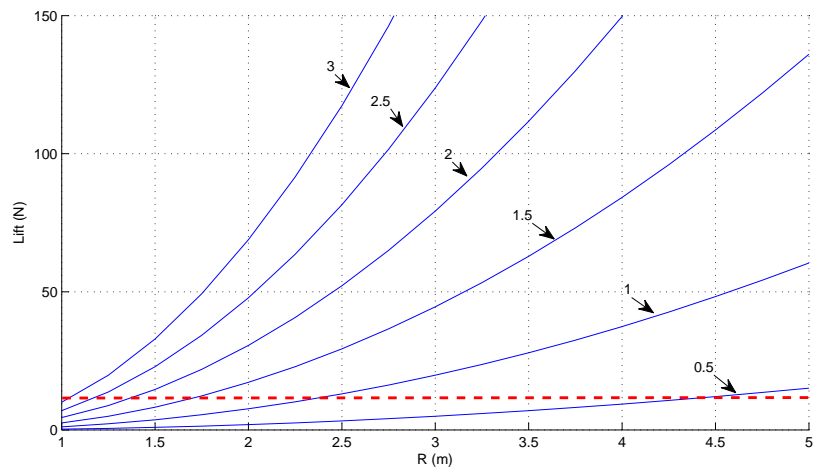


Figure 4.33: Generated lift against radius for different rotational velocities

Conclusion and recommendations

The simplified approach described in this paragraph shows that the ailerons have enough influence on the lift coefficient to control the bank angle of the aircraft, even when rotating at a small radius. The 1 MW aircraft is expected to also have ailerons closer to the root of the wing, decreasing the effect of the 'fixed' C_L (for given angle of attack), therefore this approach is expected to give similar better results (smaller R) in case of the 1 MW aircraft. On the other hand, the wing loading (W/S) is larger, a higher overall velocity will be required. The effect of the ailerons and total lift is expected to be most important for feasibility. Though, the ability of the rudder to keep the yaw moment such that the radius of turn can be kept properly should also be investigated. Due to time restrictions no further research is done on the 1 MW aircraft with this approach.

4.9.4 Test set-up proof of concept with rotating platform

As a proof of concept and to get some hands-on experience and a feeling for launching and landing with a rotating platform, a test set-up is built. The main goal to achieve with this first test is to complete some take-off and landing cycles.

Setup

The set-up for this test is shown in figure 4.34 and consists of:

- A wooden disk, mounted on a steel frame via a vertical axle and a horizontal bearing. The disc is supported by wheels.
- A battery powered DC motor, which drives the disk via a wheel.
- A wooden beam with a tethered pivot-able arm.
- An L-shaped, foam padded cradle.
- A remote controlled winch with 40 meters of nylon cable, holding a strength of up to 100N.
- Two RC controlled model-air planes. A sturdy multiplex Fox and a larger home-made aerobatics air plane with a lower wing loading.

The cable tension keeps the plane in its cradle, as the platform spins up to its desired velocity. Then the cable can be winched out, while the plane is controlled by a RC pilot.



Figure 4.34: Test set-up of rotating platform with aircraft attached

Observations

For a first observation the set-up was tested indoor in a space confined by concrete columns, which were standing 10 meters apart. Therefore the maximum achievable radius to fly without hitting the columns was about 6 meters. Within these limits a full cycle of increasing velocity, reeling out, flying up and reeling in to return the aircraft into its cradle again could be achieved with both aircrafts. The larger plane was able to fly slower and performed more smoothly, while the smaller plane reached a higher altitude. If the aircraft started to oscillate into an unstable pattern, reeling in the cable while increasing the velocity resulted into a stable circular flight again, because of the dominant centrifugal forces.

The outdoor test was performed at a calm day with wind of 1-2 Beaufort. Unfortunately the uneven ground caused the platform to rock back and forth a couple of centimetres, resulting in a slipping wheel and therefore a fluctuating rotational velocity. Because of this, it was not possible to fly the large plane steadily. The Fox however, was able to fly at an increased velocity and even though it started oscillating into a crash every time, it reached a height of about 5 meters, as shown in figure 4.35.



Figure 4.35: Screen shot of field test with rotating platform

Conclusion and recommendations

It was not possible to fly a complete test cycle in outdoor conditions due to the shortcomings of the initial test set-up. Still the indoor test and the achieved height with the outdoor test gave promising results. Before executing other tests, the rotating platform should be improved. Besides that a different bigger aircraft with a lower wing loading would simplify the control of the aircraft in the initial unstable stage of the launch. Even so, it is uncertain if a stable launch can be obtained by manual control. Quick

control actions are necessary to adapt to oscillations. Time delay between seeing what happens, giving the command on the remote control and the actual setting of the control surfaces will make it hard to control the aircraft manually. Therefore an autopilot might be vital for a successful launch.

4.10 Conclusion

Using different methods resulted in an overview of the various functions launching and retrieving the aircraft incorporates. These functions again can be fulfilled by several design options. Some of these options are easy to grasp, others need more extensive analysis. The analysis done in this chapter revealed several options which in the end would never accomplish their function within the requirements. But it also provides partial solutions which seem feasible to use in the final design recommendation, but still need to prove themselves in the big picture. In the next chapter these options are put together in concepts. This chapter provides the basis of these concepts and gives the knowledge required to analyse these concepts as a whole.

Chapter 5

Concepts

Now the main bottlenecks in the functional analysis diagrams are clarified in chapter 4, three main concepts are generated by walking an 'educated path of least resistance' through the functional analysis diagrams. Educated in this sense means making use of the knowledge gathered in the former chapter, intuition and discussion with other people working on the Powerplane. Besides that, the rotating platform concept is partly based on the concept described in an internal document of the company[Lansdorp, 2009]. The paths taken in the functional analysis diagrams are represented by different coloured arrows for every concept, as shown in figure 5.1.

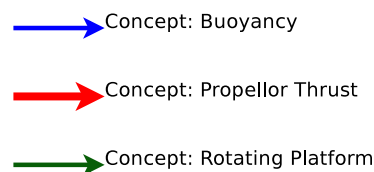


Figure 5.1: Arrows representing the path taken for every concept

The chapter ends with a trade-off in which the concepts are analysed on how they fulfil the requirements, defined in chapter 3. The concept with the highest score in the trade-off is the concept on which deeper analysis will be done in the following chapter to provide the design recommendation for the final system.

5.1 Concept: Buoyancy

This concept will counteract the gravity force on the aircraft with the help of buoyancy. Hydrogen will be used as lifting gas inside a 'zeppelin' shaped balloon. The balloon will keep its shape by either extra pressure or with internal beams. How to cope with gas leakage is not decided yet, but it will probably have a permanent refill tube, so hydrogen generated on the ground can always be pumped into the balloon. This way the height, lifting force and shape of the balloon also can be controlled. The balloon will be attached to the ground by means of two lines with a certain distance between each other and with attachment points on the sides of the balloon in such a way that the path from one to the other line is always perpendicular to the wind. The aircraft will be pulled up with a winch on the ground with a cable through a pulley attached to the balloon, in between the cables. There is an attachment unit which connects the aircraft to the two lines, so it remains in line with the wind speed. When the aircraft reaches the appropriate height, it will be released from the attachment unit to fall down in a diving flight until it reaches its controllable velocity. To land the aircraft will fly into the attachment unit again to be caught from the air, releasing its kinetic energy as described in paragraph 4.4.5. The winch will slowly release the cable to make the aircraft and the attachment unit reach the ground again.

5.2 Concept: Propeller thrust

This concept represents the most conventional approach to launch the aircraft. The aircraft will be attached to a cart on a straight rail. It has the ability to accelerate in two directions, to cope with different wind directions. The cart will accelerate the aircraft to at least its minimum launch velocity. Then the aircraft will be released to fly itself to minimum height with the help of a propeller and a battery powered electro motor. Reaching operational height will be done by reversed pumping or winching (Appendix B) Landing will also take place on the cart which than will be used to decelerate the aircraft. During climbing, and landing, the ground station releases or retracts the cable in such a way that the tension is just enough to keep the cable from getting tangled but does not influence the aircraft its performance too much. Using the cable for positioning while landing is optional.

5.3 Concept: Rotating platform

This concept consists of a carousel which carries the ground station and an aircraft cradle that is attached to a launch arm. A conceptual sketch of this set-up with the ground station is shown in figure 5.2. During launch the carousel spins up to the take off velocity of the aircraft. After achieving this velocity, the tether is reeled out and the aircraft becomes airborne. The carousel keeps on rotating while simultaneously elongating the tether. As soon as the proper length for winching is achieved, the arm goes down and the aircraft reaches its operating height by reeling the tether in and out. Landing is achieved by retracting the aircraft. As soon as the aircraft reaches a proper distance it will fly a circular pattern around the platform. The platform will rotate again to follow this pattern, while retracting the cable until the aircraft lands in its cradle. A conceptual sketch of all steps of this procedure is shown in the following paragraphs.

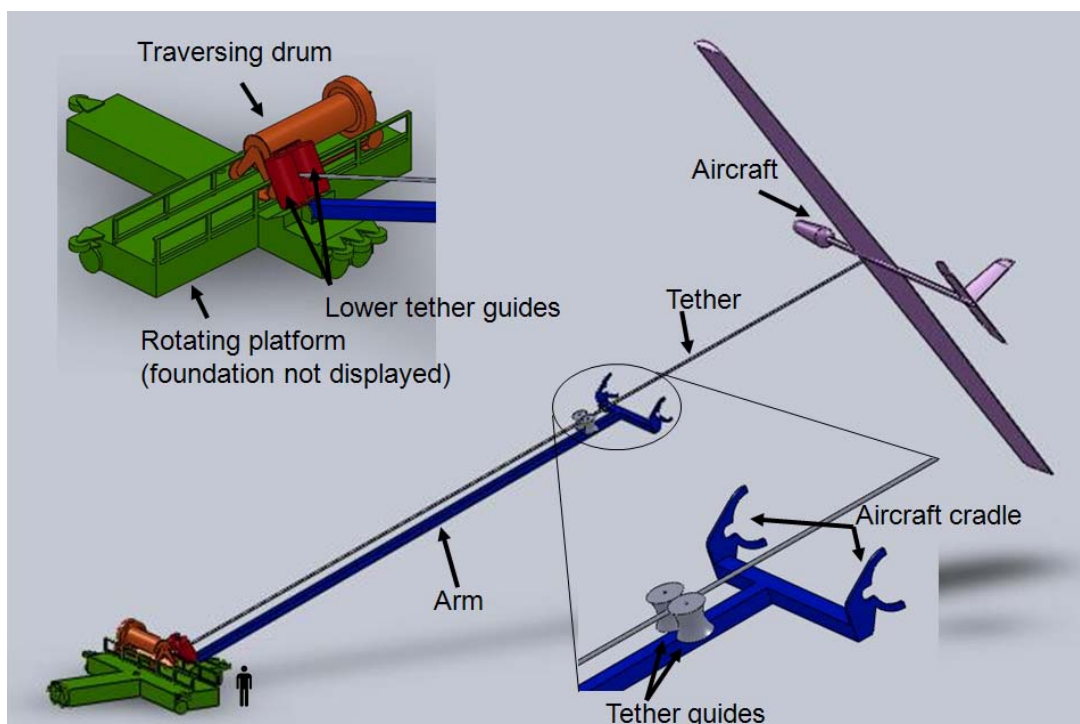


Figure 5.2: Powerplane system with rotating platform

5.4 Operational procedure rotating platform

This paragraph is loosely cited from [Lansdorp, 2009]. In “Idle configuration”, the arm is lowered; the aircraft is horizontal and might be stored in a hangar (5.3, left). Then the system goes into “launch configuration”, where the arm is elevated to the launch altitude and the aircraft is tilted in the right direction. The tether is under tension and the platform is spun up to the launch velocity of the aircraft (5.3, right). During this procedure, the tether guides located on the arm are positioned around the tight

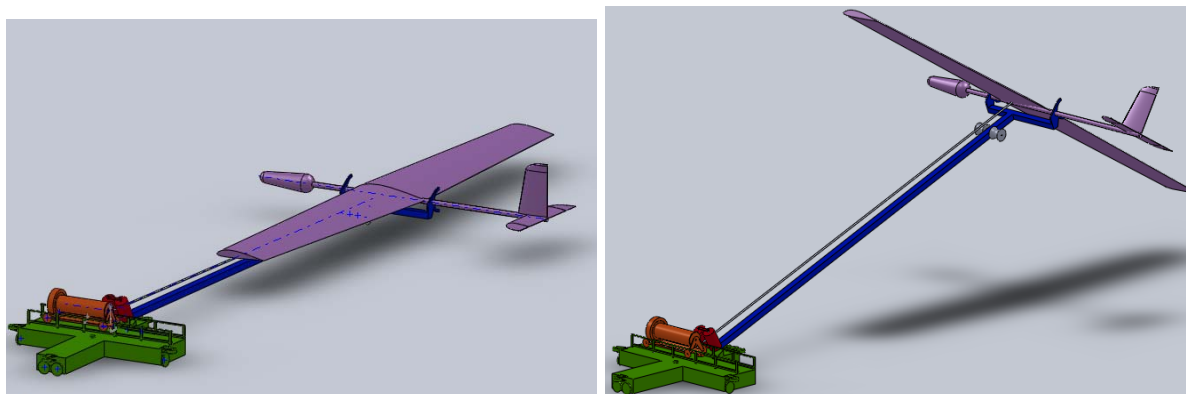


Figure 5.3: left: Idle configuration, right: Launch configuration

tether (Figure 5.4, left). Then take-off takes place by extending the tether such that the aircraft takes off from the support (Figure 5.4, right). While the tether is released, the aircraft slowly moves backward

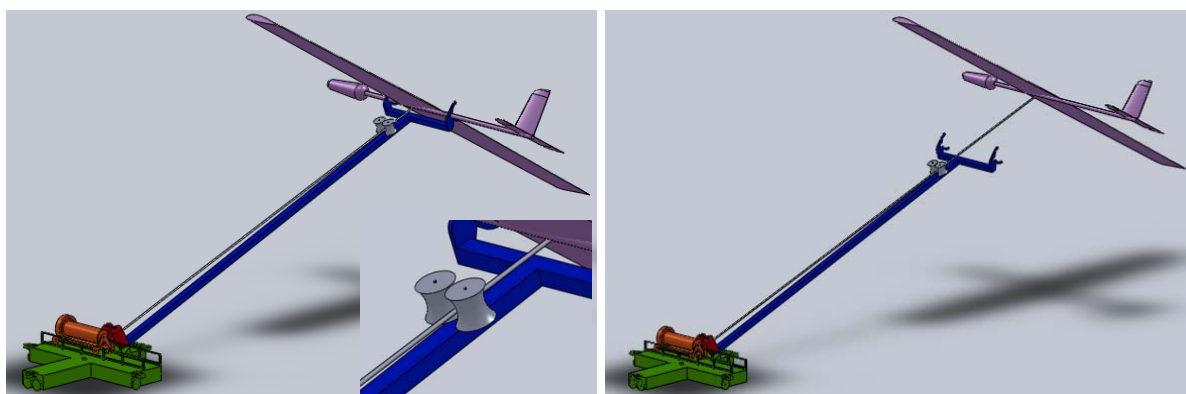


Figure 5.4: left: Tether guide positioning, right: Take-off

compared to the arm, because the arm is pulling the aircraft forward (Figure 5.5, left). When the target tether length is achieved, the angle between the arm and the tether (lag angle) is almost 90 degrees. The rotation of the platform is stopped such that the arm is exactly in the downwind direction (Figure 5.5, right).

With the rotation of the platform stopped, the angle between the tether and the arm decreases until it is around 0 degrees (Figure 5.6, left). At this moment, one of the tether guides at the arm is lowered, such that the tether can continue in the direction of flight of the aircraft while the arm is standing still (Figure 5.6, right).

Then the arm is lowered out of the flight path of the tether (Figure 5.7, left). The aircraft can now use the wind to extend the tether to operating length while flying patterns in the sky. When the operating length is achieved, power production is begun (Figure 5.7, right).

The figure shows an illustration of figure 8 pattern flying. The actual optimized flight path will only loosely resemble the here depicted flight path. The aircraft flies cross wind patterns to maximize the tether tension. The tether is pulled from the generator windlass drum, causing the generator to rotate and produce electrical power. This sequence will approximately take 1 minute. The tether will be pulled

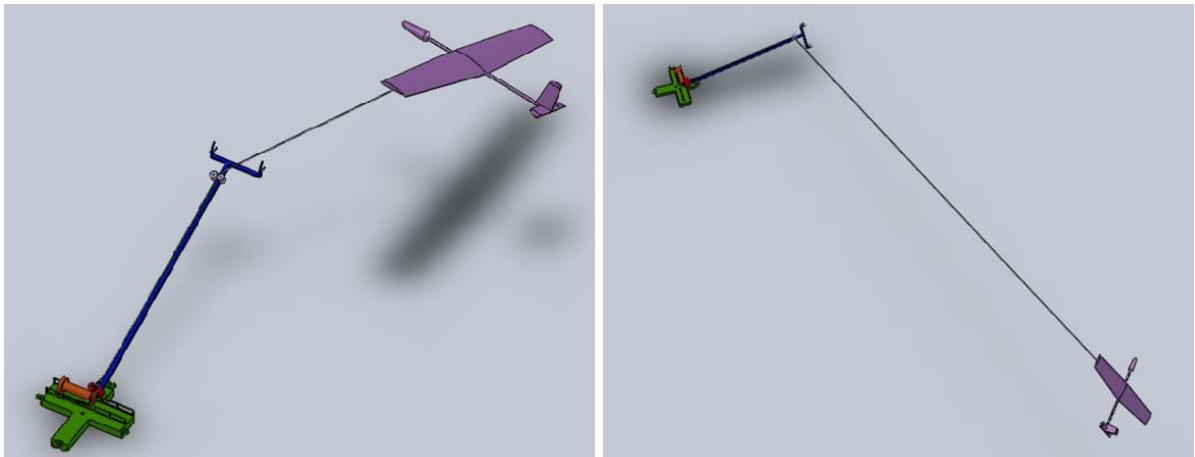


Figure 5.5: left: Tether elongation, right: Target tether length

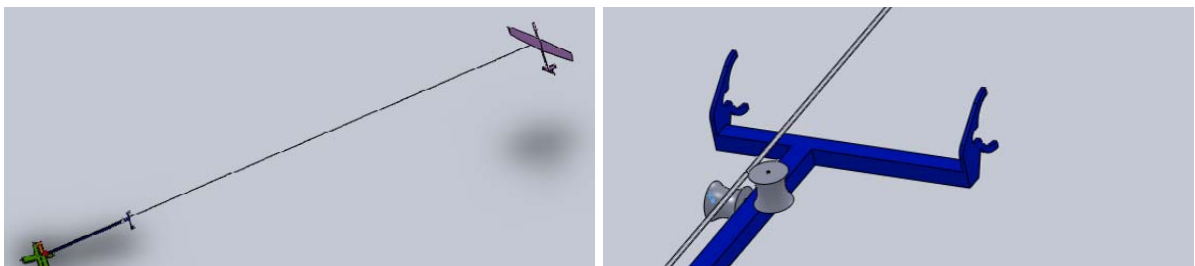


Figure 5.6: left: Tether straightening, right: Arm tether guide release

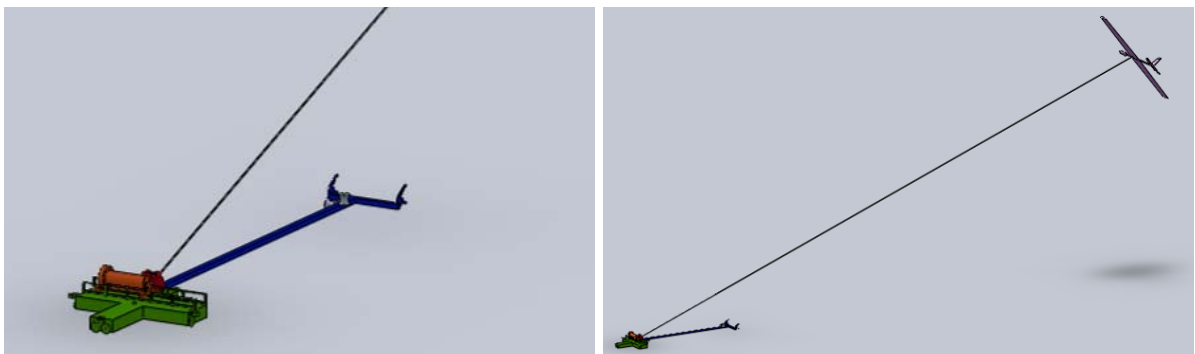


Figure 5.7: left: Arm lowering, right: Tether extension

from the windlass drum with a velocity close to $1/3$ the wind velocity (Figure 5.8, left). During retraction the aircraft dives towards the ground station, while the windlass drum retracts the tether. This phase takes about 10 seconds. The aircraft attitude is set to produce low lift and therefore the tether tension is minimal (Figure 5.8, right).

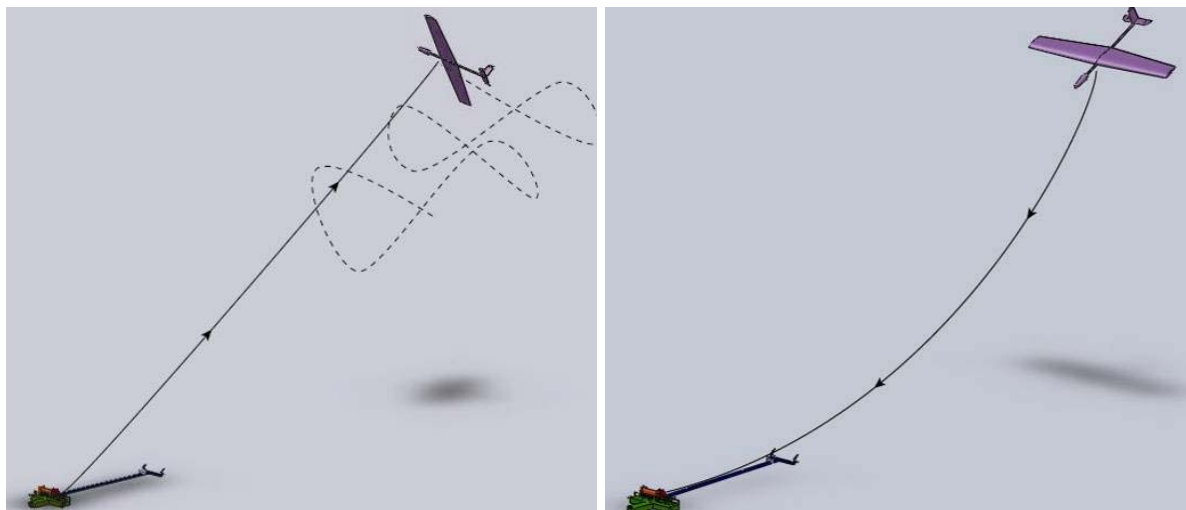


Figure 5.8: left: Power production, right Tether retraction

To land the aircraft, it is steered into a circular flight path around the launch platform. The arm is elevated to the altitude of the tether (Figure 5.9, left). The arm tether guides are positioned around the tether (Figure 5.9, right).

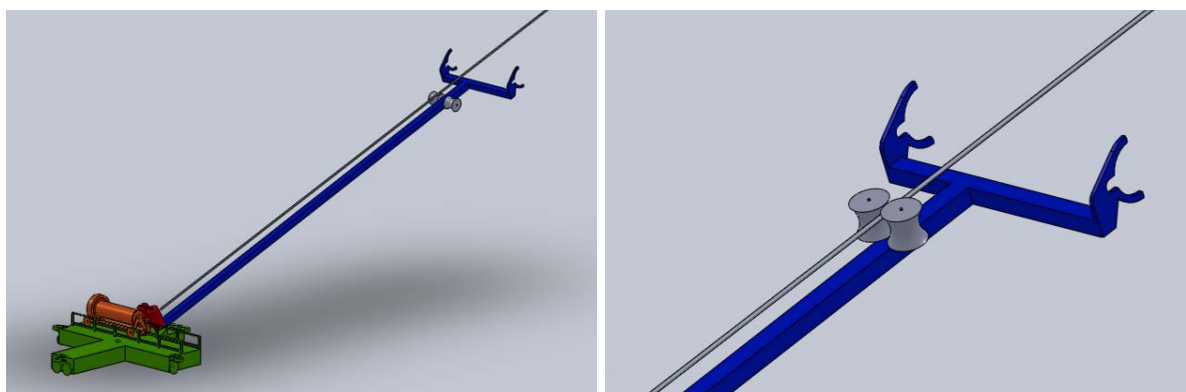


Figure 5.9: left; Landing procedure, right; Tether catching

When the guides are at the right position, the tether is retracted. During tether retraction the tether remains straight because the tether is not driving the aircraft. The aircraft is slowed down by its drag (Figure 5.10, left). The tether is further retracted until the aircraft touches down on the arm (Figure 5.10, right).

Then tether is tensioned and the arm tether guides are disengaged (Figure 5.11, left). Subsequently the platform is spun down and the arm is lowered (Figure 5.11, right).

5.5 Comparison

Even though all three concepts differ fundamentally in their approach of accomplishing the main function, it is hard to predict which one meets the requirements in the most desirable way. To facilitate this process a trade-off is made (table 5.1. The chart represents the main requirements where the importance of these

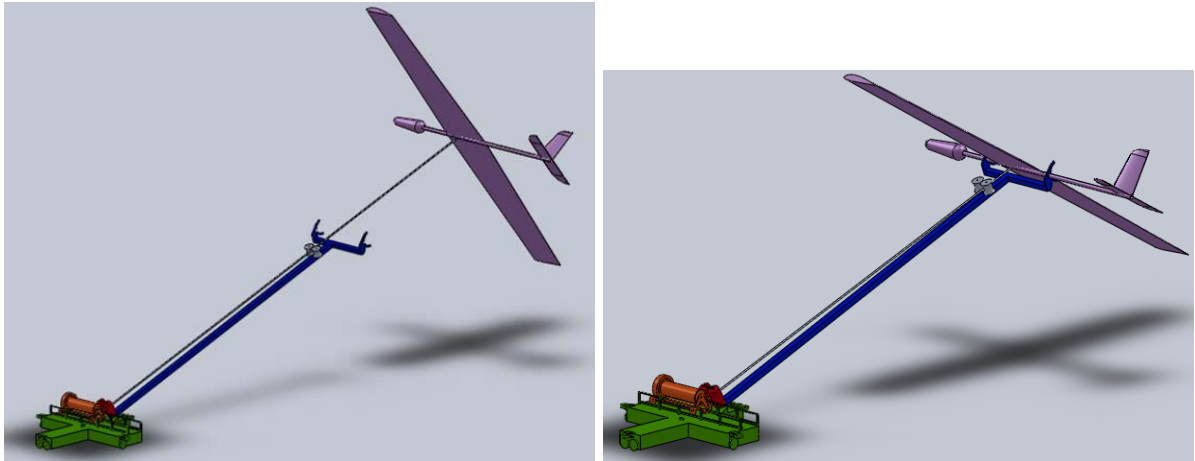


Figure 5.10: left; Tether retraction, right; touchdown

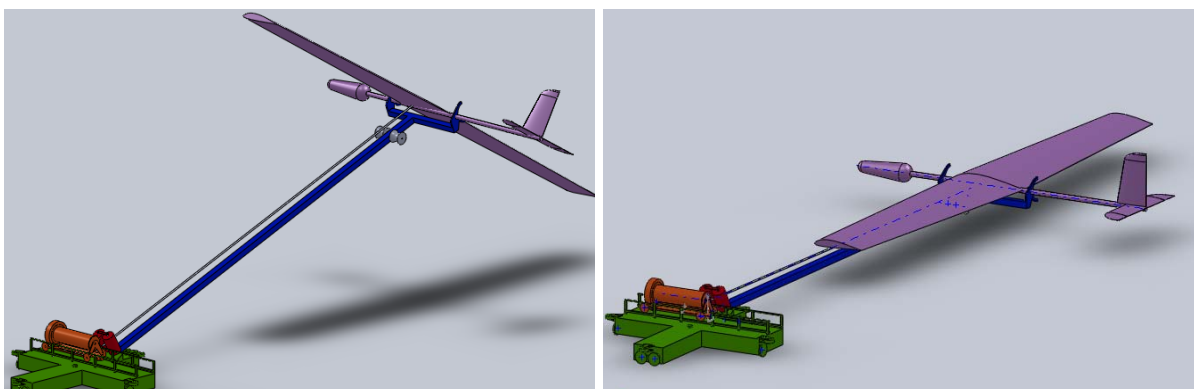


Figure 5.11: left; Arm tether guide disconnection, right; Idle configuration

requirements is graded with a weight factor of 1 to 5. Every concept is graded on how it meets a given requirement, where 1 is a low and 5 is a high score. The weighed total results in a score of 0 to 100. The highest score represents the best concept. Next to the requirements of chapter 3 “Technological risk” is added to the chart. This point is related to how much the concept makes use of proven technology.

Table 5.1: Trade-off concepts

	Factor	Buoyancy	Propeller thrust	Rotating platform
Aircraft related requirements				
Main dimensions	5	5	5	5
Minimum velocity	2	3	5	4
Maximum velocity	5	5	5	5
Maximum acceleration	5	5	5	5
Landing controllability	5	5	5	5
Additional weight on aircraft	3	5	2	5
Operational boundaries				
Minimum altitude/ cable length	5	5	4	4
Operating conditions	3	3	4	5
Time span for launching	2	3	5	5
Time span for landing	4	3	5	5
Forces on aircraft	3	5	5	5
Extreme forces	5	4	5	4
Peripheral requirements				
Prepared for park setup	4	3	4	5
Operating area	4	3	4	4
Autonomous operation	5	3	5	4
Safety	5	3	4	4
Lifetime	4	3	4	4
Initial cost	5	2	4	4
Operational cost	5	2	3	4
Reliability	5	2	3	4
Cable wear	5	3	5	3
Technological risk	5	2	4	3
Weighed total		69	87	86

5.6 Discussion of trade-off results

All concepts have a relatively high total score. This is simply due to the fact that all concepts are defined to be able to meet the requirements. The small differences are briefly discussed in the following paragraphs.

5.6.1 Aircraft related requirements

On these requirements, scores are quite equal for all concepts. The buoyancy concept has a low score on the minimum velocity, since at the moment the aircraft is released it flies below its minimum velocity for some time, making this a tricky part of the procedure. In case of the rotating platform, unforeseen wind gusts in combination with a big lag angle could also cause the aircraft to get below the minimum velocity. The concept with the propeller scores low on the additional weight requirement since the propeller, motor and batteries add a significant amount of weight to the aircraft.

5.6.2 Operational boundaries

With the buoyancy concept, its quite certain the aircraft reaches operational altitude. The other two concepts both rely on the winching or reverse pumping procedure, which adds some uncertainty, therefore their score is a bit lower on this requirement. The buoyancy concept is more sensitive to weather conditions. The wind direction is no issue to the rotating platform, while it could effect the propeller concept, since it only has two launch directions. The time it takes for landing and launching is expected to be more for the buoyancy concept. Extreme forces on the aircraft are expected to be negligible in case of flying with a propeller. For buoyancy, docking in the sky and the free fall could lead to extreme forces. With the rotating platform their might be unforeseen cases where a sudden high tether tension can take place.

5.6.3 Peripheral requirements

The buoyancy concept has more additional parts that require airspace, have a chance of breaking down, need to be controlled, and have their initial and operational costs. Therefore this concept scores low on these requirements. The propeller driven concept relies very much on batteries, causing it to score average on reliability and operational cost. On the other hand, low cable wear is a strong point of this concept. Besides that flying up with a propeller is a proven technology and therefore has the lowest technological risk.

5.7 Conclusion

Three concepts are defined in this chapter. One based on buoyancy, a concept making use of propeller thrust and one which uses a rotational platform to launch the aircraft. Using a trade-off chart revealed that the buoyancy concept stays very much behind the other two concepts. But the "Rotating platform" and the "Propeller thrust" option come out very close. For this reason no decision on these two concepts is made based on the chart. More research will be done on both options in the following chapters.

Chapter 6

Climbing with aircraft thrust

The comparison of the different concepts turned into a very small difference between the rotating platform and the propeller climb. Therefore more research on these different concepts should be done. In this chapter more practical things such as winch operation and the flight path are investigated. Besides that, the concept of flying with propeller thrust is improved by eliminating its weaker parts and adding strong parts of the rotating arm concept.

6.1 Winch limitations

Reeling out the cable should take place in such a manner that it should not hinder the aircraft too much, as cable tension must be balanced with thrust. Therefore the reel out velocity should be relatively similar to the aircraft velocity. For an estimation of the maximum required reel velocity two scenarios are possible.

- Flying with headwind: In this case the maximum reel velocity is required when there is negligible wind, so the total velocity relative to the aircraft is fully defined by the winch. This results in a velocity equal to V_{min} which is 22 m/s
- Flying with tailwind: For launching with tail wind the maximum reel out speed takes place with maximum wind. Now maximum wind speed of 14 m/s is added to the V_{min} , resulting in a maximum reel out speed of 36 m/s

Paragraph 2.2 describes that the winch will be designed for an operational velocity of 900 RPM during the retraction phase [Lansdorp, 2009], the drum diameter of the winch will be approximately 0.5 meter. This means that for energy generation, the winch is designed to reel out at a maximum speed of 23.6 m/s. Therefore no special measures for the winch have to be taken to launch with headwind. Launching with tailwind on the other hand, does require modifications.

6.2 Different approach to minimum height

As described in chapter 3, launching should take place to lengthen the cable until it is long enough for winching up the aircraft. This does not necessarily have to be at a height of 200 meters. When the aircraft flies away to one of the corners of the field, and the ground station is in the center, it can already reach a distance of more than 400 meters. In this case the cable is long enough for winching while the height remains below the specifications. The minimum height is based on the aircraft properties now, as for winching the aircraft has to make a turn of 180 °before it reaches the limits of its area. To be able to make this turn, it needs a minimum manoeuvre height. This height is estimated to be 1.5 times the wingspan, so about 53 meters. Using this procedure means less battery energy is required for climbing, resulting in a weight and cost reduction.

6.2.1 Flight path

A certain flight trajectory must be followed to stay within the operating area, which is limited to a patch of 600 x 600 m. Moreover the aircraft thrust and energy reserves should be as small as possible to reduce weight and cost. Besides that, the system should operate at a range of different wind conditions.

6.2.2 Launch with headwind

In terms of energy and winch parameters, a headwind launch seems to be the best option. But having a headwind start means that the aircraft must circle the ground station to be winched with headwind as well. Figure 6.1 shows a possible trajectory for this flight. The aircraft starts at the ground station, then it flies to the corner of the field, where it makes a turn with a large radius. This radius will be at least 80 meters, so the bank angle remains below 30°, as described in paragraph 4.9.1. Consequently not too much lift will be lost, giving the possibility to maintain a velocity below 25 m/s. After reaching the other end of the field (blue dot in the figure), winching or reverse pumping will start. The climb rate required to reach a height of 53 m. before making the turn is calculated by

$$RC = \frac{V_{\infty} h_{min}}{d_{climb}} \quad (6.1)$$

With a d_{climb} of 350 m. and a V_{∞} of 22 m/s, RC becomes 3.3. Which means that the motor weight and cost as calculated in chapter 4.5 remain within the requirements when using average values. Launching with headwind does requires battery energy to fly the half circle to the other side of the field. The energy required for this flight can be calculated by adding a climb of 53 meters to 1000 m of cruising flight. The equations from paragraph 4.5 can be used to calculate the energy of the climb part by climbing with a rate of 3.3 until d_{climb} is reached. This gives a climbtime t_{climb} of 16 seconds with a shaft power of 221 W resulting in a battery energy need of nearly 1 kWh. The cruising flight part can be calculated by only taking the cable and the aircraft drag into account. The V_{∞} is increased to 23 m/s to compensate for the banked turn. The aircraft will fly this path in 43 seconds t_{fly} with a power of 95 kW, which results in 1.3 kWh of battery power. So the total energy need and battery mass for this procedure becomes respectively 2.3 kWh and 18 kg. With a motor of 220 kW, weighing about 90 kg.

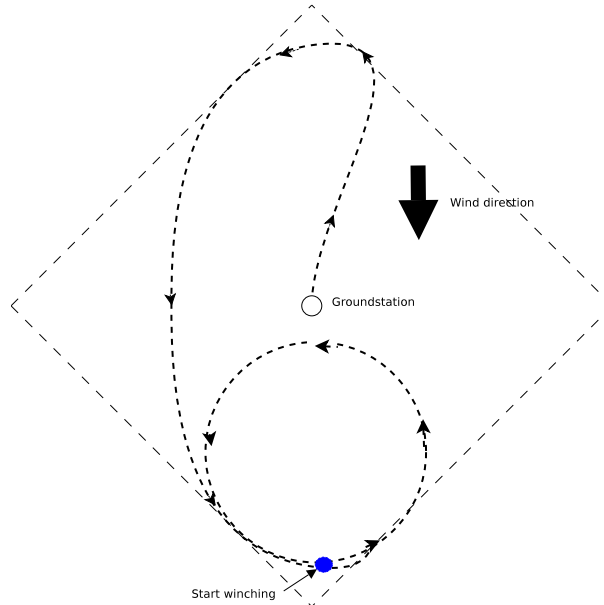


Figure 6.1: Trajectory for starting with headwind

6.2.3 Launch with tailwind

Launching the aircraft with the wind in the back, means that the optimum aircraft velocity (V_∞) will be added to the wind velocity (V_w) to calculate the velocity relative to the ground (V_g). As the ground speed increases, the aircraft reaches the end of its operating area faster, which means that a larger RC is required. In case of maximum wind V_w of 14 m/s, RC is calculated with

$$RC = \frac{(V_\infty + V_w)h_{min}}{d_{climb}} \quad (6.2)$$

Resulting in an RC of 5.5 m/s. Figures 4.17 and 4.18 show that weight and cost for such an RC remain within the requirements, but this option involves a bigger adaptation of the winch and aircraft. Also a higher acceleration is required for launching, resulting in a bigger system and larger forces on the aircraft. The only advantage of this approach is saving 1.3kWh of battery power, which is required for making the turn. Therefore launching with headwind is preferred.

6.3 Climbing to operational altitude with aircraft thrust only

The installed battery energy and motor power can be optimized for weight and cost by with optimizing the collaboration of aircraft and winch. But the other way around, operation can be simplified by using the aircraft thrust only to climb to operational altitude. To estimate an optimum weight and cost for this approach, the calculations of paragraph 4.5 are repeated with an end height (H_e) of 500m. The aircraft starts flying a similar trajectory as in figure 6.1, but instead of flying small circles on one side of the ground station, circles with a 300 meter radius are made until operational height is achieved. This results in a cost and weight graph as function of the climb rate as shown in figure 6.2.

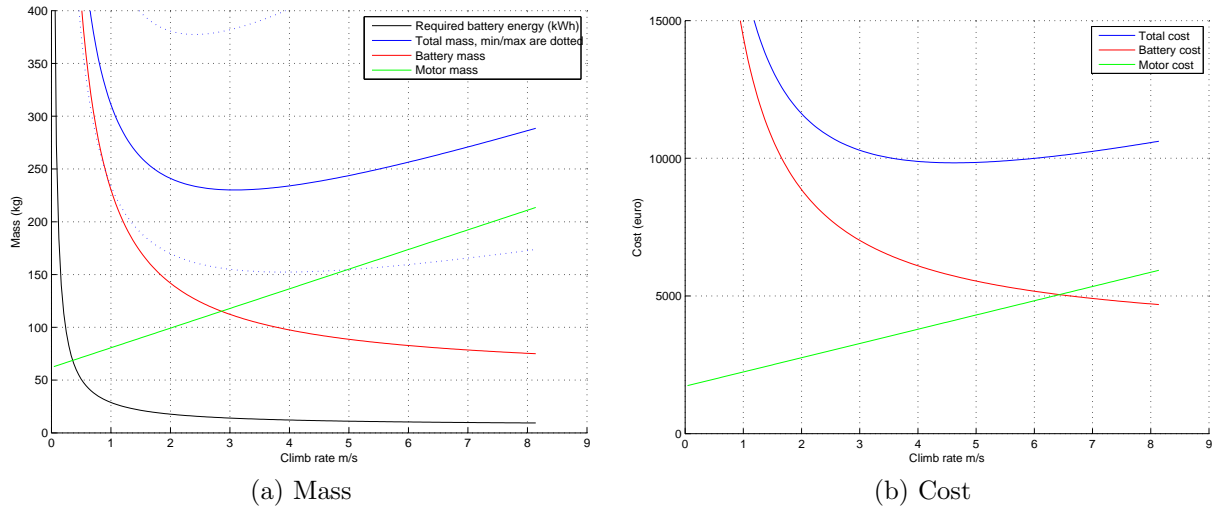


Figure 6.2: Required Mass and Cost as function of climb rate when flying to 500m. altitude

When RC is chosen to be 3.3 m/s, the required shaft power is around 315 kW and almost 13.3 kWh must be available from batteries. In this case it takes about 150 seconds to reach an altitude of 500 meters, while the aircraft has made almost 2 circles around the ground station. Figure 6.2 shows that with an estimated cost of just more than 10 k€ and a weight below 250 kg for motor and batteries together this option can be quite attractive, even though it does not comply with the weight requirements.

6.4 Launch with a circular track

One of the main advantages of using a circular track is the fact that the such a track has infinite length. Hence the ground run distance in this case is not an issue. Therefore combining such a track with a propeller climb means that the power for climbing is also sufficient for reaching lift off velocity V_{LOF} .

Besides that, take off can take place at any location on the track, in any direction. For a conventional launch, the centrifugal forces are a big disadvantage of using such a track, but since the tether can easily balance the centrifugal force as soon as the aircraft takes off, this is not such an issue. Figure 4.21 illustrates that in case a 300 kW motor is used, launch distance becomes around 75 meter. The energy of around .5 kWh for accelerating to V_{LOF} (figure 4.22) could either be stored in batteries or supplied to the aircraft via a ground connection.

6.5 Improved Propeller thrust concept

Combining the findings from the former paragraphs and the concept described in paragraph 5.2, provides an improved propeller launch concept. This concept is only powered by its own propeller and motor and makes use of a circular path instead of a straight path with two directions. The circular track can be made by a kind of roller coaster rail. On this rail a light weight attachment device can run freely, with low friction in the rotational direction, but in any other direction it is locked so it will not come off the track. The function of the attachment device is to hold the aircraft during launching and landing (figure 6.3). On the ground, battery charging takes place by means of a grid connection. As soon as the aircraft is able to fly its energy generating patterns, the batteries are charged again by using the propeller as a turbine and the motor as generator.

6.5.1 Launch and climb

Acceleration takes place as shown in figure 6.3a. The aircraft is held by the attachment unit and accelerates in a circular path by means of its own propeller until it reaches lift off velocity, while heaving a headwind heading. At this moment it is released from the attachment unit and flies a relatively straight path with headwind (figure 6.3). Before it reaches the end of the operating area, it makes a turn to climb further by means of a circular path just within the borders of the operating area.

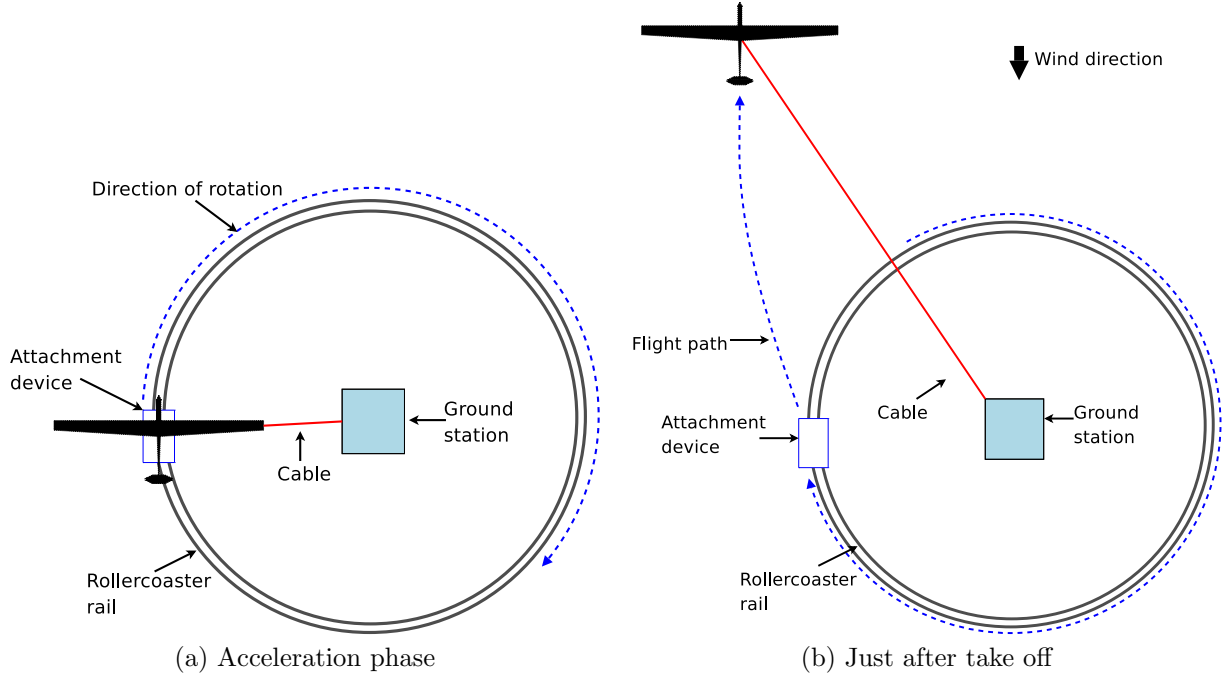


Figure 6.3: Schematic representation of launch device making use of a circular track and propeller thrust

6.5.2 Landing on a circular track

When the aircraft still has significant distance from the ground-station, it is controlled such that cable tension is low. At this moment the cable is lead through the attachment unit by means of a system later

to be defined. Landing is initiated by making the aircraft fly a circular path around the ground station while reeling in the cable. The lightweight attachment unit follows this path since it is being pulled by the cable and has the ability to move with very low friction. Cable reel in continues until the aircraft and the attachment unit their positions coincide. Now braking takes place by using the propeller reversibly until the aircraft stands still.

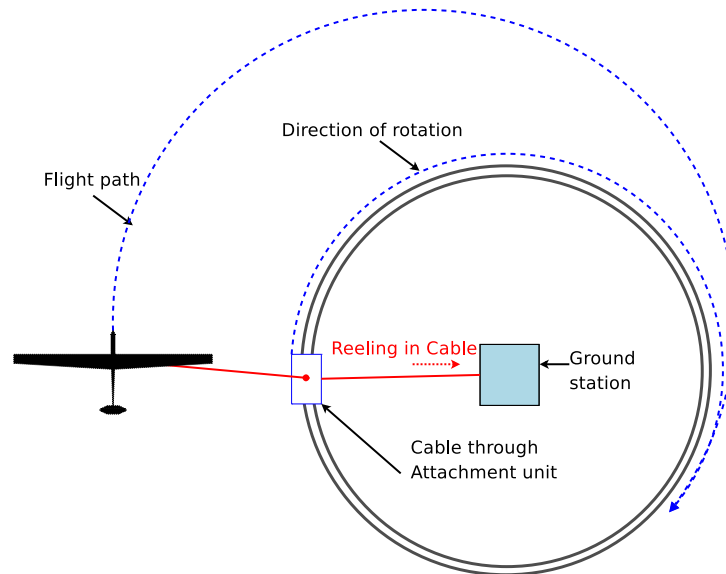


Figure 6.4: Landing on circular track with help of cable

6.5.3 Discussion of concept

The main advantages of this approach are

- The driving force for acceleration, climbing and deceleration relies on one system only. This improves the reliability and the simplicity of the total concept.
- Even though the use of an electric motor with battery power is relatively new, the use of such a system for accelerating an aircraft and climbing to a certain altitude can be regarded as proven technology.
- Using a rotational path facilitates launching and landing with wind coming from any direction.
- Having a propulsion system on the aircraft increases controllability of the aircraft. Making the Powerplane a saver system in general.

The main disadvantage is that the added weight of batteries, motor, propeller and related equipment to the aircraft could effect the system performance during power production. The importance of the drawback can only be found by a more extensive research on the Powerplane concept itself. This research lies beyond the scope of this thesis. Further on the calculations on which the power and energy requirements are based rely on several (carefully made) assumptions. A recommendation is to support the calculations by simulating the take off, fly-out and land manoeuvre in a simulation environment.

6.6 Conclusion

The concept of propeller thrust is improved such that it has clear advantages compared to the concept described in chapter 5. The disadvantage of increased weight requires more analysis in future research. Before real statements can be made on how this concept relates itself to the rotating platform, the rotating launch is analysed more deeply in the following chapter.

Chapter 7

Simulation of a rotating launch

As described in paragraph 4.9.4, a physical test might be hard to do without the help of an autopilot. This conclusion is supported by research of the Kite Power Group of the KU-Leuven [KU-Leuven, 2010]. A masters student in this group built and tested a research set-up for a rotating launch based on computer vision [Geebelen and Gillis, 2010]. What this system consists of, is shown in figure 7.1. A model aircraft is equipped with different coloured LEDs, which are monitored by a camera and recognition system. This way the attitude of the aircraft can be estimated without the need of an IMU, GPS or any other system, keeping the set-up simple and lightweight. Further research will be mainly based on finding stable conditions in which the aircraft could increase height without the need of an autopilot, but only by changing the rotational velocity. Especially when wind influences the orbit, this will be hard to obtain. Even though this is an interesting approach, the Powerplane is equipped with an autopilot anyway, so why not make use of it? To investigate how the aircraft can be launched by means of a rotating platform with the help of an autopilot, a Matlab Simulink simulation is utilized. This chapter discusses what this model consists of, how the simulation is done and finally comes up with some results and recommendations.

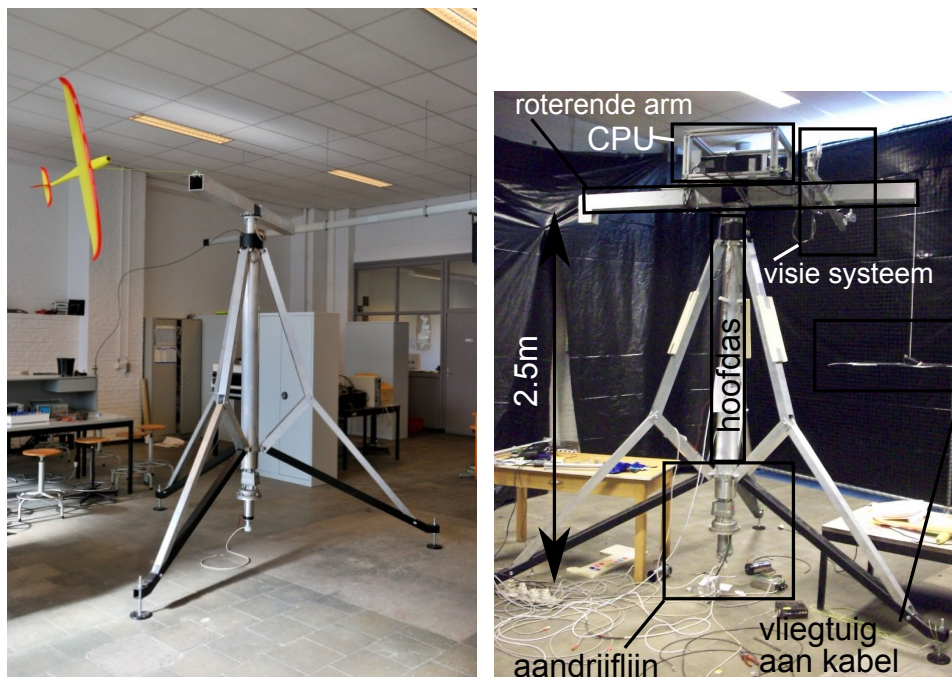


Figure 7.1: Test set-up of Kite Power Group with (right) and without measurement system (left) [Geebelen and Gillis, 2010]

7.1 Simulation model

Chapter 1 described that the Powerplane will operate as a completely autonomous system. Therefore the aircraft requires a safe, reliable and rigid autopilot. To set-up and test this autopilot a simulator is built in MATLAB-Simulink. This simulator is called AGENT, which stands for Atmospheric GEneric Non-linear Table-base simulator. It contains three types of databases, the aerodynamic database, the geometric database and the mass database. Ampyx currently optimizes the databases of the 10 kW test aircraft by performing flight patterns based on fixed commands and logging the resulting attitude of the aircraft. Besides using it for this system identification, the architecture of AGENT is such that it can easily be expanded to different environments [Sieberling, 2009]. The simulation of a launch with a rotating platform therefore can also be accomplished with the help of this model.

7.1.1 Model structure

AGENT consists of seven basic building blocks as shown in figure 7.2. Each block performs its particular part of the simulation. All blocks together form a closed loop which simulates the non-linear behaviour of the aircraft. Figure 7.2 also illustrates how the simulation consists of four basis vectors that enter most states, known as:

- State vector: Contains aircraft states such as the angles of attack and side-slip and position, velocity and heading, static and dynamic pressures, but also cable tension and length, lag and launch angle, wind velocity etcetera.
- Mass vector: Contains information on the mass (M), the centre of gravity (CG) and the inertia (J).
- Control vector: Contains all control settings, δ_a for the ailerons, δ_e is the elevator, δ_r for rudder. In case of additional thrust on the aircraft δ_t is the trust setting. When spoilers end flaps are used δ_s and δ_f define these settings. Finally the landing gear is set by δ_g
- Acceleration vector: Contains translational (XYZ) and rotational accelerations (LMN)

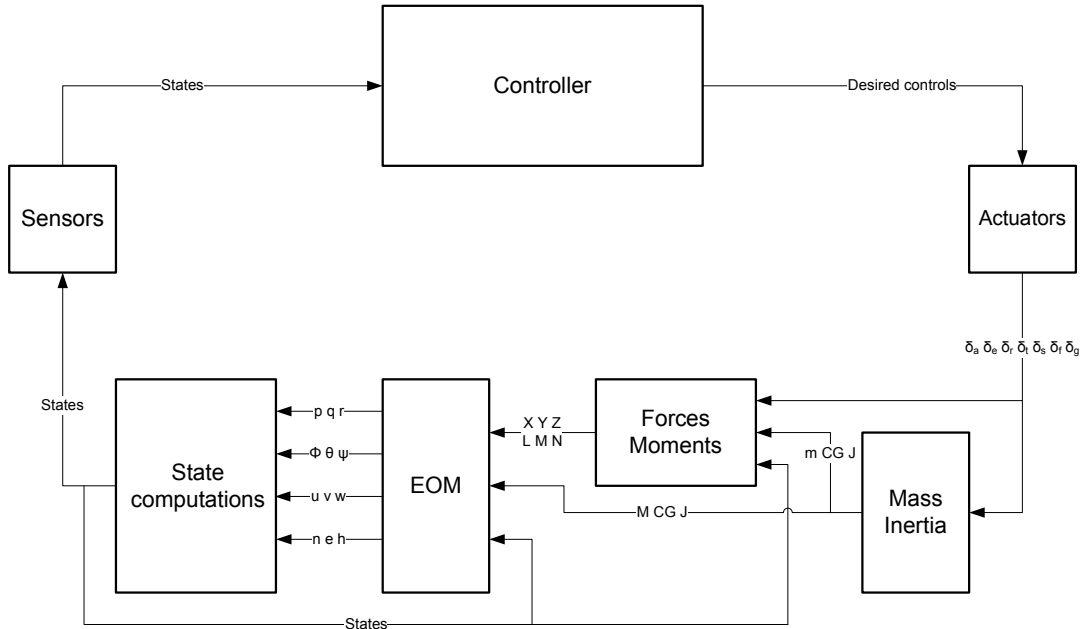


Figure 7.2: Block diagram of simulation environment AGENT

The following sections briefly describe the mathematical background of each block, drawn in figure 7.2. These descriptions are for quick reference only. More extensive information about the AGENT

simulator itself can be found in [Sieberling, 2009] which is also the main source of this content. To acquire a full derivation of the formulas used in these paragraphs [Mulder et al., 2006] provides extensive information.

7.1.2 Mass and inertia block

A regular aircraft consumes fuel during flight. The change of mass and also the variation in center of gravity due to this fuel usage is an important issue. In case of the Powerplane fuel consumption will not take occur, thus mass (m_{total}) is assumed to be constant. The mass of the tether is modeled as an external force on the aircraft. Therefore the actual inertia of the flying aircraft is similar to the empty weight inertia, which is provided in table 7.1

Table 7.1: Moments of Inertia of different Powerplanes

	10kW	1 MW
J_{xx}	34.51	131000
J_{yy}	23.19	91000
J_{zz}	57.08	21000
J_{xz}	0.11	11

7.1.3 Forces and Moments block

The computations behind this block all result in forces and moments. The inputs are the mass properties, control settings and the states. From these inputs stability and control derivatives are obtained and force and moment coefficients are made dimensional by means of lookup tables. Also the forces produced by gravity and tether tension are computed. The main sub blocks behind this Forces and Moments block are described in the following paragraphs.

Lookup tables

The lookup tables contain information about the aircraft in a non-dimensional form. For this reason the inputs to the lookup tables need to be non-dimensionalised correctly. [Mulder et al., 2006, Tables 4.1 to 4.8] show lists of how rates can be non-dimensionalised. For example the roll rate (r) which has the dimension t^{-1} becomes non-dimensional by making use of the wing span (b) and the velocity (V) as

$$r_{non-dimensional} = \frac{rb}{2V} \quad (7.1)$$

The pitch rate (q) can be non-dimensionalised by means of the mean aerodynamic chord (\bar{c}) and V .

$$q_{non-dimensional} = \frac{q\bar{c}}{V} \quad (7.2)$$

Multiplying the force coefficients with $0.5\rho V^2 S$ and the longitudinal and lateral moment coefficients with $0.5\rho V^2 Sc$ or $0.5\rho V^2 Sb$ provides the dimensional forces again.

Gravity

The gravity force acting on the aircraft is simply mass (m) times earth gravitational acceleration (g). This force acts along the Z axis of the vehicle carried normal earth reference frame (F_O) while the directions of the aircraft (X_b, Y_b and Z_b) are in the body fixed reference frame (F_B). The transformation matrix T_{BO} below is used to transform the gravity to the proper frame. A derivation of T_{BO} can be found in [Sieberling, 2009, Appendix C]. Figure 7.3 shows how this matrix is built up by means of three rotations of ψ , θ and ϕ .

$$F_B = T_{BO}F_O = \begin{bmatrix} \cos\theta\cos\psi & \cos\theta\sin\psi & -\sin\theta \\ \sin\phi\sin\theta\cos\psi - \cos\phi\sin\psi & \sin\phi\sin\theta\sin\psi + \cos\phi\cos\psi & \sin\phi\cos\theta \\ \cos\phi\sin\theta\cos\psi + \sin\phi\sin\psi & \cos\phi\sin\theta\sin\psi - \sin\phi\cos\psi & \cos\phi\cos\theta \end{bmatrix} \begin{bmatrix} 0 \\ 0 \\ mg \end{bmatrix} \quad (7.3)$$

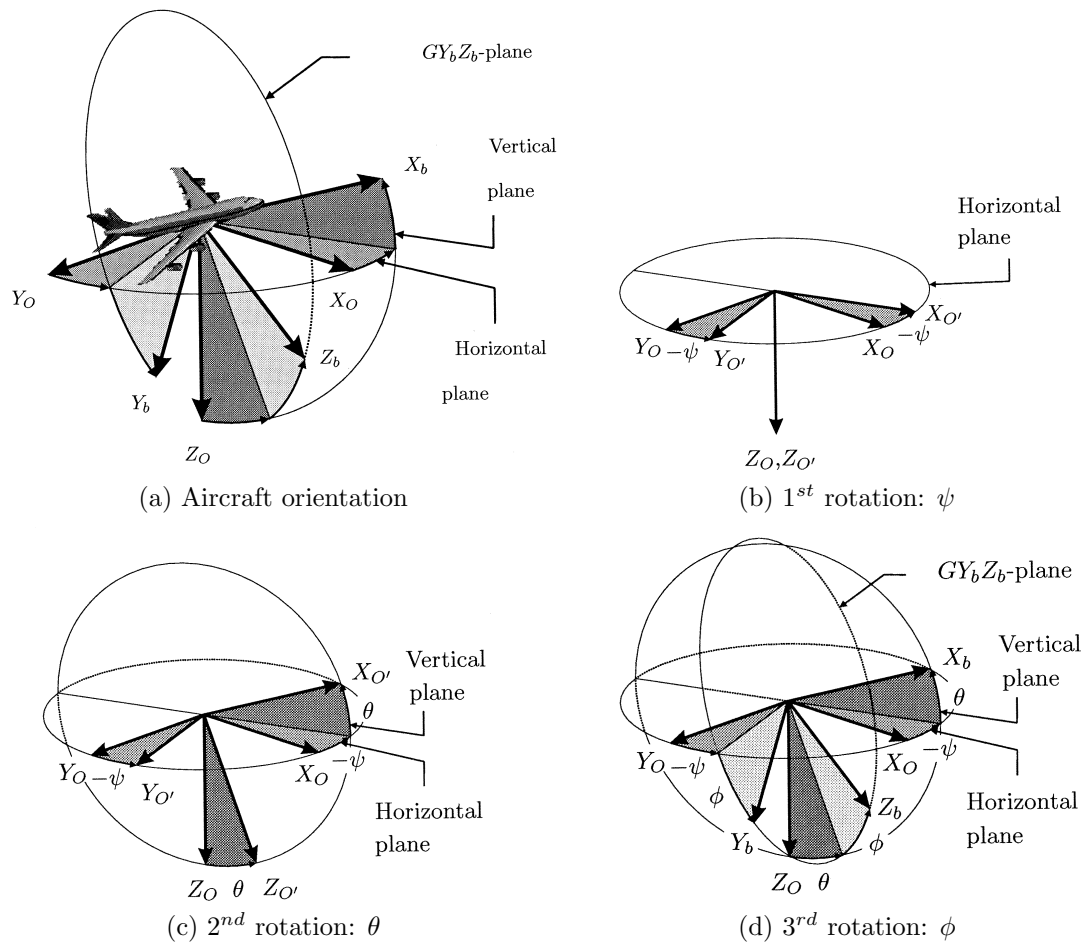


Figure 7.3: Transformation from vehicle carried normal earth reference frame F_O to the body fixed reference frame F_b , from [Mulder et al., 2006]

As already described the gravity force only acts in the Z_O direction, therefore the gravity force F_B can be simplified to

$$F_B = mg \begin{bmatrix} -\sin\theta \\ \sin\phi\cos\theta \\ \cos\phi\cos\theta \end{bmatrix} \quad (7.4)$$

Engines

An engine (for example a battery powered electric motor) could be used for additional thrust. The engine forces are computed by scaling the throttle setting, which is a number between 0 and 1, with the maximum thrust. The force is acting along the body fixed X-axis. To increase realism rate saturation and a delay on the engine response are also implemented in this block. The moments produced by the engine is the force multiplied by the distance to the CG

$$\bar{M}_{engine} = (\bar{x}_{engine} - \bar{x}_{CG}) \times \bar{F}_{engine} \quad (7.5)$$

7.1.4 Equations of Motion

The computations around the equations of motion in the body fixed reference frame are handled in this block. The translational dynamic equations of motion are a combination of the resulting gravity vector, the aircraft mass and the accelerations in the X_b, Y_b and Z_b direction, \dot{u}, \dot{v} and \dot{w} . Where the upper-dot defines that the time derivative of the underlying parameter is used. p, q , and r are the rotational rate of the aircraft around the X_B, Y_B and Z_B axes, which also effect the relative displacements of the aircraft. are the accelerations of the The dynamic and kinematic relations of the translational equations of motion are shown in equation 7.6 and 7.7. Where 7.7 consists of a transformation matrix, comparable to the one in 7.3.

$$\begin{bmatrix} \dot{u} \\ \dot{v} \\ \dot{w} \end{bmatrix} = g \begin{bmatrix} -\sin\theta \\ \sin\phi\cos\theta \\ \cos\phi\cos\theta \end{bmatrix} + \frac{1}{m} \begin{bmatrix} X \\ Y \\ Z \end{bmatrix} - \begin{bmatrix} qw - rv \\ ru - pw \\ pv - qu \end{bmatrix} \quad (7.6)$$

$$\begin{bmatrix} \dot{x}_O \\ \dot{y}_O \\ \dot{z}_O \end{bmatrix} = \begin{bmatrix} \cos\psi\cos\theta & -\sin\psi\cos\phi + \cos\psi\sin\theta\sin\phi & \sin\psi\sin\phi + \cos\psi\sin\theta\cos\phi \\ \sin\psi\cos\theta & \cos\psi\cos\phi + \sin\psi\sin\theta\sin\phi & -\cos\psi\sin\phi + \sin\psi\sin\theta\cos\phi \\ -\sin\theta & \cos\theta\sin\phi & \cos\theta\cos\phi \end{bmatrix} \begin{bmatrix} u \\ v \\ w \end{bmatrix} \quad (7.7)$$

The dynamic and kinematic relations of the rotational equations of motion are shown below. Instead of mass and translational vectors, the inertia vector J and the rotational state vectors L, M, N are taken into account. Equation 7.9 again shows how a transformation matrix changes the rotational velocities (p, q, r) of the aircraft body fixed reference frame to rotational velocities ($\dot{\phi}, \dot{\theta}, \dot{\psi}$) in the normal earth reference frame.

$$\begin{bmatrix} \dot{p} \\ \dot{q} \\ \dot{r} \end{bmatrix} = \bar{J}^{-1} \left\{ \begin{bmatrix} L \\ M \\ N \end{bmatrix} - \begin{bmatrix} p \\ q \\ r \end{bmatrix} \times \bar{J} \begin{bmatrix} p \\ q \\ r \end{bmatrix} \right\} \quad (7.8)$$

$$\begin{bmatrix} \dot{\phi} \\ \dot{\theta} \\ \dot{\psi} \end{bmatrix} = \begin{bmatrix} 1 & \sin\phi\tan\theta & \cos\phi\tan\theta \\ 0 & \cos\phi & -\sin\phi \\ 0 & \frac{\sin\phi}{\cos\theta} & \frac{\cos\phi}{\cos\theta} \end{bmatrix} \begin{bmatrix} p \\ q \\ r \end{bmatrix} \quad (7.9)$$

The wind itself is a constant parameter, it can be prefixed to a specific value and direction or randomly obtained. The wind velocity is a vector which is modeled in the normal earth reference frame. Additional to this constant value, turbulence is added by means of 'band limited white noise' in x_0, y_0 and z_0 direction.

$$\begin{bmatrix} \dot{x}_O \\ \dot{y}_O \\ \dot{z}_O \end{bmatrix}_{wind} = \begin{bmatrix} Northern_wind_constant \\ Eastern_wind_constant \\ 0 \end{bmatrix} \quad (7.10)$$

The total ground speed can then be obtained by adding the three components

$$\begin{bmatrix} \dot{x}_O \\ \dot{y}_O \\ \dot{z}_O \end{bmatrix}_{total} = \begin{bmatrix} \dot{x}_O \\ \dot{y}_O \\ \dot{z}_O \end{bmatrix}_{EoM} + \begin{bmatrix} \dot{x}_O \\ \dot{y}_O \\ \dot{z}_O \end{bmatrix}_{wind} + \begin{bmatrix} \dot{x}_O \\ \dot{y}_O \\ \dot{z}_O \end{bmatrix}_{turbulence} \quad (7.11)$$

7.1.5 State computations block

The remaining parameters that define the state of the aircraft are computed in this block. Most important are the aerodynamic angles and flight path angles, but also Mach number, atmospheric properties etc. are taken into account. The state vector of the aircraft is defined by the combination of the parameters of this block and the parameters from the equations of motion block. This state vector is again fed back into the force and moments computations and the equations of motion block.

Aerodynamic angles

The angle of attack α is defined by its relations to the velocity in the body fixed reference frame.

$$\alpha = \arctan\left(\frac{w}{u}\right) \quad (7.12)$$

Analogous the angle of side-slip β is computed by

$$\beta = \arcsin\left(\frac{v}{\sqrt{u^2 + v^2 + w^2}}\right) \quad (7.13)$$

Flight path angles

The kinematic translational equations of motion (equation 7.7) define the velocities to the north, east and in vertical direction. Flight path angle (γ) and heading (χ) can be easily determined by these values. The heading is obtained by the arctangent of the velocity to the east (\dot{y}_O) divided by the velocity to the north (\dot{x}_O).

$$\chi = \arctan\left(\frac{\dot{y}_O}{\dot{x}_O}\right) \quad (7.14)$$

Similarly γ is computed by means of the total velocity in the horizontal plane and the vertical velocity

$$\gamma = \arctan\left(\frac{-\dot{z}_O}{\sqrt{\dot{x}_O^2 + \dot{y}_O^2}}\right) \quad (7.15)$$

Atmosphere

The calculations in paragraph 4.5 assume that the projected height variation of 0 to 500 meter does not result significant differences in atmospheric conditions. The simulator however, does incorporate these variations for a higher accuracy and usability at larger altitudes. Also temperature variations are taken into account. The equations of the standard atmosphere [ISO 2533:1975,] are used to obtain these values.

$$\rho = \rho_0 \left(1 + \left(\frac{\lambda h}{T_0}\right)\right)^{\left(\frac{g_0}{R\lambda} + 1\right)} \quad (7.16)$$

$$T = T_0 + \lambda h \quad (7.17)$$

$$a = \sqrt{\gamma RT} \quad (7.18)$$

In these equations ρ is the air density and ρ_0 is the density at sea level. The same holds for temperature T and T_0 . λ is the temperature lapse rate, or temperature variation with altitude h , which is -0.0065° per meter. R is the gas constant for dry air and equal to $287.05 \text{ m}^2/\text{s}^2\text{K}$. Finally the Mach number M (V/a) is determined by the speed of sound a which is also a function of the specific heat capacity ration γ which is 1.4.

7.1.6 Sensor dynamics

Sensors are expected to introduce certain time delays, biases and measurement noise into the system. The dynamics of different sensors are incorporated in this block. For example the measurements of the angle of attack, pressures in the pitot tube for the airspeed, IMU-outputs, gps-data etcetera. The values for the sensor dynamics are obtained from the actual data of the 10 kW test aircraft. The sensor equipment of the 1 MW system is not expected to deviate much from the 10 kW system, therefore these values are also applicable in this case.

7.1.7 Actuator dynamics

After the control block has handled the states and the desired conditions of the aircraft. It provides an output to the actuators to make the desired adjustments. The controllable actuators in this case are the left and right aileron, the elevator and the rudder. For a realistic output of these adjustments, this block incorporates the minimum and maximum deflection rates of the control surfaces and also the deflection limits which are set to $\pm 30^\circ$ for every actuator.

7.1.8 Cable

The cable is modeled such that one end acts 10 cm under the center of gravity of the aircraft. To transform the forces and moments from 0.01 m. in the Z_b -direction to the center of gravity a transformation matrix is used again. The location of the other end of the cable is at the end of the arm, which is given by coordinates in the normal earth reference frame. In current simulations it does not have a weight, although it adds drag to the aircraft, as a force opposite to the velocity. The cable can take up pulling force, and no pressure. It is a straight line from the ground station to the aircraft. During operation the cable length can be changed with a velocity which is limited similar to the limitations of a realistic winch, for example, the maximum reel out acceleration is $\pm 3 \text{ m/s}^2$. The cable tension is calculated as a function of Youngs modulus (E_c) and the difference between the measured distance from the ground station, given by the aircraft coordinates (L_m) and the cable length (L_c) as given by sum the initial length and the length that has been reeled out.

$$T_{cable} = \frac{EA_c(L_m - L_c)}{L_c} \quad (7.19)$$

Youngs modulus of the cable is calculated by means of the graph in C. and equation 7.20. The graph shows an average strain ε of 2% for 60% break force. With a break force of 1314 kN, a diameter of 0.04 m. results in a E_c of 31.4 GPa

$$E_c = \frac{\sigma}{\varepsilon} = \frac{0.6F_{max}}{\frac{1}{4}\pi D_c^2 \varepsilon} \quad (7.20)$$

7.1.9 Rotating launch

The arm rotation is modeled by varying the arm end coordinates in the x_0 and y_0 plane such that a rotation with a given radius R_{arm} and a rotational velocity ω_{arm} takes place. The coordinates are modeled as way points, which are defined by the arm length (R_a) and the rotational velocity (ω). The aircraft follows this path because it is being pulled by the other end of the cable. In the mean time, the cable length extends with a given velocity (V_{cable}). The rotational velocity is defined such that a given aircraft velocity is maintained, how this works is explained in paragraph 7.4.

7.1.10 Start of simulation

During the simulation the settings of the aircraft control block are such that the bank angle first remains zero. This is necessary, because at the start the location of the aircraft is at 0 altitude. Banking under these circumstances results in the wing tips going through the ground, which makes the simulation stop. Further on the aircraft is controlled such that the cable must maintain a given angle ξ relative to the ground, as shown in figure 7.4. Lengthening the cable by reeling out now automatically results in an altitude gain of the aircraft.

Now the most important parts of the aircraft simulator are known, input is required to make this system take-off by means of rotation. The simulation starts with an initialization phase of 70 simulation seconds. It takes 60 seconds for the Karmann filter to initialize, then 10 seconds are left for setting up the control surfaces.

7.2 Simulation approach

The default settings of the simulation model give satisfactory results for the 10 kW aircraft. These settings were determined via trial and error. Satisfactory means that the aircraft did not crash during

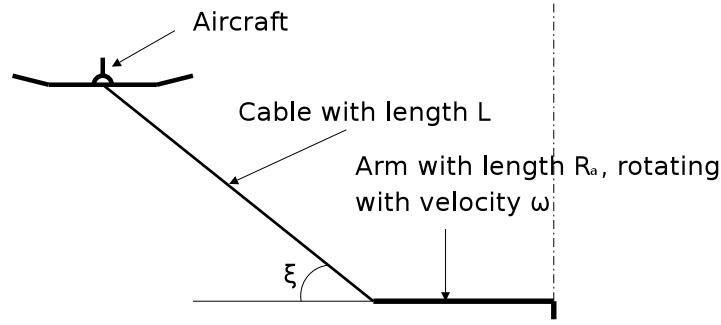


Figure 7.4: Schematic representation of angle ξ which aircraft must maintain during simulation

the launching procedure before reaching a height of about 60 meters with a wind velocity of 10 m/s. The default settings are taken as a 'point of departure'. These settings are used as a basis for a reference simulation. Then a sensitivity analysis is done by changing main parameters to find more optimum trajectories or launch strategies. Based on these results estimations can be made on what a rotational platform launch system as part of a 1 MW Powerplane is capable of. A launch can be regarded as successful when it complies to the main requirement of chapter 3. Meaning that the aircraft should reach an altitude of 200 m. with a cable length of 400 meter with a wind speed of 14 m/s. But an altitude of 125 m. with 10 m/s wind can also be regarded as a promising result.

7.3 Simulation results

Even though launching with wind gives a more realistic proof of concept for different weather conditions, the data of a launch without the periodic wind effects, is easier to analyse. Besides that the condition of a wind velocity of 14 m/s is an extreme which cannot be regarded to as a normal operating condition. For these reasons analysis of the simulation results in the following paragraphs takes place with a set wind speed of 0 m/s although some effect of turbulent winds is still present. The effect of wind will be implemented again in a separate paragraph.

7.3.1 Reference simulation

This paragraph shows the results of a simulation with settings as in table 7.2. An arm length of 36 meters is chosen because an arm length similar to the wingspan of the aircraft intuitively seems to be a possible and applicable option. The simulation results in a path as shown in the 3d graph of figure 7.5. The blue line, represents the coordinates of the aircraft in the normal earth reference frame. It starts at -36 meters (arm length) to the East at 0 altitude and 0 meters to the North. Then it rotates around the origin in the North-East plane, slowly gaining altitude. At the start of the simulation the path is quite irregular, this is merely due to the non-optimal way the first seconds of the launch are modeled. Although these first seconds are important for setting up a proper autopilot for the aircraft, for now it is neglected as it does not cause the simulation or the aircraft to crash. The aircraft continues to ascent and the radius of the turn increases with the cable length until the aircraft suddenly leaves the circular pattern, flies an irregular path and crashes.

Table 7.2: Settings for first simulation

R_a	$V_{aircraft}$	V_{cable}	V_{wind}	Φ
36 m.	40 m/s	0.5 m/s	0 m/s	0 °

7.3.2 Coordinates

Figure 7.7a shows the aircraft coordinates plotted separately against time. The altitude is a negative value because it is taken from the perspective of the aircraft. The graph also represents how the aircraft

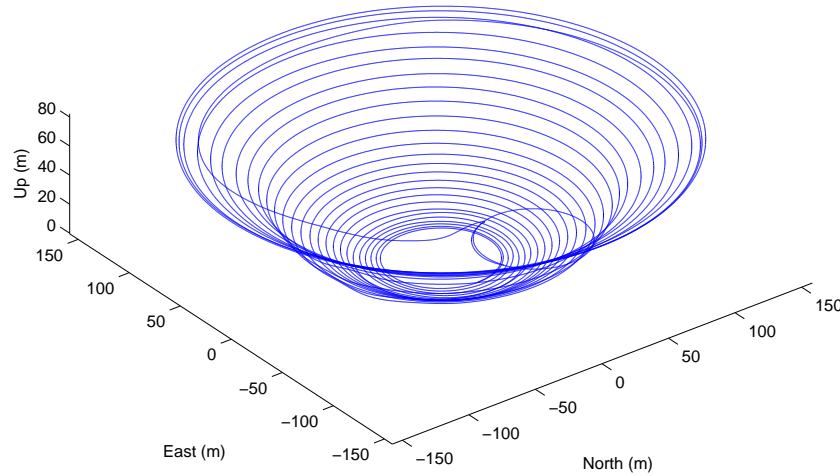


Figure 7.5: 3 dimensional plot of the path of the aircraft during simulation

remains on the same spot until $t=70$. Then it starts rotating and ascending. After about 420 seconds it reaches a maximum altitude of 82 m, then it descends slowly until it suddenly loses altitude very fast. The radius of the circle also increases together with the altitude and becomes 152 meter. Then it decreases again, as the aircraft breaks its circular path, just as in figure 7.5 .

7.3.3 Lag angle ζ

The lag angle ζ , is defined as in figure 7.6, and plotted in figure 7.7b. It slowly increases to 90 degrees while the aircraft reaches its maximum altitude. After reaching this value, the flight becomes unstable, since the component of the cable tension in the heading direction of the aircraft decreases to below zero. ζ keeps on increasing up to 180 degrees and then jumps to -180 since half a circle behind physically can also be regarded to as half a circle ahead. The large peaks at the start seem to represent that the flight path starts with lagging $\pm 1\pi$ behind, this phenomena is neglected since physically the aircraft cannot really lag behind as there is very little cable reeled out. At $70 \leq t \leq 150s$ there is some oscillation in the value of ζ . This can be overshoot of a controller, which could be solved by optimizing the controller with proper gains especially at low cable length. .

7.3.4 Launch angle ξ

Physically a launch angle can only be measured when the cable reels out, because from that moment the launch starts. A ξ of 90 degrees at the start and the jump to -90, when rotation starts, therefore do not really make sense, but also do not influence the simulation such that it has to be stopped. When the cable lengthens, ξ gradually increases to 27 degrees, which means that there is a small error of 3 degrees with the desired launch angle. As soon as ζ reaches 90 degrees, ξ also loses its stable value.

7.3.5 Cable

The oscillations in the lag angle are also reflected in the cable tension (Figure 7.8a), which starts at an (averaged) value of 150 kN and then decreases with time to 0. From $t=180$ s. there are some prominent peaks in the cable tension, which are repeated with a period similar to the rotation of the aircraft. During the simulation there is a point in the circular path where the aircraft makes a small dive, goes up and then stabilizes again. The reason for this phenomena is unclear, but as the controller restores it every time, also for different simulations with different settings, no effort is put in repairing this bug. It might have something to do with a tangent giving an infinite output in one of the underlying calculations. Figure 7.8b shows how the cable length starts at 36 m and then increases linearly with 0.5 m/s. Contrary to the other outputs, there is no feedback at the reel speed. Thus, even though the

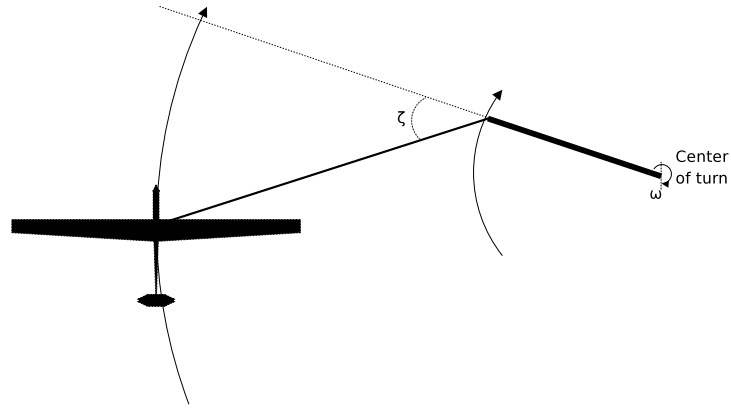


Figure 7.6: Schematic representation of lagangle ζ of the aircraft, compared to the arm

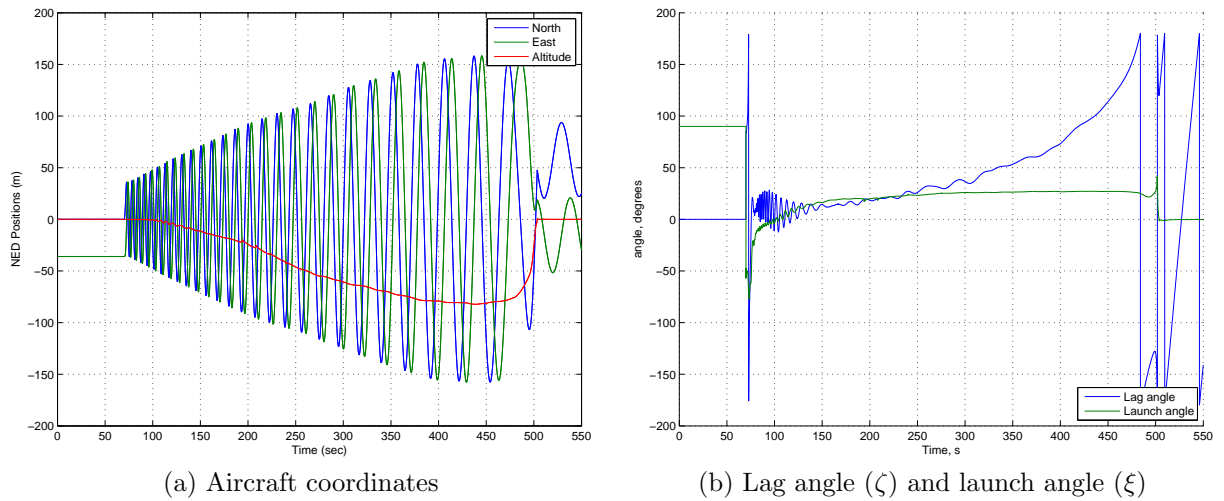


Figure 7.7: Results of reference simulation

aircraft is crashed, the cable length keeps increasing at constant rate. The start length of 36 meters is because the winch is estimated to be in the centre of rotation. This means that there is always 36 m. of cable reeled out, which means that there can also be some strain, causing the aircraft to take off a little already before the cable is being reeled out. When the first seconds of the simulation are optimized, this effect should be kept in mind. Since there is no feedback, cable length L_c can also be calculated as a function of time with the following equation

$$L_c = R_a + V_r(t - 75) \quad (7.21)$$

Where R_a is the arm length and V_r is the reel out speed. 75 seconds is the time of initialization, before the cable starts reeling out.

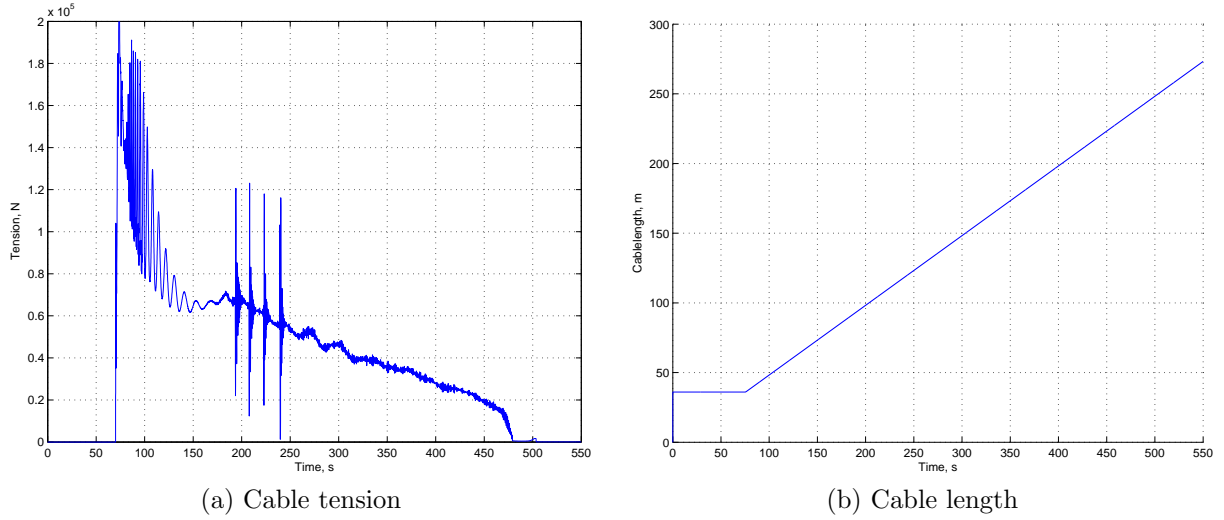


Figure 7.8: Results regarding the cable of reference simulation

7.3.6 Velocities

Figures 7.9a and b show how the rotational velocity of the platform results in the aircraft velocities. At the start ($t=70$), the airspeed is just above 40 m/s, which is similar to the product of ω and the arm length plus turbulent wind velocities and measurement errors. The airspeed remains near the set 40 m/s, although it decreases with time. An explanation for this is the way the desired airspeed is calculated. This is described and improved later in this chapter. The peaks in the cable tension discussed earlier are also clearly visible in the upward velocity.

7.3.7 Attitude and actuator demands

To have an indication of the state of the aircraft during the simulation it is useful to have a look at the actuator demands. The servo demands for the simulation are shown in figure 7.10b. As described already, the maximum setting for every surface is ± 30 degrees. It appears that at the start of the simulation, the desired rudder setting is quite large. This is probably due to the fact that the rudder must provide sufficient yaw moment to keep the small circular path at the high velocity. Nevertheless, the side-slip angle remains constant at -4 degrees. The elevator only crosses its limits right at the start and at the previously described 'bumps'. It also reaches maximum setting as soon as the flight becomes unstable, at the end of the simulation. The ailerons remain almost constantly at 4 degrees during the start and then slowly decrease in deflection with time, they remain within their limits. How these control settings effect the aircraft attitude is shown in figure 7.10a. It clearly takes time before the aircraft sets to the desired bank angle. This is most probably due to an inappropriate controller. During the start of a launch like this, the difference between the wind velocity at the outer wing and the velocity at the inner wing is significant (figure 7.11. This difference will result in a roll moment directing towards the center of rotation, giving a bank angle in this direction. The ailerons should compensate for this difference.

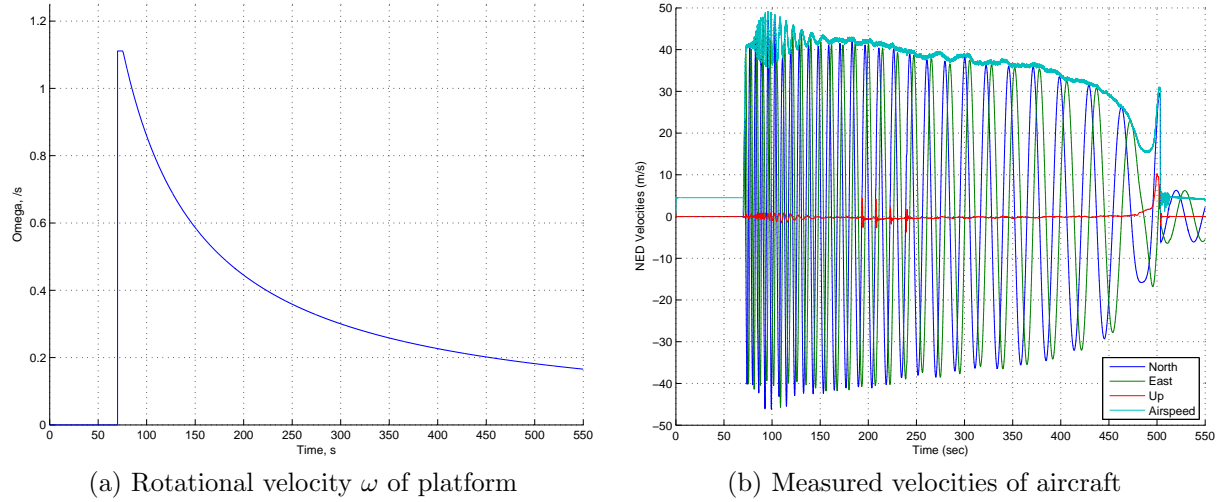


Figure 7.9: Velocities during reference simulation

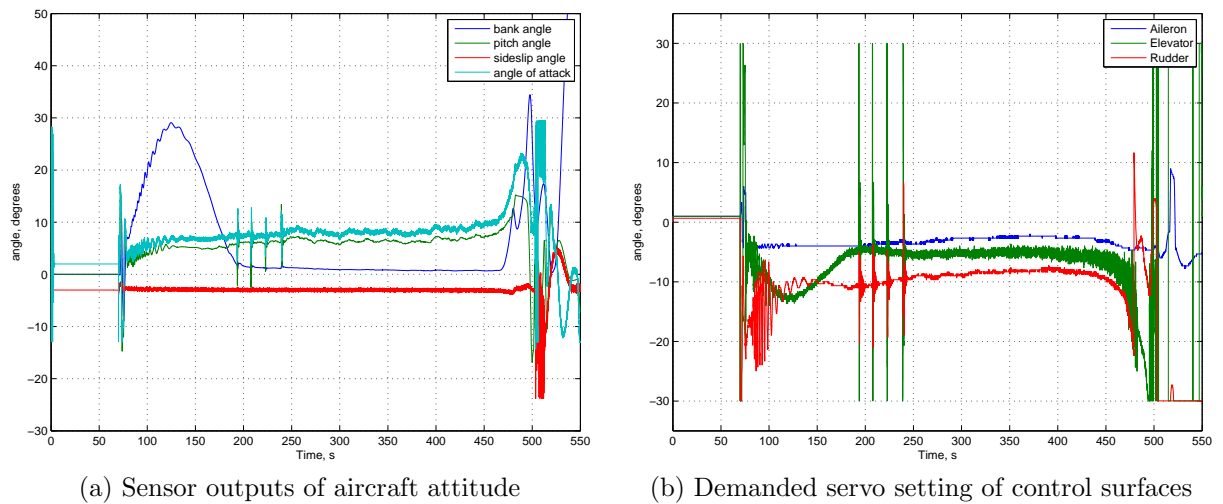


Figure 7.10: Graphs of aircraft state during reference simulation

Figure 7.10b shows that the aileron servo setting remains constantly around 4 degrees, which is far below its maximum, so there must be enough room for adjustment, but the controller lacks to make use of this room. The bank angle also results in the aircraft to fly towards the center of rotation. Since the aircraft banks up to 30 degrees, the elevator setting also can influence this path, which it does, since the side-slip angle remains below an acceptable 4 degrees. As the radius of turn becomes larger, the effect of the velocity difference decreases hence the bank angle finally finds its proper setting after 200 seconds.

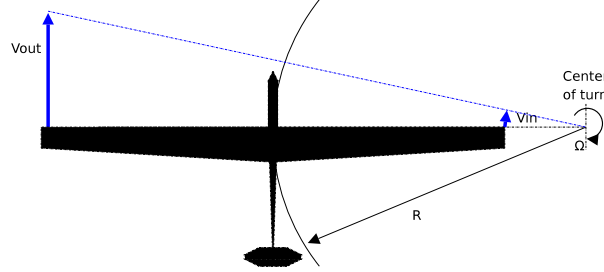


Figure 7.11: difference in wind velocity along aircraft with small radius

7.3.8 Optimizing controller

Extensive unraveling of the controller in and outputs revealed the reason for the aileron setting remaining at a maximum of 4 degrees. For an unclear reason the output of the controller had a saturation block which was set to ± 5 degrees. Changing this value to ± 30 (the actual physical maximum) resulted in the aircraft to find its desired bank angle much faster (figure 7.12a). Even though control still can be optimized to decrease the fluctuations in the servo settings, the changes result in a much more desirable aircraft attitude. Now also the elevator setting is much smaller. Additional simulations as described in paragraph 7.5.2 reveal that optimization of controller only influences the aircraft attitude at the start of the simulation, and no significant altitude gain is reached by this optimization. This indicates that to reach higher altitudes, especially the second half of the simulation should be optimized.

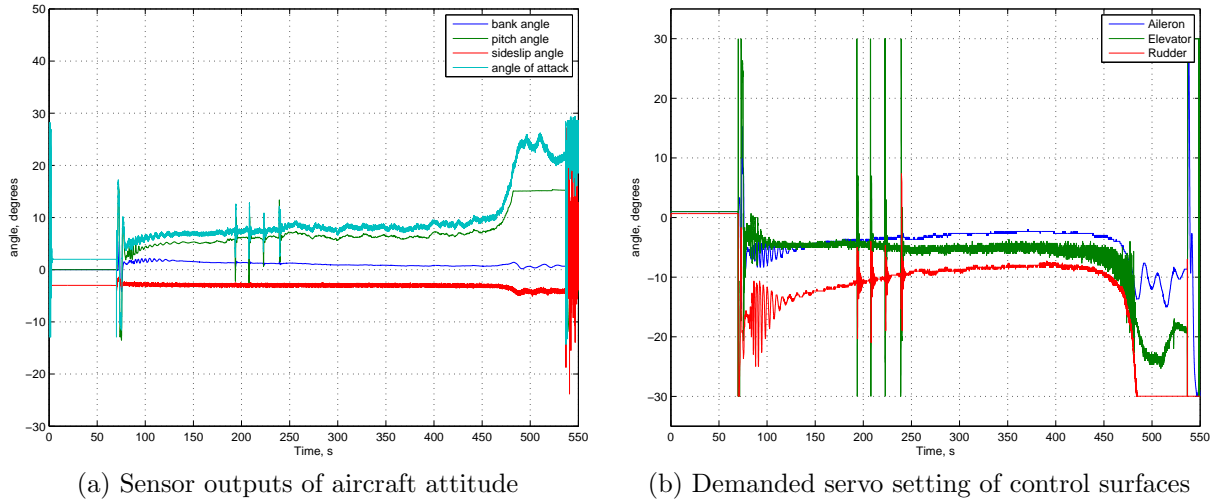


Figure 7.12: Graphs of aircraft state with optimized aileron controller

7.4 Optimizing airspeed

The rotational velocity ω can be calculated as function of the radius (R) and the desired velocity V

$$\omega = \frac{V}{R} \quad (7.22)$$

In the simulation at the start R is given as the arm length, but as cable is being reeled out, the radius increases. Currently the resulting radius is calculated as a function of the desired airspeed V_{des} , the desired launch angle ξ , which is $1/3\pi$, the arm length R_a and the cable length L_c .

$$\omega = \frac{V_{des}}{R_a + (L_c - R_a)\sin(1/3\pi)} \quad (7.23)$$

The sine of ξ is used in this equation while one would expect this to be the cosine, this is due to the way ξ is defined in the simulation. During the simulation there is actually a static error between the desired ξ and the real launch angle. Besides that, the arm length also decreases with increasing lag angle ζ . So for a more realistic approximation the measured ξ and ζ are used for defining ω

$$\omega = \frac{V_{des}}{R_a + (L_c - R_a)\sin(\xi)\cos(\zeta)} \quad (7.24)$$

This results in an omega shown as in figure 7.13a and an airspeed as in figure 7.13b. In reality it would be hard to control the angular velocity of an 36 m. arm in such a way. Besides that, having feedback on this value causes instabilities of the control system. This is clearly visible in the vividly changing ω demand which finally results in an unstable loop. Optimizing this control can be interesting and useful, but at this state of the research it is not the most necessary approach. Therefore the current optimum ω is set by iteration with a factor until the measured airspeed remained near the desired speed until the end of the simulation. Now the starting velocity remains similar, but when L_c increases, ω decreases a bit less, which results in an airspeed remaining above 40 m/s for a bit longer. Which results in a maximum altitude of 87 meters, 7 meters higher than the reference simulation.

$$\omega = \frac{V_{des}}{R_a + (L_c - R_a)\sin(1/3\pi)0.85} \quad (7.25)$$

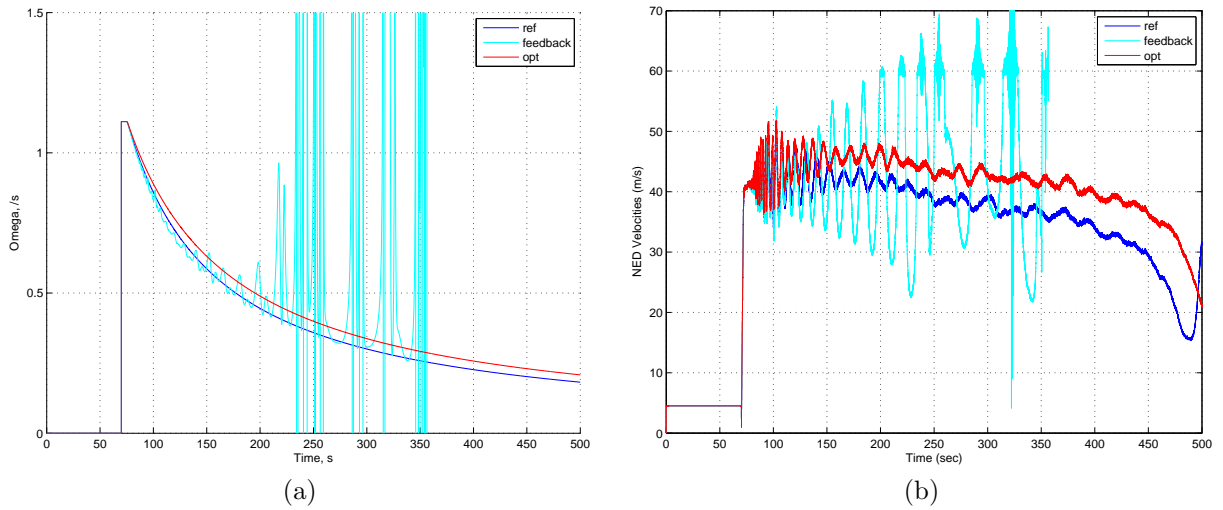


Figure 7.13: (a) Optimization of ω with and without feedback. (b) Resulting airspeed with optimization steps

7.5 Sensitivity analysis

Now the basis of the simulation is understood and some reference simulations are run, the effect of changing several parameters is investigated. This will give insight on how to improve the set-up to optimize the results.

7.5.1 Effect of wind

Obviously the system will not generate wind energy without wind. To show how the wind effects the performance, some simulations with different wind speeds are completed. The effect of the wind is clearly visible, as the rate of ascent varies periodically with the same frequency as the rotation (figure 7.14a). This is due to the constantly varying airspeed of the aircraft, since the wind direction changes compared to the aircraft while it rotates. With the maximum wind speed the effect on the obtained altitude is significant, the aircraft just reaches 79 meters, while without wind goes up to 88 m. A wind velocity of 7 m/s only results in 1 meter difference compared to no wind. This effect is also visible in the lagangle. Figure 7.14b shows that the lag angle has the same periodic variation as the altitude, the maximum wind speed makes the lag angle increase faster. Therefore it reaches the 90 degrees lag about 50 seconds earlier, proclaiming the end of the circular pattern.

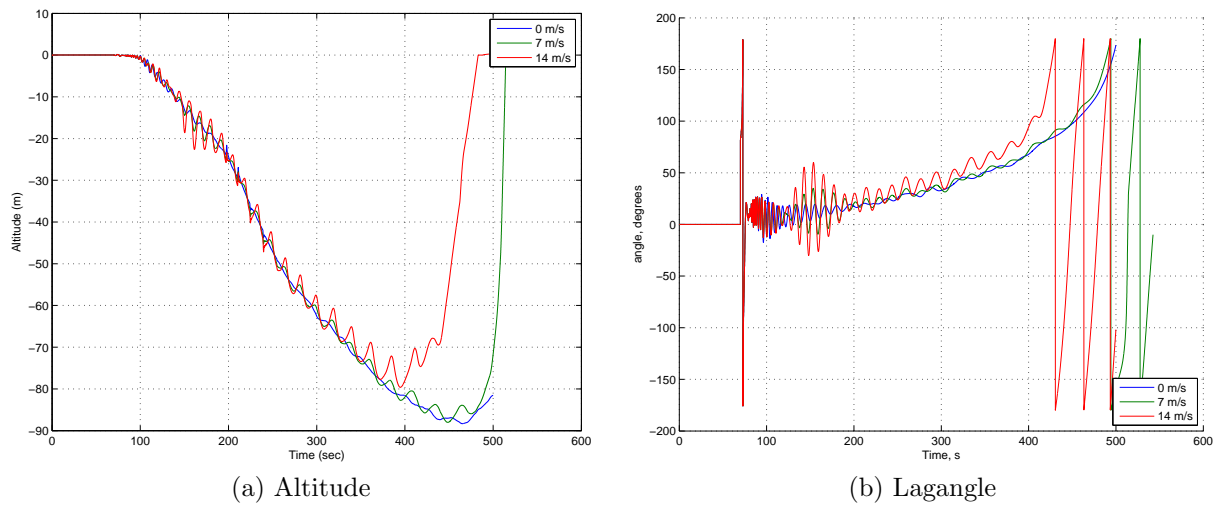


Figure 7.14: Simulation results with optimized ω and varying wind

7.5.2 Changing desired bank angle

An increasing lag angle results in the aircraft to loose velocity and finally stop climbing. Setting up the bank angle such that cable tension increases could influence the lagangle such that the aircraft reaches a higher altitude. Simulations with varying bank angles are run to verify this hypothesis. Figure 7.15a indeed shows an increasing cable tension, which does lead to a higher altitude as shown in figure 7.15b. But the stable gradual climb starts having more oscillations in both altitude gain and cable tension after reaching above 110 meters. Remarkably, below 200 seconds the bank angle setting seems not to influence cable tension nor altitude. The reason for this is shown in figure 7.16a, where it clearly takes time before the aircraft sets to the desired bank angle. An explanation for this phenomena is given in paragraph 7.3.7.

Increasing the bank angle significantly results in a much higher altitude. Compared to flying without bank angle and flying with bank angle, the altitude gain is up to 60%. The aircraft now reaches up to 140 meter, which is very promising as it crosses its minimum required altitude of 125 m. The cable length after 700 seconds is 350 meters, which is almost the required 400 meter.

Changing bank angle with optimized controller

Since the aileron controller is optimized in a later stage of the research, this simulation is repeated with the optimized controller setting. Comparing figure 7.16a and b shows how the bank angle now almost immediately finds its desired setting and keeps it as long as the stable climbing flight is maintained. Only a large bank angle of -40 degrees shows some large fluctuations at the start. These fluctuations are also clearly reflected in the cable tension which peaks up to 600 kN. A bank angle of -25 results in a

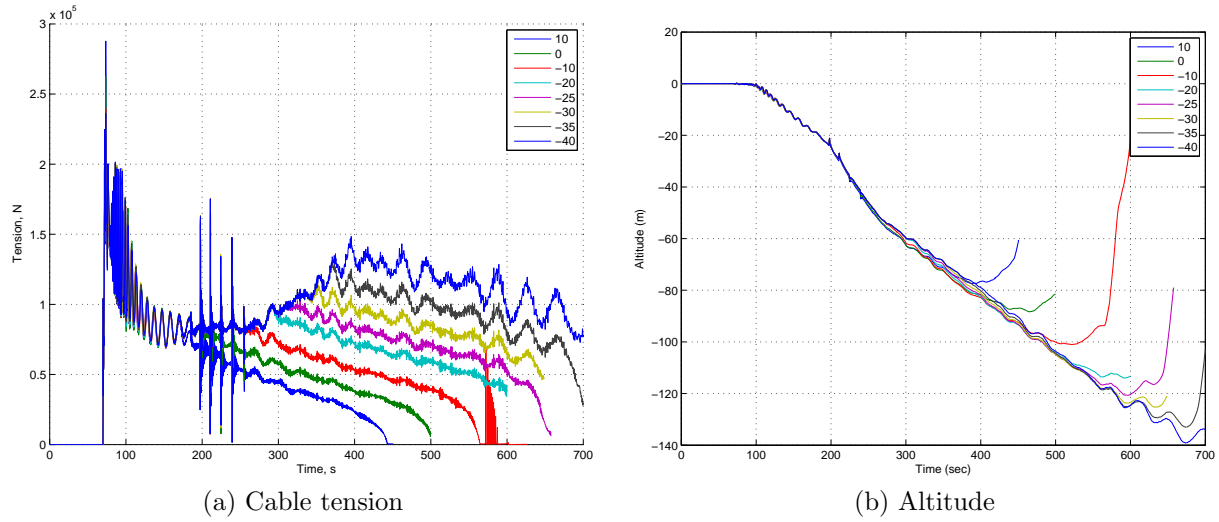


Figure 7.15: Results of simulation with varying bank angles

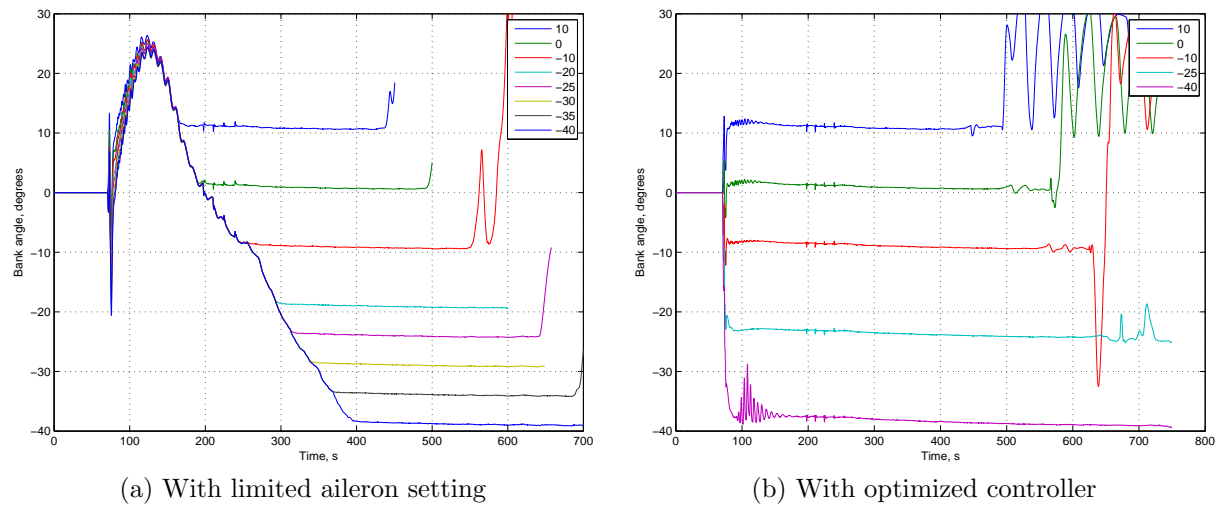


Figure 7.16: Measured bank angle during simulation

more steady tension and climb. The altitude gain, however, does not change significantly, although the altitude rises more steadily, with less fluctuations at the end.

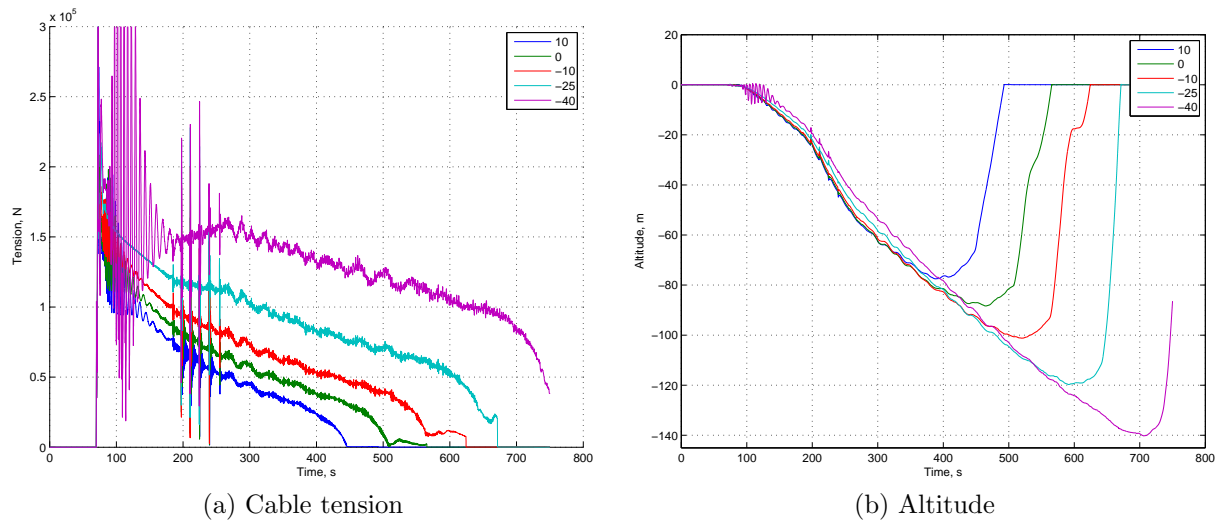


Figure 7.17: Results of simulation with varying bank angles and optimized aileron controller

Adding wind

An increased bank angle does result in a smaller component of the lift balancing the weight. When wind speed is added to the simulation, the aircraft flying with tail wind will have a smaller airspeed relative to the wind, compared to flying with no wind. When the lag angle increases, changing the rotational velocity to compensate this becomes more difficult. In the mean time, the lag angle decreases due to the increased cable tension. Therefore there is most probably an optimum bank angle for every wind speed. The simulation of the former paragraph is repeated with a wind speed of 7 and 14 m/s. How this effects the altitude is shown in figures 7.18a and b. A wind speed of 7 m/s results that in no real altitude difference between banking with -25 and -40 meters. Still an altitude of almost 120 m. is reached. Just as in paragraph 7.5.1 a 14 m/s wind influences the altitude gain more negatively. But still a bank angle of up to 25 degrees has a better results than with 0 bank angle. For this reason a bank angle of 25 degrees is regarded as an optimum for further simulations.

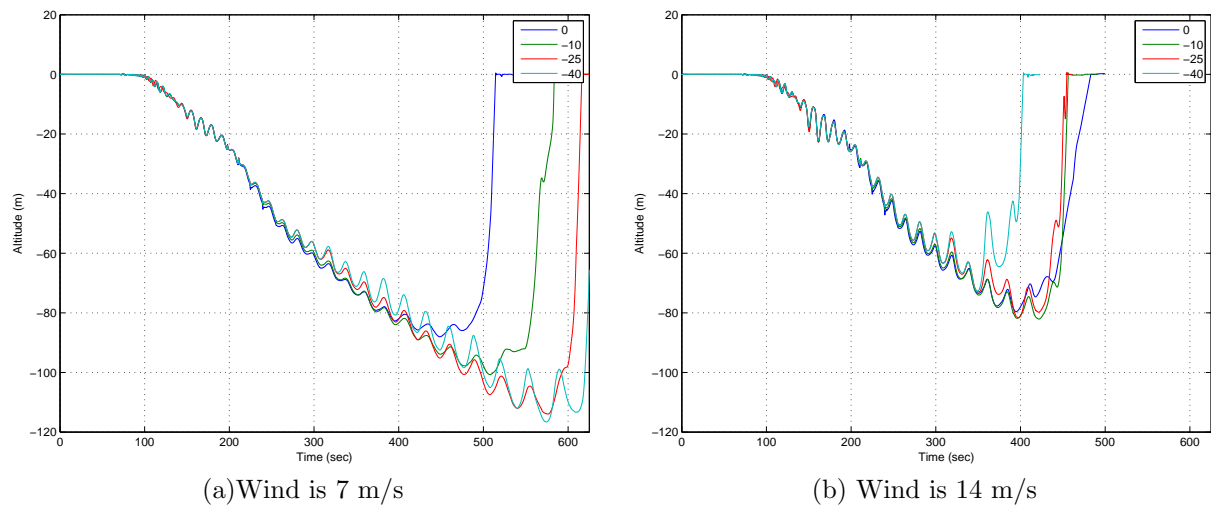


Figure 7.18: Altitude as function of time for different bank angles.

7.5.3 Varying desired velocity

Increasing the velocity also has different advantages and disadvantages that could influence the end height. For instance, flying at an increased velocity increases the centrifugal force, thus cable tension and consequently could decrease the lag angle. On the other hand, cable and aircraft drag increases as well, increasing the lag angle. To estimate the result of these influences, simulations with different desired velocities are run. For these simulations a bank angle of -25° is chosen as this gives the best results for different wind speeds. The lowest desired velocity plotted is 36 m/s. Below this value the aircraft did not take off any more.

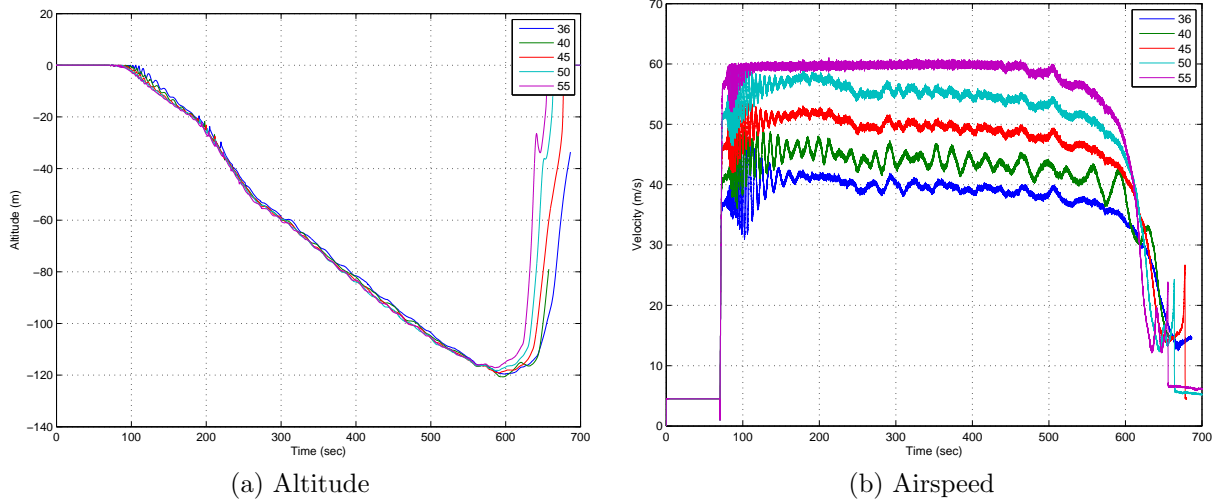


Figure 7.19: Simulation results for different desired velocities

Figure 7.19a shows that varying the desired velocity does not influence the reached altitude very much. It even shows that the 40 m/s used as a reference is indeed the optimum setting. At higher and at lower values the altitude decreases, even though it only varies about 8%. At a higher velocity the maximum altitude is reached in a bit less time, which also means that there is less cable rolled out yet. In figure 7.19b can be seen that the real measured airspeed from the simulation is slightly above the desired setting. There is also a clear maximum of 60 m/s, which the aircraft does not exceed, which most probably is a result of drag forces increasing with the square of the velocity, keeping the aircraft below this maximum.

7.5.4 Varying desired reel out speed

As described before, the cable length is an important parameter for the possibility to increase altitude by flying patterns or by means of 'reverse pumping'. Since the cable length is a linear function between the reel out speed V_r and time, simulations of flying with different reel out speeds are executed. The bank angle and wind settings for these simulation where -25° and 0 m/s respectively. The results, shown in figure 7.20 show that the maximum altitudes differ only about 4 % where an optimum lies in between 0.5 and 0.6 m/s. Using equation 7.21 results in a cable length of almost 300 meter at maximum altitude at a reel out speed of 0.7. Since it takes more time to reach maximum altitude with lower V_r , a V_r of 0.4 m/s gives a similar final length. Repeating this calculation for all these simulations reveals that the simulation reaches its maximum altitude when the cable length is around 300 meters. This means that there could be a relation between these values which should be investigated more.

7.5.5 Varying arm length

The arm length is an important factor, it defines the size of the system not only in length. Bending moments which increase with the arm length will also define the thickness of the arm, the weight of the structure, drive train criteria etc. Preliminary simulations showed that the wind velocity has a big influence on the possibility to take off with a small arm length. Hence a V_w of 7 m/s is used to perform

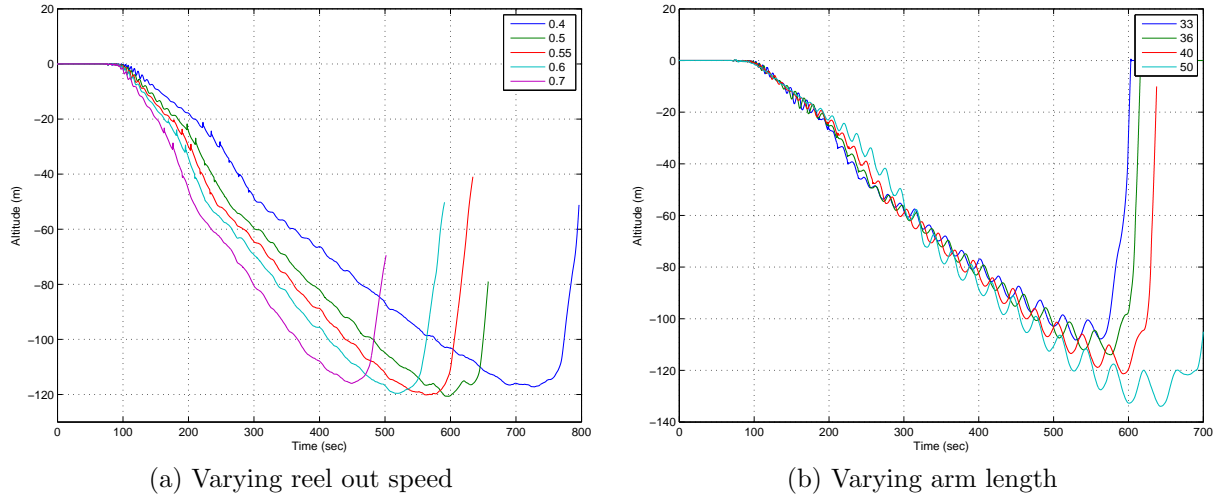


Figure 7.20: Altitude as function of time for different parameters

these simulations. The bank angle is again -25 degrees. Below an arm length of 33 meters, no take off was possible. Figure 7.20b shows that the reached maximum altitude increases with arm length. With an arm of 50 meters an altitude of 135 meters is reached in 650 seconds. Since V_r is 0.5 m/s, the cable length becomes over 325 meter which is still not enough to meet the requirements.

7.6 Required power

The required power is a measure of size and cost of the drive train of the system, hence power required is calculated for some simulations as described in this paragraph. As mentioned before, power is

$$P = T\omega \quad (7.26)$$

Where T is the torque in the plane of rotation, which is a function of the cable tension T_c , the arm length R_a and the launch and lag angle ξ and ζ .

$$T = R_a T_c \sin \xi \sin \zeta \quad (7.27)$$

So the power to drive the platform P_p becomes

$$P_p = R_a T_c \sin \xi \sin \zeta \omega \quad (7.28)$$

The power required is plotted for different simulations in figure 7.21. The energy at first stage after take off is quite high, due to the peaks in cable tension. The drive train could be able to level out those peaks, for example with a spring damper system. Integrating the elasticity of the arm in the simulation would already decrease the peaks. When looking at the mean between these peaks the required power to launch the aircraft this way, is in the range of 0.5 MW. Only at very strong winds (14 m/s) the required power is much larger. Further on, the periodic variation in required power in the simulations with wind are explained by the varying tension due to the wind speed.

The system will be located at a spot where it can deliver at least 1 MW of power while it is generating. The power connection can also be used the other way around, so requiring power of maximum 1.5 MW for the launch system is not a big issue. Further on, the average power requirement during launching is about 0.5 MW. Multiplied with a timespan of 500 seconds this results in an energy need of roughly 70 kWh. Since this is similar to the amount of energy the Powerplane will produce within half of the start up time and after one launch it will stay airborne for several days, the energy use is negligible.

7.7 Physical appearance

To indicate the physical appearance of how a machine, capable of resisting a force of 150 kN at an arm length of 36 meters and able to rotate, similar machines on the market are investigated. A tower crane

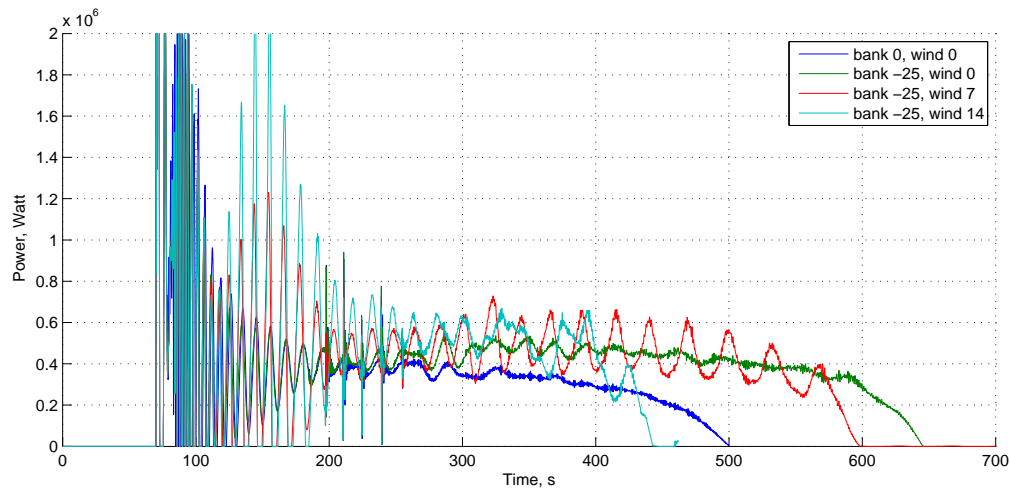


Figure 7.21: Requested power for different simulations

lifts heavy loads, at big arm lengths. Even though the forces are mainly in one direction (gravity), the altitude at which the arm is situated also leads to dynamic forces of wind. Besides that, moving a load from one point to another also results in forces in different directions. For these reasons as an indication, the arm of a tower crane (in these set-ups known as 'Jib') is a good start.

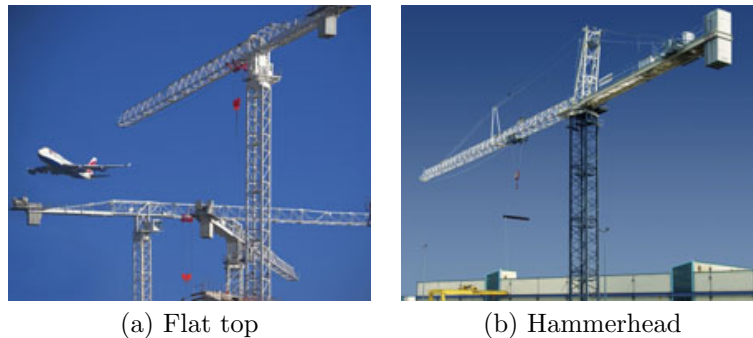


Figure 7.22: Different types of tower cranes [Terex-Cranes, 2010b]

Figure 7.22 shows two different tower crane set-ups. The hammerhead crane has an extra beam above the jib, which decreases the bending moments in the jib. In case of the hammerhead cranes, the jib itself must resist these bending moments, resulting in a wider and stronger jib. When a jib is used as arm for the rotating platform launch, forces will act in different directions. This requires beams in different directions to deal with the resulting bending moments. Therefore the jib itself becomes smaller, though the whole set-up with beams and beam connections becomes much larger. Hence a jib of a flat top crane is used as an indication for the arm. In a later stage of specifically designing the system, optimization with the help of supporting beams could be investigated.

The Terex CTT 561/A-24 HD23 has a lifting capacity of 15.8 tonne at 39 m length [Terex-Cranes, 2010a]. More data about this crane can be found in appendix G. The jib consists of triangular trusses (figure 7.23) with sizing and weight as shown in table 7.3. This means that the arm starts with a width of 2.54 m, and a height of 2.54 and ends with a width and height of 1.87 and 2.5 meters. The total weight of the arm becomes 24.400 kg. The weight of section 23 includes a trolley winch and accessories and also stretches out in opposite direction. Considering only an arm, from the center of rotation the total weight is estimated to be about 16 tonnes. Since forces will act in different directions, the ratio between height and width will also be different.

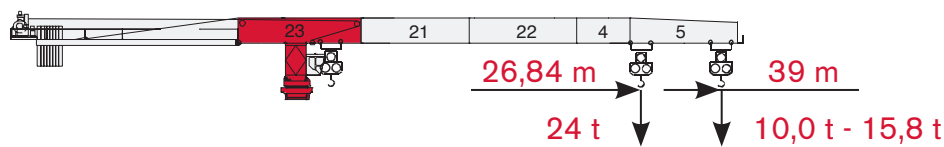


Figure 7.23: Jib components with component numbers

Table 7.3: Weights and measures of jib components

Section number	Length	Width	Height	Weight
23	12	2.54	2.54	11000
21	10.29	1.87	2.54	4900
22	10.34	1.87	2.5	4000
4	5	1.87	2.5	1800
5	10	1.87	2.5	2700
Total	47.63			24400

7.8 Circular track

The large moments appearing at base of the arm require a strong foundation and adequate balancing. A way to avoid this is to use a circular track instead of an arm to maintain the circular motion (figure 7.24). This track can be made by a kind of roller coaster rail. On this rail an attachment device is put, which has the ability to drive around the track. In any other direction it is locked so it will not come off the track. The function of the attachment device is to hold the aircraft during launching and landing, but also to provide the rotational motion as soon as the aircraft takes off. The cable is lead through the attachment unit, so the motion of the unit is passed on to the aircraft through the cable similarly as it would have been when using an arm instead. The power of the motor driving the attachment unit should be sufficient to launch the aircraft. Since there is no difference in power when using an arm or circular track, the attachment device in this case requires a motor of about 0.5 MW (paragraph 7.6). This motor can also be put on the ground and moving the attachment device through some kind of conveyor belt principle. Having a lightweight attachment device decreases the inertia in the system. This provides the ability to reduce peak forces in the cable by, for example, having a friction connection between attachment device and motor.

7.9 Conclusion and recommendations

The results of the simulation and the translation to a physical system show that the concept of using a rotating platform for launching the aircraft of the Powerplane system is promising, but does not fully fit to the requirements. First of all it is necessary to reach a higher altitude and cable length. The achievable altitude and cable length are limited for this system because drag forces increase with cable length and altitude. This makes the path of the aircraft lag behind the motion of the arm, until the aircraft lags so much behind that the cable tension in the heading direction of the aircraft decreases to below zero. Research could be done on finding ways to postpone this phenomena until higher altitudes are reached, for example by decreasing drag or adapting flight paths to the wind direction. Anyhow, it is not expected that this would lead to such an improvement that the aircraft reaches the operational altitude of 500 m. Therefore the rotational platform should always be supported by another technique. Reverse pumping (chapter B) will most likely work in this case and does not need additional equipment, though it is not proven yet. Using a propeller-motor combination as described in chapter 4.5 to reach higher altitudes is an option, but this results in a more complex system which undermines the main advantage of using a rotating platform: Its simplicity. Because, even though the system performance of the rotational platform is a bit tricky to predict, the concept itself is simple and straightforward.

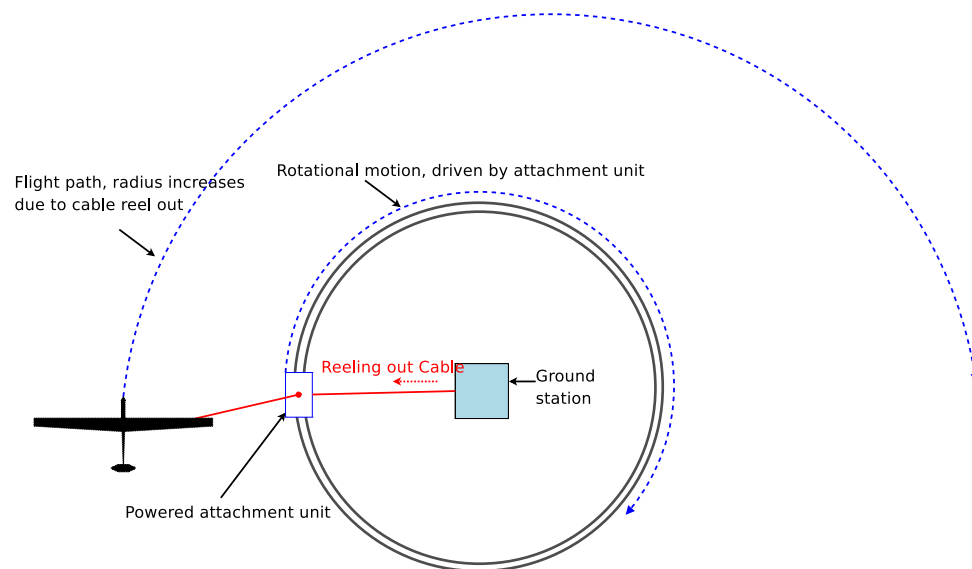


Figure 7.24: Example of a circular track with powered attachment unit

Chapter 8

Conclusion and recommendations

The objective of this research was to find out how the aircraft of the Powerplane system can be launched and retrieved such that it will be a competitive system for wind energy generation. In the first chapters of this report, the main principle of crosswind power and the Powerplane system were described to provide a framework for the requirements given chapter 3. Chapter 4 describes how different design methods were used to come up with several design options. Some of these options were analysed more extensively in this chapter by means of literature study, calculations and a physical test setup. The most promising design options were put together in three concepts, defined in chapter 5. A trade-off chart resulted in abandoning a concept based on buoyancy, but also resulted in the decision to continue researching on the two other concepts. This led to two improved concepts with both their advantages and disadvantages.

One concept can be regarded as a more conventional method, it makes use of a battery powered propeller to accelerate and gain altitude. A description of this concept can be found in paragraph 6.5. Its main drawback is a possible decline in energy generating performance due to an increased aircraft weight.

The other concept physically seems very straightforward and does not effect the aircraft performance. It makes use of a rotational platform to provide thrust via the cable. The performance of this method is analysed by means of a computer simulation in chapter 7. Even though simulation results were promising, no proof was given that the operational height could be reached by this method. Therefore the main drawback of the rotational platform concept is the fact that it has not proven itself yet. To make a definite decision of which concept is most feasible, research should continue, based on following recommendations.

8.1 Research on reversed pumping

The ability of making use of the winch for gaining altitude is an important enabling principle which is useful for the propeller powered concept but vital for the rotating platform. Reversed pumping is kind of taken for granted throughout the thesis. Nevertheless, this procedure is not proven technology yet.

The decision on which concept to choose heavily relies on the end height that has to be reached. If reversed pumping does not work, the rotational platform requires an additional system to gain more altitude. The need of such a system most probably cancels out the main advantage of reversed pumping: the fact that it is a simple and straightforward system. In case of the other concept saves roughly 75% of the required battery power, which significantly reduces the weight of this system on the aircraft.

Therefore more effort should be put in analysis of the possibilities of reversed pumping. A close cooperation with OPTEC of the KU Leuven about this topic is highly recommended, but investigating the procedure in a simulation model is a good start.

8.2 Improve and utilize simulation model

The simulation model is a very powerful tool to use as a starting point for continuing research. It should be used and improved on the aspects stated below.

8.2.1 Specifications 1 MW aircraft

A proper simulation of a 1 MW Powerplane flying energy generating patterns in different wind conditions will provide knowledge on, for example, the loads on the aircraft. This is also important for defining the aircraft design of the system in general, since the requirements tend to differ significantly from conventional aircraft. More important to estimate for this research, is the effect of added weight on the performance of the aircraft.

8.2.2 Rotating launch

Using the simulation model to estimate the performance of a rotating launch incorporated several adjustments on the model itself. The first seconds of the simulations provide unrealistic results. This part should definitely be improved. An improved model will provide more reliable and probably even more desirable results.

8.2.3 Reversed pumping and winching

The simulation model provides the ability to define flight paths and adjust the cable length. Therefore reversed pumping and winching can and should be investigated with the help of this model. This is probably the fastest way to

8.2.4 Winch parameters

Having more knowledge on how the system performs during energy generation also provides the winch parameters required for this operation. These parameters will also tell if reversed pumping or winching need additional requirements on the winch.

8.2.5 Propeller thrust

Adding propeller thrust to the simulation model provides the capability of recalculating the power and energy need of the concept outlined in 6.5. Also the performance at different wind conditions and with different flight paths can be estimated.

8.3 Modular prototype

Beside simulations, a physical setup to test both of the concepts is desirable. Using a modular approach to build a prototype is highly recommended. Both concepts make use of a circular track for launching and landing, such a track can be designed and built for the 10 kW prototype and placed around the ground station on the test field.

Putting the attachment unit on a cart with a detachable drive system, enables the possibility to test both concepts with the same setup. Complementary to this a detachable aircraft propulsion system, consisting of an electric motor, a battery pack, a (foldable) propeller and the required control system could be designed and built to use at the existing 10 kW aircraft.

Bibliography

- [ACA, 1911] ACA (1911). Report of the advisory committee for aeronautics. *Flight*, 3(106):546–547.
- [Aerospace, 2009] Aerospace, A. (2009). Homepage of aerwin aerospace c.v. <http://www.zeppelinvlucht.nl/>. viewed on 20-06-2009.
- [Anderson, 2008] Anderson, J. D. (2008). *Introduction to flight*. McGraw-Hill, 6th edition.
- [Brown, 1998] Brown, D. (1998). Ucla news: Hydrogen didnt cause hindenburg fire. <http://www.seas.ucla.edu/hsseas/releases/blimp.htm>. Viewed 12-08-2009.
- [Burton, 2001] Burton, T. (2001). *Wind Energy Handbook*. John Wiley & sons, Ltd.
- [Canada, 2010] Canada, E. (2010). Wind data of governmental weather office of canada. http://www.weatheroffice.gc.ca/canada_e.html. viewed on 18-05-2010.
- [DeWind, 2010] DeWind (2010). Dewind d8.2 2000 kw wind turbine. <http://www.dewind.de/services-en/produkte/d82.index.htm> and <http://www.sandia.gov/wind/2008BladeWorkshop/PDFs/Mon-05-Sanner.pdf>. viewed on 20-04-2010.
- [Diehl, 2010] Diehl, M. (2010). Reversed pumping. Private communication.
- [Doyle et al., 1995] Doyle, M., Samuel, D., conway, T., and Klimowski, R. (1995). Electromagnetic aircraft launch system - emals. *IEEE Transactions on magnetics*, 31(1):528–533.
- [DWIA, 2003] DWIA (2003). *Wind energy reference manual*. Danish Wind Industry Association. <http://www.windpower.org/en/stat/units.htm>, Viewed 19-03-2010.
- [EWEA, 2009] EWEA, E. W. E. A. (2009). *Wind Energy - the facts*. Earthscan.
- [Fulton, 2008] Fulton, C. G. (2008). *Airship Progress and Airship Problems*. Wildside Press LLC.
- [Geebelen and Gillis, 2010] Geebelen, K. and Gillis, J. (2010). Modelling and control of rotational start-up phase of tethered aeroplanes for wind energy harvesting. Master’s thesis, KU Leuven.
- [GeneralAtomics, 2010] GeneralAtomics (2010). Electromagnetic launch system (emals). <http://atg.ga.com/EM/defense/emals/index.php>. viewed on 19-03-2010.
- [ISO 2533:1975,] ISO 2533:1975. *Standard Atmosphere*. ISO, Geneva, Switzerland.
- [Jackson and Pearson, 1974] Jackson, D. R. and Pearson, M. K. (1974). Investigation of a stored energy launch system for gliders. *AIAA*.
- [JobyEnergy, 2010] JobyEnergy (2010). Homepage of joby energy, inc. <http://www.jobyenergy.com/>. viewed on 12-07-2010.
- [Klok, 2010] Klok, M. (2010). Structural design of a powerplane. Master’s thesis, TU Delft.
- [KU-Leuven, 2010] KU-Leuven (2010). Homepage of the kite power research group of the ku- leuven. <http://www.kuleuven.be/optec/research/projects/kitepower>. viewed on 15-06-2010.
- [Kühn, 2009] Kühn, D. (2009). Modelldaten für fms flugmodellsimulator. http://www.multiplex-rc.de/cms/vorschau/upload/d-software/m-easyglider_e.zip. viewed on 10-11-2009.

- [Lange-Aviation, 2010] Lange-Aviation (2010). Homepage of lange-aviation. <http://www.lange-aviation.com/>. viewed on 12-02-2010.
- [Lansdorp, 2009] Lansdorp, B. (2009). Powerplane technical document. Technical report, Ampyx Power.
- [Lansdorp and Ockels, 2005] Lansdorp, B. and Ockels, W. (2005). Design of a 100 mw laddermill for wind energy generation from 5 km altitude. In *Beijing: 7th World Congress on Recovery, Recycling and Re-intergration*, pages 1–6. 7th World Congress on Recovery, Recycling and Re-intergration.
- [Liao and Pasternak, 2009] Liao, L. and Pasternak, I. (2009). A review of airship structural research and development. *Progress in Aerospace Sciences*, 45(4-5):83 – 96.
- [Lipman and Delucchi, 2006] Lipman, T. E. and Delucchi, M. A. (2006). A retail and lifecycle cost analysis of hybrid electric vehicles. *Transportation Research Part D: Transport and Environment*, 11(2):115 – 132.
- [Loftin, 1985] Loftin, L. K. (1985). *Quest for Performance: The Evolution of Modern Aircraft*. Number NASA SP-468. NASA Scientific and Technical Information Branch.
- [Loyd, 1980] Loyd, M. L. (1980). Crosswind kite power. *Energy*, 4(3):106–111.
- [Magenn, 2010] Magenn (2010). Homepage of magenn power inc. <http://www.magenn.com/>. viewed on 14-06-2010.
- [MakaniPower, 2010] MakaniPower (2010). Homepage of makani power. <http://www.makanipower.com/>. viewed on 03-08-2010.
- [MT-Propeller, 2010] MT-Propeller (2010). Homepage of mt propellor. <http://www.mt-propeller.com/>. viewed on 12-02-2010.
- [Mulder et al., 2006] Mulder, J., van Staveren, W., van der Vaart, J., and de weerdt, E. (2006). *Flight dynamics, Lecture notes*. Delft University of Technology.
- [Nemry et al., 2009] Nemry, F., Leduc, G., and Munoz, A. (2009). Plug-in hybrid and battery-electric vehicles: State of the research and development and comparative analysis of energy and cost efficiency. Technical Report JRC 54699, EC JRC Institute for Prospective Technological Studies.
- [PML, 2006] PML (2006). Specifications of hi-pa drive from pml flightlink ltd. http://www.pmlflightlink.com/motors/hipa_drive.html. viewed on 27-05-2010.
- [Ruijgrok, 2007] Ruijgrok, G. (2007). *Elements of airplane performance*. VSSD.
- [Ruiterkamp, 2009] Ruiterkamp, R. (2009). Powerplane sizing and optimization. Technical report, Ampyx Power.
- [Scrosati and Garche, 2010] Scrosati, B. and Garche, J. (2010). Lithium batteries: Staus, prospects and future. *Journal of Power Sources*, 195:2419–2430.
- [Sieberling, 2009] Sieberling, S. (2009). Design of a robust generic flight control system using incremental nonlinear dynamic inversion. Master’s thesis, TUDelft / NLR.
- [Stevenson et al., 2005] Stevenson, J., Alexander, K., and Lynn, P. (2005). Kite performance testing by flying in a circle. *Aeronautical Journal*, 109(1096):269–276.
- [TCOM, 2009] TCOM (2009). Homepage of tcom aerostats. <http://www.tcomlp.com/tcom-home.html>. viewed on 12-08-2009.
- [Terex-Cranes, 2010a] Terex-Cranes (2010a). *Flat top tower crane CTT 561/A-24 HD23*, tc-ds-me/f/g/i/s-ctt561a-24 hd23-04/10 edition.
- [Terex-Cranes, 2010b] Terex-Cranes (2010b). Homepage of terex cranes corporation. <http://www.terexcranes.com>. viewed on 08-07-2010.

- [Torenbeek, 1982] Torenbeek, E. (1982). *Synthesis of Subsonic Airplane Design*. Delft University Press.
- [Turman et al., 1995] Turman, B., Marder, B., Rohwein, G., and Aeschliman, D. (1995). The pulsed linear induction motor concept for high-speed trains. Technical report, Sandia National Laboratories.
- [UQM, 2010] UQM (2010). Vehicle propulsion systems of uqm technologies. http://www.uqm.com/propulsion_specs.php. viewed on 27-05-2010.
- [White, 2008] White, F. M. (2008). *Fluid Mechanics*. McGraw-Hill, 6 edition.
- [Worthington, 2010] Worthington (2010). Homepage of worthington cylinders sci aviation cylinders. <http://www.worthingtoncylinders.com/Products/composite-cylinders/SCI-Aviation.aspx>. viewed on 09-04-2010.
- [Yuneeec, 2008] Yuneeec (2008). Specification of e430 electric aircraft from yuneeec ltd. http://yuneeccouk.site.securepod.com/Aircraft_specification.html. viewed on 27-05-2010.

Appendix A

List of symbols

Symbol	Meaning	Symbol	Meaning
a	Acceleration	r	Radius
A	Area	R	Radius
b	Wing span	RC	Rate of climb
c	Chord	s	Distance
C_D	Drag Coefficient	S	Surface
C_L	Lift Coefficient	t	Time
CF	Capacity Factor	T	Torque
CG	Centre of gravity	T	Tension
d	Diameter	T	Temperature
d	Distance	u	Energy
D	Drag	V	Velocity
e_w	Energy to weight ratio	W	Weight
E	Energy	z_0	Ground roughness
E	Youngs Modulus		
F	Force	α	Angle of attack
g	Gravity	β	Side slip angle
h	Altitude or height	χ	Heading angle
I	Impulse	δ	Deflection
l	Length	η	Efficiency
L_c	Cable length	γ	Flight path angle
L	Lift	γ	Climb angle
m	Mass	λ	Temperature lapse rate
M	Moment	ω	Angular Velocity
n	Load Factor	ϕ	Bank angle
p_w	Power to weight ratio	ρ	Air Density
P	Power	ε	Strain
P	Pressure	ξ	Launch angle
r	Roll rate	ζ	Lag angle

Appendix B

Increase altitude with help of the winch

Winching is a way to make the aircraft increase height, which is a generally used way to launch sail planes. This method can also be used subsequently when the aircraft is already airborne to gain more altitude. Since the aircraft is attached to the winch with the tether during its whole operation, this method does not require additional equipment. Even though a prove of concept of utilizing this method has not been made yet. Ampyx Power has a strong believe that this method will work. Therefore it is regarded as a fixed solution that can be made use of anyhow. Modelling or proving this methodology is regarded to be beyond the scope of this thesis.

B.1 Airborne winching

Winching can be done by retrieving the cable while the aircraft flies with adverse wind. The apparent wind at the wing is increased, creating lift which brings the aircraft to a higher altitude. After reaching a point where no height can be gained any more, the aircraft flies away from the ground station with tailwind at minimum velocity, exchanging height for velocity, while the cable is being reeled out. Since the lift force increases with the square of the velocity, and the velocity during cable retraction is higher than at reeling out, altitude is gained during the whole cycle. This cycle repeats until the aircraft has reached its operational height (figure B.1).

B.2 Reversed pumping

Instead of winching, another way of gaining altitude by making use of the winch is called 'reversed pumping'. Reeling the cable in and out while the aircraft flies a path, can be done such that the net energy gain at the aircraft to gain altitude is positive. It is kind of similar to winching as described above, though the frequency in which reeling in and out takes place does not necessarily have to be linked to flying with headwind or tailwind. This methodology is currently being investigated by the kite power group of the K.U. Leuven and seems promising [Diehl, 2010, Geebelen and Gillis, 2010]. Though, real test results have not been published yet.

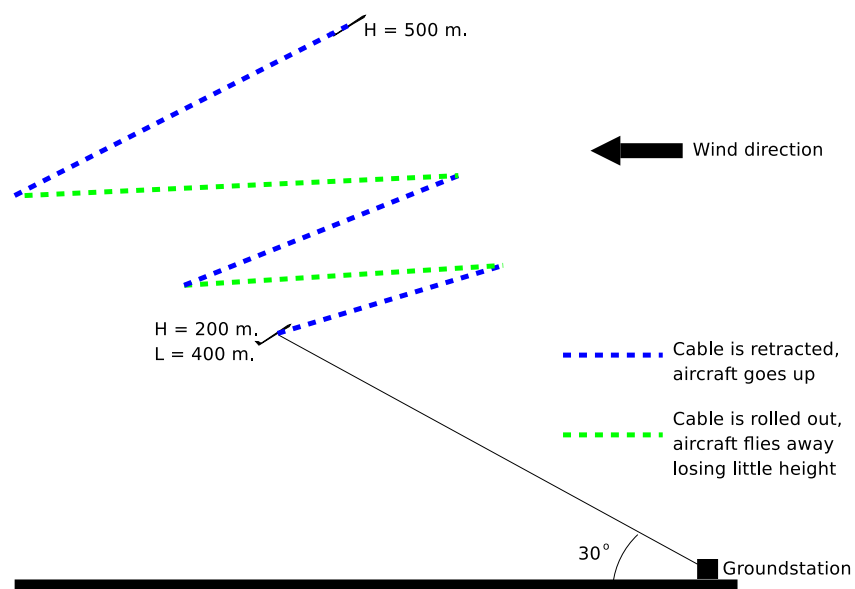



Figure B.1: Increasing altitude by winching

Appendix C

Specifications Dyneema Cable



High performance ropes EURONEEMA®

Lankhorst/Ropes


R-9

FIBRE ROPES



12 strand braided rope, made of UHMWPE yarns. This rope forms an excellent alternative for heavy and cumbersome steelwire ropes in situations requiring manual handling of the rope. The strength is higher than that of conventional steelwire rope and the corresponding weight is 7 times lower! The better handling characteristics are especially appreciated in towing and mooring applications. This rope is floating!

When replacing fibre rope the reduction in diameter can lead to substantial saving of weight and size of e.g. the mooring winches, and when incorporated in the design of the vessel at newbuilding to a saving of cost as well.

EURONEEMA®

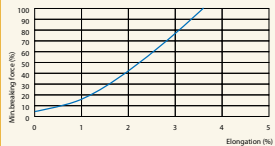



SPECIFIC GRAVITY • 0,98 UV-RESISTANCE • excellent ABRASION RESISTANCE • excellent CHEMICAL RESISTANCE • good ELONGATION • see graph MELTING POINT • approx. 165°C	CONSTRUCTION • 12-strand plaited TCLL VALUE • 100% COLOUR • yellow WATER ABSORPTION • 0%
--	---


Art.number	Circ. (inches)	Diameter (mm)	Weight (kg/100m)	MBF (kN)
092.006	3/4	6	2,2	35
092.008	1	8	4,0	62
092.010	1 1/4	10	6,0	97
092.012	1 1/2	12	9,3	137
092.014	1 3/4	14	10,7	184
092.016	2	16	15,0	244
092.018	2 1/4	18	19,6	303
092.020	2 1/2	20	23,1	374
092.022	2 3/4	22	26,9	450
092.024	3	24	33,5	533
092.026	3 1/4	26	38,5	612
092.028	3 1/2	28	45,5	701
092.030	3 3/4	30	52,5	789
092.032	4	32	59,0	887
092.034	4 1/4	34	65,0	991
092.036	4 1/2	36	71,0	1076
092.038	4 3/4	38	80,0	1191
092.040	5	40	88,5	1314
092.044	5 1/2	44	109	1559
092.048	6	48	126	1853

Diameter, weight and MBF (as well as other mechanical and physical properties) are determined according ISO 2307:2005





01112007
www.lankhorstropes.com
 member of the Royal Lankhorst Euronete Group


 GROUP BV

Appendix D

Design options

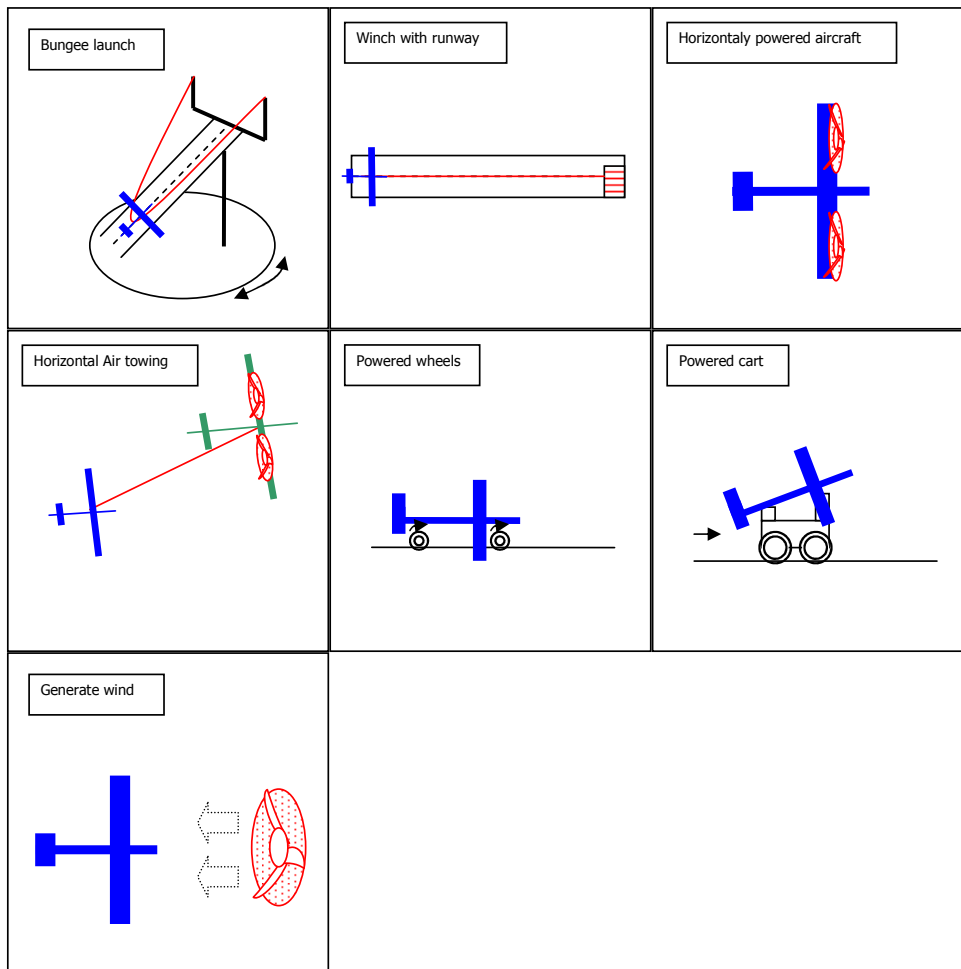


Figure D.1: Launch with runway

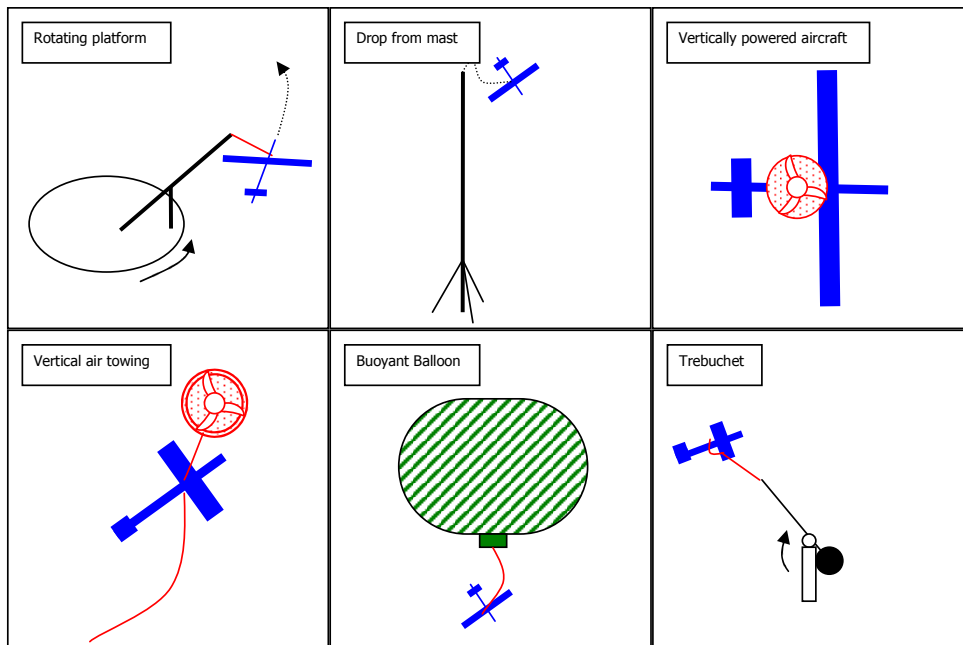


Figure D.2: Launch without runway

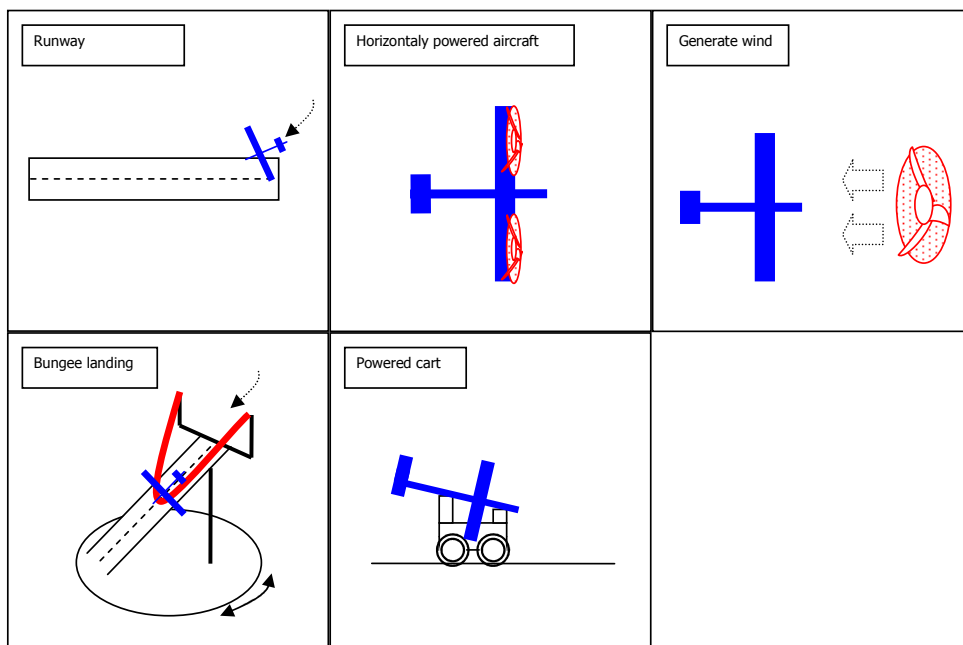


Figure D.3: Land with runway

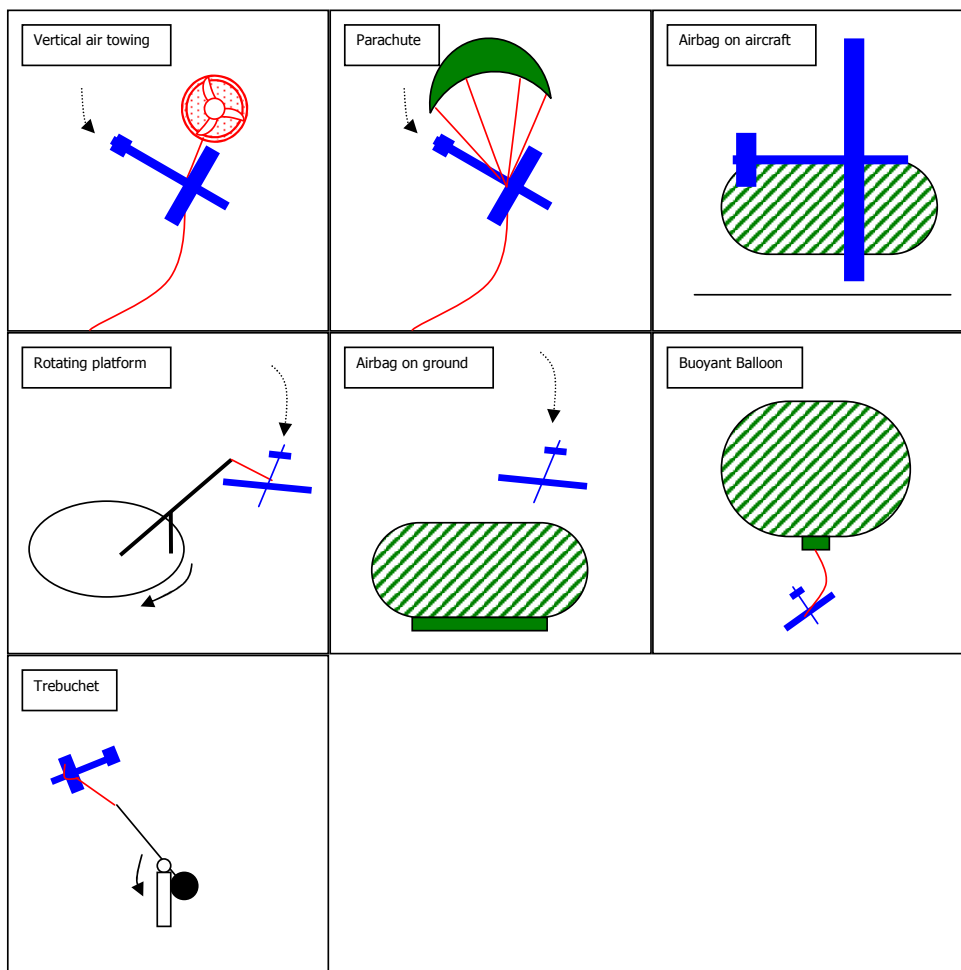


Figure D.4: Land without runway

Appendix E

Functional Analysis Diagrams

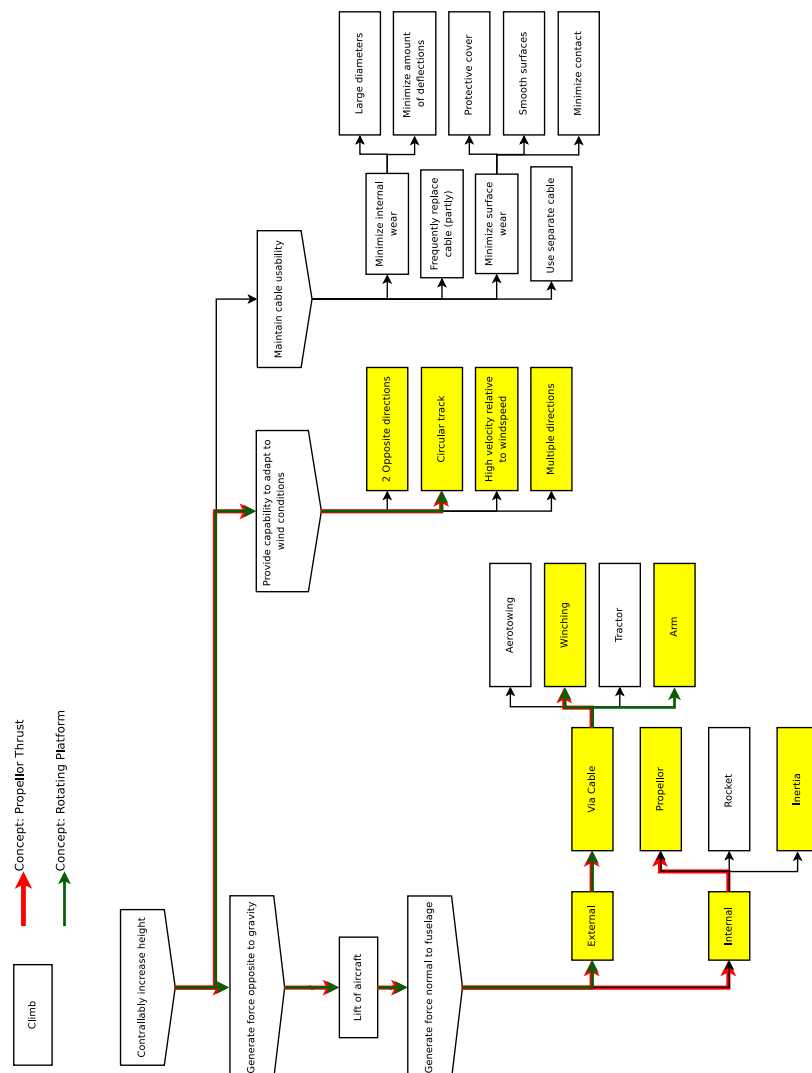


Figure E.1: Functional analysis of climb out

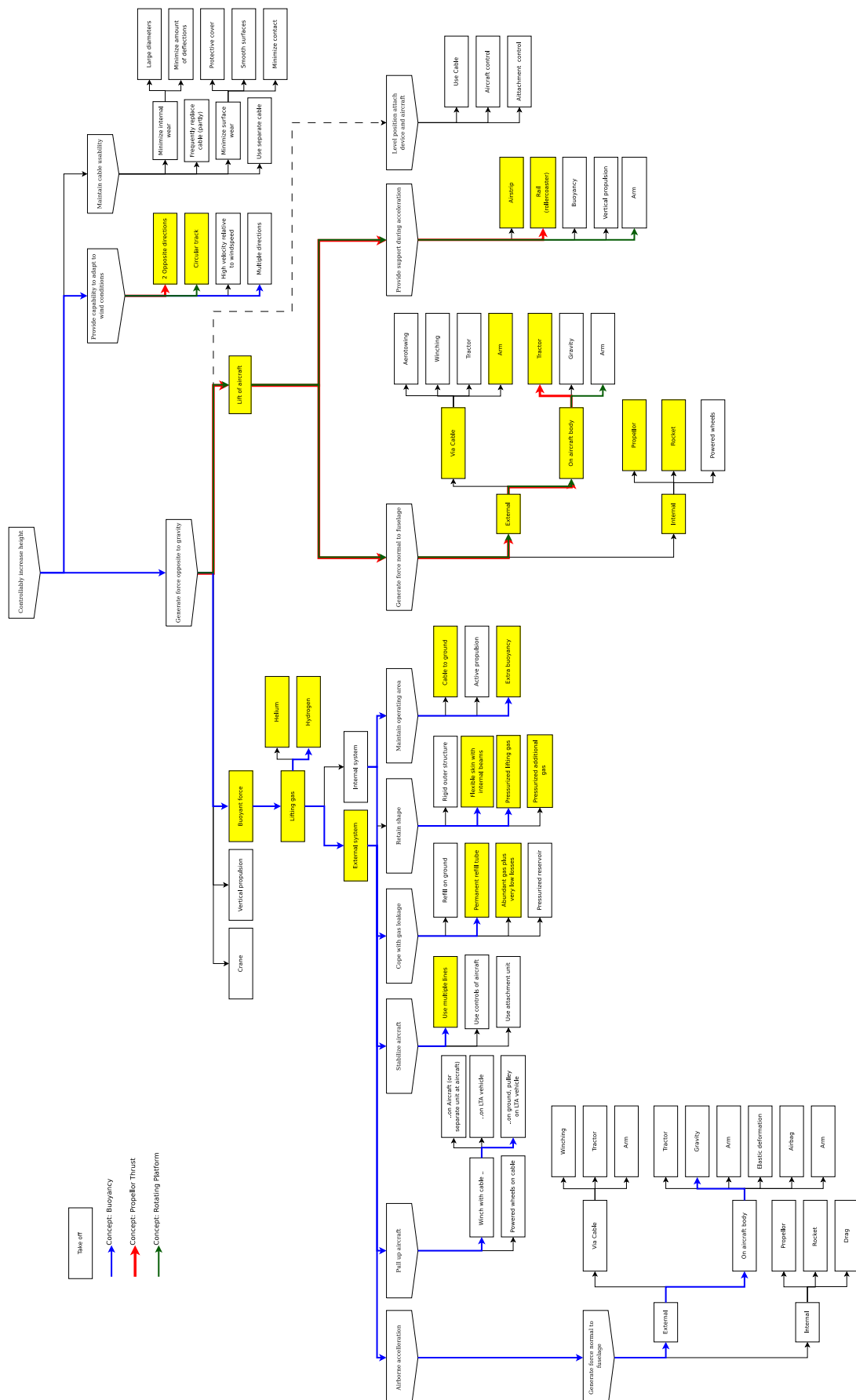


Figure E.2: Functional analysis of take-off
Up! How to Launch and Retrieve a Tethered Aircraft

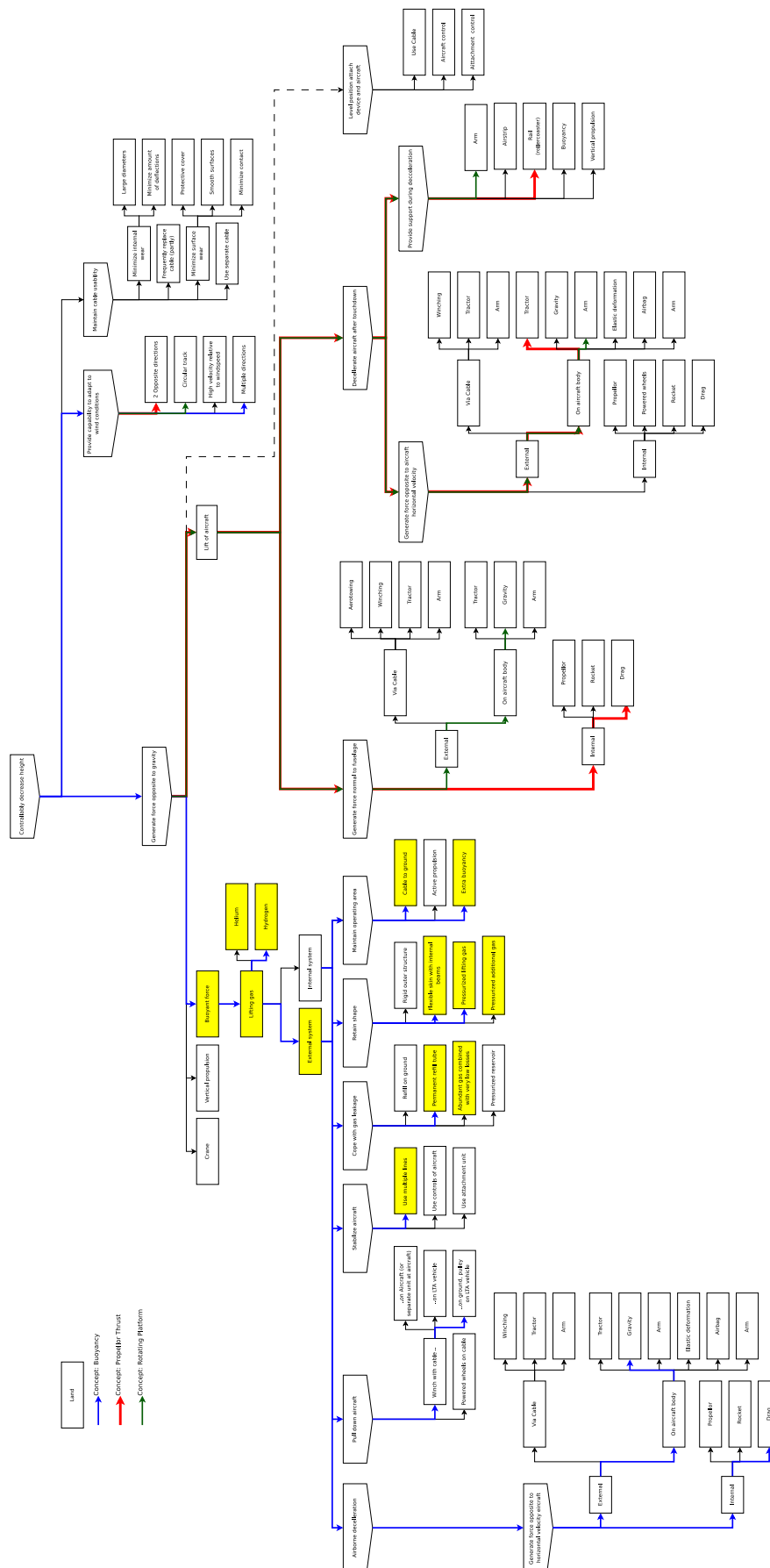


Figure E.3: Functional analysis land
Up! How to Launch and Retrieve a Tethered Aircraft

Appendix F

Airfoil characteristics Easyglider

The air foil data of the Easyglider was not given with the aircraft documentation. The website of the manufacturer only provided model data to use with a flight simulator. ([Kühn, 2009]) To make sure this data agrees with the aircraft some additional analysis has been carried out. The air foil surface was copied with tinfoil and scanned providing the picture shown in F.1



Figure F.1: Scan of airfoil

The picture was used to trace and digitize the geometry of the airfoil with digitizing software (Engauge). This geometry was put in Javafoil. Some tinkering with the design till a smooth velocity distribution occurred resulted in the final airfoil coordinates, which are shown in figure F.2. A two dimensional analysis of the airfoil by Javafoil provided the lift and drag polar of the aircraft (figure F.3) and a graph of the lift coefficient as a function of the angle of attack (figure F.4). The maximum lift coefficient of 1.3 which can be found by this method agrees with a C_l of 1.4, found in the flight simulator characteristics ([Kühn, 2009]). Further characteristics of the Easyglider are shown in table F.1.

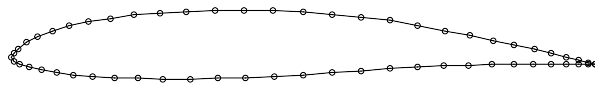
Wingspan b	Overall length l	Chord c	Surface S	Max Lift Coeff. $C_{L_{max}}$	Weight W	Wing loading W/S
1.8 m	1.13 m	0.20 m	0.416 m ²	1.3	8.63 N	20.7 N/m ²

Table F.1: Characteristics of Easyglider Electric

Airfoil Geometry Easyglider

10/22/09 / 2:21 PM

Airfoil Shape



x	y	x	y
0.99900545	-0.01220119	0.10534898	-0.02883292
0.99167822	-0.01063328	0.13858552	-0.03163318
0.97967872	-0.00769197	0.17532070	-0.03367328
0.96311391	-0.00345614	0.21517543	-0.03496066
0.94206287	0.00171222	0.25774788	-0.03550946
0.91667934	0.00755150	0.30261487	-0.03537854
0.88722967	0.01408868	0.34933552	-0.03460112
0.85401865	0.02135421	0.39745392	-0.03322971
0.81736236	0.02926272	0.44650174	-0.03129198
0.77760336	0.03769090	0.49600174	-0.02880615
0.73509837	0.04643295	0.54546656	-0.02569793
0.69022794	0.05525551	0.59441764	-0.02206141
0.64327883	0.06323849	0.64237941	-0.01794284
0.59457963	0.06918283	0.68904075	-0.01550629
0.54476666	0.07382566	0.73386957	-0.01364591
0.49437354	0.07732280	0.77641320	-0.01197871
0.44391400	0.07967600	0.81627004	-0.01074207
0.39389897	0.08085025	0.85305294	-0.00990399
0.34483669	0.08079602	0.88640537	-0.00946925
0.29723089	0.07946817	0.91600282	-0.00941404
0.25157697	0.07685949	0.94155671	-0.00968321
0.20836086	0.07294514	0.96281821	-0.01018756
0.16805267	0.06775989	0.97958055	-0.01084442
0.13110740	0.06135079	0.99168007	-0.01157741
0.09796027	0.05381495	0.99900545	-0.01220119
0.06902909	0.04528697		
0.04471626	0.03596141		
0.02539585	0.02615477		
0.01141452	0.01634235		
0.00300044	0.00732280		
0.00001890	0.00055102		
0.00312825	-0.00592013		
0.01412102	-0.01097149		
0.03006375	-0.01618887		
0.05077108	-0.02102059		
0.07596732	-0.02527743		

Created by JavaFoil © 2001–2009 © Martin Hepperle

Figure F.2: Airfoil geometry Easyglider

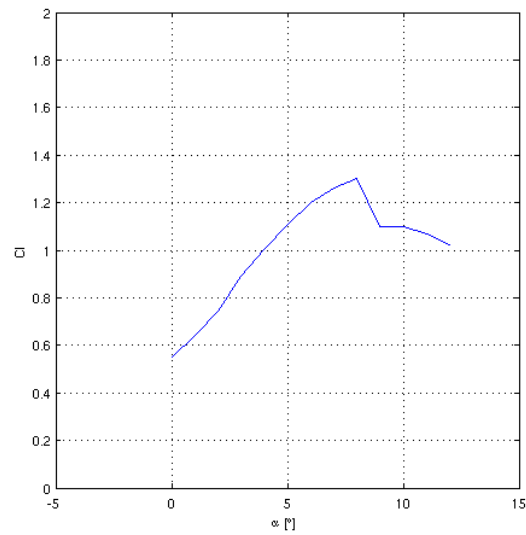


Figure F.3: Lift coefficient versus Angle of Attack of Easyglider

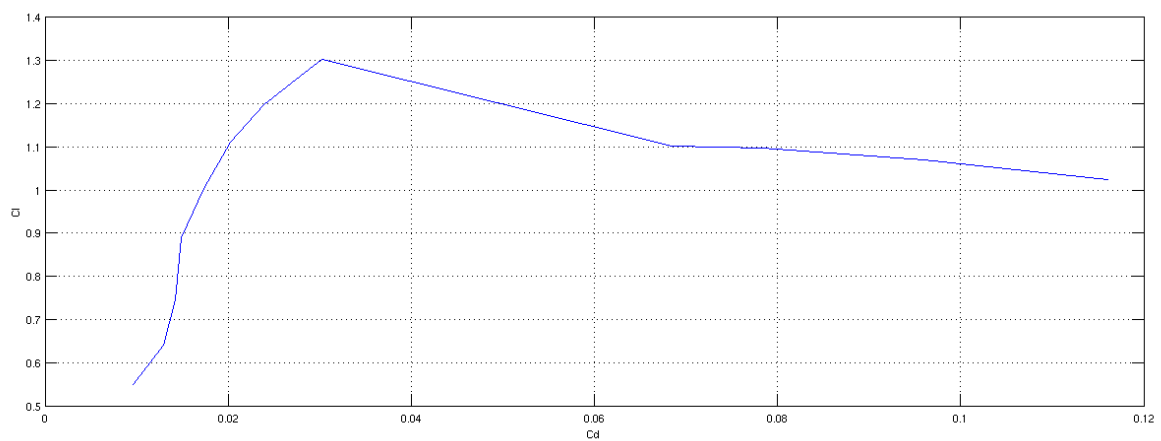


Figure F.4: Lift drag polar of Easyglider

Appendix G

Data of Terex Crane

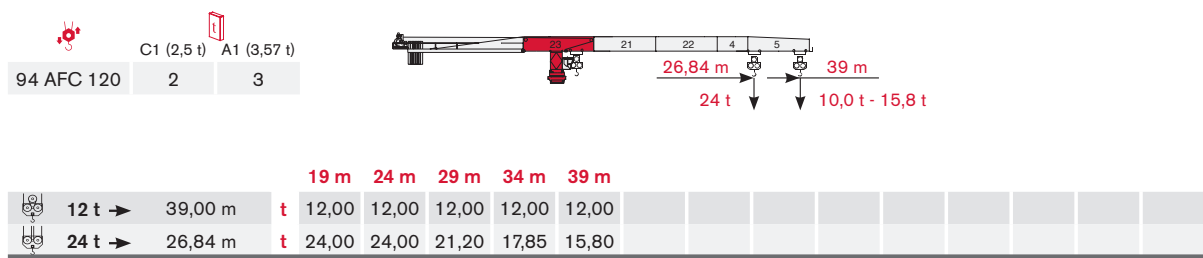


Figure G.1: Load curve of crane, with component numbers



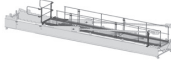







CTT 561A -24 HD23	DESCRIPTION · BESCHREIBUNG · DESCRIPTION · DESCRIPCIÓN · DESCRIZIONE	LENGTH · LÄNGE · LONGUEUR · LONGITUD · LUNGHEZZA	WIDTH · BREITE · LARGEUR · ANCHURA · LARGHEZZA	HEIGHT · HÖHE · HAUTEUR · ALTURA · ALTEZZA	QUANTITY · MENGE · QUANTITÉ · CANTIDAD · QUANTITÀ	WEIGHT · GEWICHT · POIDS · PESO · PESO
	CAB SUPPORT PLATFORM	5,54 m	1,87 m	2,69 m	1	2000 kg
	CAB TOWER SECTION	1,90 m	2,50 m	3,23 m	1	3050 kg
	COUNTERJIB "1C"	7,16 m	1,99 m	0,86 m	1	3950 kg**
	COUNTERJIB "3C"	11,66 m	2,21 m	1,10 m	1	5800 kg**
	JIB SECTION-23 23TT19 23.12	12,00 m	2,54 m	2,54 m	1	11000 kg***
	JIB TROLLEY 20-24 t	2,38 m	2,29 m	1,45 m	1	765 kg
	JIB SECTION-21 21TT19 23.10	10,29 m	1,87 m	2,54 m	1	4900 kg
	JIB SECTION-22 22TT19 23.10	10,34 m	1,87 m	2,50 m	1	4000 kg
	JIB SECTION-04 TT19 23.05	5,00 m	1,87 m	2,50 m	1	1800 kg
	JIB SECTION-05 TT19 23.10	10,00 m	1,87 m	2,50 m	1	2700 kg
	JIB SECTION-06 TT19 20.10	10,29 m	1,87 m	2,18 m	1	1930 kg
	JIB SECTION-07 TT1920.05	5,28 m	1,87 m	2,18 m	1	900 kg
	JIB SECTION-08 TT1917.05	5,25 m	1,87 m	1,86 m	1	780 kg

Figure G.2: Component data of crane